University of Nevada

Reno

Study of Airflow Over Rough Surfaces

A thesis submitted in partial fulfillment of the requirements for the degree of

Master of Science in Mining Engineering

by

Indu Mohan Konduri

Pierre Mousset-Jones, Thesis Advisor

May 1994

The thesis of Indu Mohan Konduri is approved:

P. Mousset-Jones

Thesis advisor

Dr. Pierre Mousset-Jones

Daeman

Department Chairman

Dr. Jaak Daeman

Dean, Graduate School

University of Nevada

Reno

May 1994

ACKNOWLEDGEMENTS

The research for this paper is supported by the Generic Mineral Technology in Mine Systems Design and Ground Control, Office of Mineral Institutes, U.S. Bureau of Mines, Grant No. G1125151. Their assistance and cooperation is gratefully acknowledged. I would like to express my sincere gratitude and appreciation to Dr. Pierre Mousset-Jones, my advisor, for his guidance, motivation, and encouragement during my studies at the University of Nevada, Reno; and to Dr. George Danko for guidance and assistance in designing, conducting and evaluating the wavy-walled wind tunnel experiments, and Dr. Felipe Calizaya for his valuable ideas, suggestions and support throughout my thesis work. I also sincerely thank Dr. Richard Wirtz, department of mechanical engineering, for his valuable comments and serving in my thesis advisory committee.

The assistance of the following persons is also acknowledged: H.P. Muller, General Manager, A.M.T., for the loan of a laser tunnel profiler, Mr. John Jordan, Chief Engineer, Sunshine Mine, Idaho, for his assistance in the collection of the field data, Dr. J.R. Carr for his advice on fractals, and Mr. Shiping He for his help in building the field and laboratory equipment.

ABSTRACT

The research project involved an investigation into the appropriate parameter to characterize the surface roughness of an underground airway. Two sections of an underground airway were laser-profiled for analysis in order to determine the impact of the surface measurement method on the calculation of coefficient of friction and friction factor. The results indicated that there is a need to remeasure friction factor values of mine airways, since the published values tend to overestimate. Fractal analysis was used to investigate the potential role of the fractal dimension as an alternative to conventional parameters. A unique laboratory of a mine airway with macro-roughness was constructed, i.e., wavy-walled, simulating the typical surface conditions of an actual mine airway developed by drilling and blasting. It was found that the macro-waviness in an airway contributes significantly to the total airflow pressure loss.

Table of Contents

List of Illustrations

List of Illustrations

List of Tables

List of Symbols and Units

The symbols and units indicated below are used throughout the text unless it is noted.

Symbols

A	area (m^2)
A_x	projected area on yz plane (m^2)
A_y	projected area on zx plane (m^2)
ASCII	American Standard Code for Information Interchange
Ave	average
a	speed of sound (m/s)
C	fast fourier transform function
C_d	drag coefficient
C_p	pressure coefficient
CLA	center line average
CV	control volume
c	constant
D	fractal dimension, dimension
D_0	topological dimension
d	hydraulic diameter (m)
dt	infinitesimal time (s)
dx	infinitesimal length in x direction (m)

dy	infinitesimal length in y direction (m)
e	mean asperity height (m), waviness (m)
F_d	drag force (N)
f	coefficient of friction, frequency (Hz)
g	acceleration due to gravity (m/s^2)
H	scaling parameter of a fractal curve
H_2O	water
Hg	mercury
h	height (m), pressure head loss (m)
i, j	integer
k	friction factor (kg/m^3), integer
L	ruler length (m)
l	length (m)
m	mass (kg), slope of the strait line
N, n	integer
p	amplitude (m)
P	pressure (Pa)
P_a	atmospheric pressure (Pa)
P_s	static pressure (Pa)
P_v	velocity pressure (Pa)
P(f)	power function
Per	perimeter (m)
Q	flow rate (m^3/s)

R	resistance ($N\ s^2/m^8$)
R_u	universal gas constant (J/kg.K)
RMS	root mean square
Re	Reynolds number
r	radius (m), scaling ratio
r_h	hydraulic radius (m)
S	rubbing surface (m^2), spectral density function
s_x, s_y	roughness parameters
T	absolute temperature (K)
T_0	reference temperature (273 K)
t	time (s), temperature (^0C)
t_d	dry bulb temperature (^0C)
t_{wet}	wet bulb temperature (^0C)
U_∞	far field velocity (m/s)
u_p	perturbation velocity, horizontal component (m/s)
V	mean velocity (m/s), fractional Brownian motion function
v	velocity (m/s)
v_{ave}	average velocity in the airway (m/s)
v_{max}	maximum/centerline velocity (m/s)
v_p	perturbation velocity, vertical component (m/s)
x_b	boundary point in x direction
β	slope
β_x, β_y	roughness geometry parameters

γ	semi-variogram function
Δp	static pressure difference (Pa)
δ	elemental length (m)
∂	partial differential
μ	viscosity (Pa. s)
μ_0	viscosity at reference temperature (Pa. s)
ϕ_p	velocity potential function
τ	shear stress (Pa)
θ	angle (radian,°)
λ	wave length (m)
ρ	mass density (kg/m^3)
ν	kinematic viscosity (m^2/s)

Units

^0C	degree centigrade
cm	centi-meter
^0F	degree Fahrenheit
ft	foot
Hz	hertz
J	joule
K	kelvin ($273.15+^0C$)
km	kilo-meter
kg	kilogram

m	meters
mm	milli-meter
s	second
in	inch
N	newton
Pa	pascal

All other unmentioned and mathematical symbols used in the text follow standard universal notations.

1. INTRODUCTION

Ventilation is a primary and an essential requirement in underground mining operations. One of the major identifiable costs in underground mining is mine ventilation (Barnes & Rellier, 1989). Airflow in mine drifts is a constant requirement for all unit mining operations, eg. development, stoping and transportation. Mine ventilation is essential for maintaining acceptable working conditions in a mine by maintaining the quality and quantity of the atmospheric environment and is the mainstay of the miner's life support and the mine's health and safety program (Hartman, 1987).

The basic components in a mine ventilation system are mine fans and a network of airways. Airflow in mine ventilation networks is primarily caused by mechanical fans, either by exhaust or forced ventilation (Hartman, 1982). Depending on the airflow requirements in a given mine, the specific size and capacity of the mine fans are selected. The fan pressure required for the supply of adequate fresh air is primarily governed by the size, shape and surface roughness of the airways, and the airflow quantity.

To date, considerable work has been performed on the effect of number, size, shape of the airways (Calizaya, et al., 1991), and other parameters such as distribution of air pollutants (Konduri, 1991, Chao & Ruston, 1989, Thakur, 1979) in mine ventilation system design. The influence of rock surface characteristics on airflow has been studied by many researchers, but there remains considerable uncertainty in predicting the effect of surface roughness on the flow distribution and power requirement. A knowledge of the airway surface roughness is necessary in planning and designing mine ventilation systems for least cost and high efficiency, because it affects the mine resistance (Wala, 1991, Gangal, et al.,

85). An immediate consequence of inaccurate estimation of airway resistances could be energy losses by running oversized mine fans. In practice, for a mine opening with particular surface characteristics, aerodynamic friction factors are chosen from published data, and used in equations derived from different experimental and analytical studies. In reality, because of the limited applicability of the theories and hypotheses from experimental results, this can lead to erroneous estimation of airway resistance for newly developed underground airways, which impacts on the designed capacity of the mine fans. Hence, it is vital to choose friction factors in the planning stages of a mine, that are sufficiently accurate to reasonably predict airway resistance losses in order to avoid over-design of the fan and the resulting energy losses.

The objective of this research is to determine a correlation between airway rock surface characteristics and friction factor under fully developed turbulent airflow conditions. Over several decades, a number of correlations between different flow parameters have been put forward by researchers in fluid mechanics (Rahim, et al., 1976). Most of these investigations were based on using the approach of sand-grain roughness in circular pipes (Nikuradse, 1933 and Moody, 1944). The concept of average asperity (roughness) to hydraulic diameter ratio was the approach taken to characterize a rough airway surface. Apart from the fact that circular pipes of limited cross-section were tested (eg. Nikuradse), the methods of estimating the basic physical flow parameters in a mine airway, such as average roughness height and mean hydraulic diameter, are not yet well established and are questioned by practicing mine ventilation engineers. Average roughness height is a gross simplification of the rock surface roughness characteristics, because the representative quantity is the arithmetic mean of the asperities. This shows that, the same average roughness height can represent two or more distinctively different rough surfaces. Consequently, different friction

factor values may be obtained for surfaces with the same average asperity (roughness) heights, which implies that just the concept of average roughness is an insufficient description of a rough surface. In reality, each distinct surface shows a specific roughness property or a friction factor. Therefore, for a practicing engineer, the notion of average asperity cannot encompass the surface roughness geometry in its totality, except for a completely random distribution of roughness elements over the surface. In order to show the distinction between various surfaces that have different friction factors, parameters that relate to airway geometry need to be taken into consideration. The airway surface roughness consists of two significant components. One is the micro-asperities which are smaller in scale and do not effect the surface of an airway significantly. The other is macro-asperities which effect the geometry of the airway significantly in the form of areal changes, etc., and can be observed by visual inspection of surface profiles.

The definition of hydraulic diameter does not hold for an airway with surface asperities considerably larger than sand-grain type roughness. This is even more the case for asperity distributions with a specific directional bias i.e. the airway offers a different resistance if the flow direction is changed. Due to the presence of relatively high roughness elements in an airflow field, localized eddies and vortices are likely to be present in the flow path. At the onset of the turbulent buffer layer, the effective cross-section will be constricted, hence, the calculated hydraulic diameter, depending on the actual geometry of the airway cross-section, would not be acceptable. This is more the case in mine airways, because their surfaces have micro-asperities superimposed on macro-asperities due to the mining excavation cycle (Konduri, et al., 1993 and Danko & Mousset-Jones, 1988).

A recent approach to characterize a rough surface, namely fractal geometry, has been

found to be quite promising. Its wide application in science and technology made it acceptable for the study of surface roughness geometry in mine airways (Banik, 1990 and Konduri, et al., 1993). This approach is unique in the sense that it can identify the surfaces of differing asperity patterns with separate fractal dimensions. This implies that two surfaces of different asperity heights can rarely have the same fractal dimension, although they can possibly have the same average heights. Recently, the fractal dimension has been used to study fluid flow on rock surfaces (Brown, 1987), to classify rockmass (Carr & Warriner, 1987), to study rock joint profiles (Huang, 1992, Carr & Warriner, 1989), and to correlate the fractal dimension and the aero-dynamic friction factor (Banik, et al, 1993).

The concept of fractal dimension is applicable to characterize many natural surfaces and an this is explained in detail in Chapter 4. Natural surfaces have random distribution, therefore fractal dimension has been successfully used for rock surface profiles, profiles of mine airways. The fractal dimension cannot show a significant difference in profiles that have same shapes but different amplitudes, for example, two sine waves ($\simeq 1.5$). In mine airways, the surface apsperities, although they are random, show a sinuosity or waviness in their longitudinal profiles. Another limitation with the fractal dimension is that it is not sensitive to the direction it is calculated for a mine airway.

In addition to the above mentioned problems, it is found that the value of the friction factor depends on the size and shape of a mine airway cross-section (Calizaya, et al., 1991). Furthermore, the friction coefficient changes with the direction of the airflow (Calizaya, et al., 1990). This anomaly is prominent in the cases of rough surfaces with relatively large asperities having a distinct directional bias in their orientation. The focus is laid on the role of macro-asperities on the pressure drop and flow patterns.

In this research, the fractal nature of mine airway rock surface has been investigated and it is described in terms of friction factor, coefficient of friction, and fractal dimension. A set of surface roughness measurements were evaluated. An airway, located on the 3100 level at the Sunshine mine, Idaho, was surveyed using a tunnel laser profiler. A part of the study carried out in the laboratory is to investigate any correlation that may exist between macro asperity height and friction factor. A wavy walled model of a mine drift was designed and built to study this relationship, and to simulate large scale surface unevenness (macro-asperities). The rectangular model has an adjustable roof and floor, which allows a wave form to be created.

The organization of this thesis is as follows: Chapter 2 focuses on a background discussion and review of previous research on airflow over rough surfaces in underground airways. Fundamental and related theories in fluid mechanics applied to mine ventilation are discussed in detail, along with their limitations and drawbacks when applied to real airways. The intent is to minimize disagreement between the results obtained by using available relationships and by making measurements in actual mine airways. Chapter 3 introduces the concept of fractals and is centered around the fundamental relationships required for determining the fractal dimension of a profile. Chapter 4 is devoted to the analysis of the field data obtained with the assistance of a laser tunnel profiler, and a discussion of fractal analysis and its potential application to characterizing rough rock surfaces. In Chapter 5, the experimental set-up (wind tunnel), methodology and data acquisition procedures are presented and analyzed in detail. In Chapter 6, the results of the whole study work are discussed, and important conclusions and recommendations for future work in this area are presented.

2. AIRFLOW OVER ROUGH SURFACES

2.1 Background

In the U.S. for different types and sizes of underground non-coal mine airways, friction factor values have traditionally been estimated on the basis of the published data reported by McElroy (McElroy, 1935). These were obtained principally from studies conducted in various metal mines. Although these values can be used for quick reference, they may be quite different from the true values determined from pressure-quantity surveys. In fact, ventilation surveys carried out in many mines have shown significant differences between measured values and those determined from qualitative descriptions of mine openings (Kharkar, 1973, Notley, 1985). A major cause of this difference is technological changes such as the use of modern excavation equipment, capable of producing relatively smooth airway rock surfaces. A further discrepancy occurs from the inaccuracies in characterizing the airway surface. The present trend in mining excavation is to drive openings larger in cross-section and smoother in surface characteristics than those developed a few decades ago. As the friction factor is a function of the relative roughness of the surface compared to the diameter of the airway under fully developed turbulent flow conditions, it is expected that friction factors may be somewhat lower in modern mine airways than those evaluated in the past.

Extensive studies have been carried out on airflow characteristics in mine airways with rough walls. In most of these investigations, the basic objective was to establish a relationship between the magnitude of pressure drop or energy loss, and wall asperity pattern and internal configuration, for various mine openings driven both in metal and non-metal mines. In general, the results of these investigations have been published in the form of tables and charts

(Hartman, 1982, McPherson, 1988). These data sets of friction factor values are applicable only to airways similar in geometry and surface characteristics to those surveyed. This imposes limitations on the use of such tables and nomogram to determine the friction factor. Very few scholars have addressed the problems of macro-asperities in relation to pressure loss and flow patterns in fluids so far. The necessity is to find a relationship between the macro-roughness and pressure loss and quantity in airways, as this study is an attempt to contribute to the literature in that direction.

Amongst the many investigators of fluid flow in pipes and airways, some of the most citated researchers are Reynolds, Prandtl, Nikuradse, Chezy, D'Arcy, Atkinson, Colebrook and McElroy (Shames, 1982).

2.2 **Review of Theories Relating to Airflow and the Friction Factor**

The established and classical theories have been oriented towards the analysis of experimental measurements in a rectangular wind tunnel. At the same time, relatively new techniques, eg. the discrete element method, are discussed in the context of the same experiment. A critical analysis of these theories helps to judge the strengths and limitations of these methods, and their applicability in the tests described in the following section. The principle objective of this study is to correlate the friction factor with the rock surface characteristics of underground mine airways, where the flow regime is turbulent. Therefore, majority of the analyses have been focused on turbulent airflow.

2.2.1 Reynolds Number

In principle, two types of flows are observed in fluids, laminar and turbulent. In laminar flows, fluid appears to move smoothly along stream lines or laminae. At high flow

rates, stream lines assume a chaotic form; this kind of complete mixing behavior is called turbulent flow. The type of flow depends upon the flow rate or velocity, density, and viscosity of the fluid. Reynolds number is defined by the following equation:

$$Re = \frac{\rho v^2}{2} \frac{1}{\mu} \frac{dy}{dv} \tag{2.1}$$

where,

ρ = density of fluid (kg m^{-3})

v = velocity of flow (m s^{-1})

μ = viscosity of fluid (N s m^{-2})

dv = change in velocity normal to flow direction (m s^{-1})

dy = change in the position of the direction to flow (m)

The change in the position of the direction of flow is dependent on hydraulic diameter, d (m), and velocity v, and Equation (2.1) reduces to:

$$Re = \frac{\rho \, v \, d}{\mu} \tag{2.2}$$

$$d = \frac{4A}{Per}$$
$$v = \frac{Q}{A} \tag{2.3}$$

where,

A = area of cross-section (m^2)

Per = perimeter of cross-section (m)

Q = quantity of flow ($m^3 s^{-1}$)

At Reynolds numbers less than 2000, viscous force prevails and the flow will be laminar. The Reynolds numbers over which fully developed turbulence exists is less well defined. It can be stated that between Reynolds numbers of 2000 and 4000 the flow is in transition from laminar to turbulent (Davies, 1972). In most underground airways Re is much greater than 4000.

2.2.2 Darcy-Weisbach's Equation

The boundary shear-stress for uniform open-channel flow and gradually varied flow at the same flow depth and velocity, are very nearly identical. When fluid flows along a channel (see Figure 2.1), the head loss is given by Darcy-Weisbach's equation and is derived in the following way.

If the pressure difference causing flow of fluid is Δp (Pa) across a cross-sectional area of A (m^2), the pressure force equals Δp A (N). A mean shear-stress, τ ($N m^{-2}$) exerts a drag force on the channel walls of τ Per l (N).

$$\therefore \tau \, Per \, l = \Delta p \, A \qquad (2.4)$$

$$But \quad \Delta p = \rho g h$$

$$\therefore \tau = \frac{A}{Per} \rho g \frac{h}{l} \qquad (2.5)$$

where,

h = head loss (m)

g = acceleration due to gravity (m/s^2)

If the flow is fully turbulent, the shear-stress or drag, exerted on the channel walls is proportional to the energy of the flow expressed as follows:

$$\tau \propto \rho \frac{v^2}{2}$$

$$\tau = f\rho \frac{v^2}{2} \qquad (2.6)$$

where,

f = dimensionless coefficient of friction

$$\therefore f \rho \frac{v^2}{2} = \frac{A}{Per} \rho g \frac{h}{l} \qquad (2.7)$$

Substituting $A = \pi d^2/4$ and $Per = \pi d$ in Equation (2.7), the following equation is derived:

$$Also, \quad \Delta p = 4f \frac{l}{d} \frac{\rho v^2}{2} \qquad (2.9)$$

$$h = 4 f \frac{l}{d} \frac{v^2}{2 g}$$

This can be expressed as a relationship between frictional pressure drop, and flow rate, Q as follows:

$$v = \frac{Q}{A} = \frac{4\,Q}{\pi\,d^2} \qquad (2.10)$$

$$\therefore \quad \Delta p = \frac{32}{\pi^2}\frac{fl}{d^5}\rho\,Q^2 \qquad (2.11)$$

2.2.3 Atkinson's Equation

In order to generalize the applicability of Darcy's equation to airways of non-circular cross-section, the concept of hydraulic diameter was introduced. For straight airways of uniform cross-section, the Darcy's equation can be written as:

$$\Delta p = \frac{4\,f\,l}{\left(\frac{4\,A}{Per}\right)}\,\frac{\rho\,v^2}{2} \qquad (2.12)$$

Further substituting v=Q/A, the following equation is obtained:

$$\Delta p = \frac{f\,l\,Per}{A^3}\,\frac{\rho\,Q^2}{2} \qquad (2.13)$$

Combining two constant terms density, ρ, and coefficient of friction, *f*, the most commonly used constant in mine ventilation practice, Atkinson's friction factor, k (kg m^{-3}) is formed (McPherson, 1987), where $k = \rho f/2$. Thus the basic Equation (2.13) transforms to Atkinson's equation:

$$\Delta p = \frac{k\ l\ Per\ Q^2}{A^3} \tag{2.14}$$

The parameter k, a function of air density, which is often different in one section of a mine from another. In order to normalize the friction factor, k against standard air density, 1.23 kg m^{-3}, Equation (2.14) is given by (McPherson, 1988):

$$\Delta p = \frac{\rho}{1.23} \frac{k\ l\ Per\ Q^2}{A^3} \tag{2.15}$$

Comparing this with the square law ($\Delta p = RQ^2$), the airway resistance, R (N s^2 m^{-8}) becomes:

$$R = \frac{k\ l\ Per}{A^3} \tag{2.16}$$

2.3 Relationship Between the Coefficient of Friction and Roughness Geometry

The skin friction factor can be significantly higher for turbulent flow over a rough surface than for an equivalent flow over a smooth surface. In turbulent flow analysis, the use of time- averaged equations leads to the necessity of formulating models with empirically obtained input parameters. In airflows with high Reynolds numbers, it was observed by many scientists (Nikuradse, Moody, etc.) that the resistance is more dependent on the airway geometry than the flow parameters. A similar situation exists in the analysis of flow over rough surfaces. Unless the equations can be solved on a grid which is fine enough to resolve

the flow over a rough surface, a roughness model with empirical input is necessary.

There are two general approaches which have been used in formulating the required roughness models - the classic sand grain approach and the discrete element approach. These are presented in detail in the next section. The goal of these approaches is to predict the value of friction factor for any given airway without actually measuring the flow parameters.

2.3.1 Sand Grain Roughness

Johan Nikuradse (1933) conducted a series of classical experiments on a number of smooth pipes of varying diameter, coated the inside of walls uniformly with grains of graded sand. The roughness of each tube was then defined as e/d ratio, where e is the diameter of sand grains and d is diameter of the tube.

From Nikuradse's investigation into the flow and analysis, it was found that the formation and maintenance of small, interacting and propagating eddies within the fluid stream, are responsible for giving very high resistance to flow in the developed turbulent regime. These small eddies in the flow necessitate the existence of cross velocities with vector components perpendicular to the longitudinal axis of the tube. There can be no cross velocities at the wall except on a molecular scale. Hence, it was understood that there must be a thin layer close to the wall over which the velocity increases from zero to some finite quantity sufficiently far away from the wall for an eddy to exist. This means that the streamline layers remain parallel to each other and to the wall, i.e. laminar flow.

Although this laminar sublayer is very thin, it has a marked effect on the behavior of the total flow in a pipe. All real surfaces (even polished ones) have some degree of roughness. If the peaks of roughenings, or asperities, do not protrude through the laminar sublayer then

the surface may be described as 'hydraulically smooth' and the wall resistance is limited to that caused by viscous shear within that fluid. On the other hand, if the asperities protrude well beyond the laminar sublayer, then the disturbance produced by the flow will cause additional eddies to be formed. Thus, consuming energy which results in a higher resistance to flow. Furthermore, as the velocity (Reynolds number) increases, the thickness of the laminar sublayer decreases. Any given pipe is then hydraulically smooth if the asperities are submerged within the laminar sublayer and hydraulically rough if the asperities project beyond the laminar sublayer. Between these two conditions there will be a transition where some, but not all, of the asperities protrude through the laminar sublayer.

Nikuradse's work marked a significant step towards predicting the coefficient of friction and hence, the resistance of any given pipe through which there is turbulent flow. However, in typical pipes, ducts, or underground airways, the wall asperities are not all of the same size, nor are they uniformly dispersed. In particular, mine airways show great variation in asperity size, shape and distribution.

When fully developed turbulence has been established in a rough pipe, the viscous forces are negligible compared to the inertial forces. The latter are proportional to the shear stress at the walls. Hence, in this state f becomes independent of Reynolds number and varies with e/d ratio. A useful equation for this behavior was suggested by Von Karman (Von Karman, 1939). The equation is:

$$f = \frac{1}{4\left(2\log_{10}(d/e) + 1.14\right)^2} \qquad (2.17)$$

The most general form of f- Re relationship in common use is the Colebrook and

White equation, given by:

$$\frac{1}{\sqrt{f}} = -0.86 \ln\left(\frac{e/d}{3.7} + \frac{2.51}{Re\sqrt{f}}\right) \qquad (2.18)$$

which is the basis for the Moody diagram (Moody, 1944, White, 1982).

Moody (1944) has constructed one of the most convenient charts for determining friction coefficients in commercial pipes.

2.3.2 Discrete Element Approach

The discrete element approach for turbulent flow over rough surfaces has been developed completely from basic principles (Taylor, et al., 1984). In this model formulation, both drag and blockage effects due to surface roughness have been incorporated as constituent parts of partial differential equations for mass momentum conservation. No single-length-scale concepts such as the equivalent sand grain roughness has been taken as the basis for the analysis of the flow characteristics. This roughness model includes the necessary empirical information on the interaction between three-dimensional roughness elements and the flow in a general way. Predictions using the model are compared with additional data for fully developed and boundary layer flows. They are found to compare equally well with both transitional and fully developed turbulent flows without modification of the roughness model.

In the discrete element method, the three-dimensional shapes of the roughness elements were taken into account. However, to simplify the mathematics, the element cross-section has been approximated as circular, i.e. the shape of a cone as shown in Figure 2.2 (Taylor, et al., 1984). The physical effects of roughness on the flow field were modelled by

considering the blockage effect of the roughness elements exerted on the fluid. In the following development, attention is restricted to roughness elements of uniform shape and spacing.

The model formulation is based on differential equations derived from mass and momentum conservation, which includes the roughness effects. In a control volume (CV) as shown in Figure 2.2, δx, an exaggerated length, is taken in the primary flow direction, as an aid to formulate the roughness effects correctly in the model. The CV includes all the fluid in the volume. As shown in Figure 2.2, roughness elements penetrate the CV.

The two dimensional, time-averaged turbulent boundary layer equations are taken as the foundation for the model. These equations are applied in the flow region below the crests of the roughness elements. Therefore, the flow variables have been averaged in the transverse (z) direction over an appropriate x distance.

The physical effects of the roughness elements on the flow field are modeled by considering the flow blockage, and by postulating the total force exerted by the elements on the flow, which can be incorporated as a drag force. It can be seen in Figure 2.2, that the area available in the yz-plane (A_x) and the xz-plane (A_y) are decreased by the presence of the roughness elements. In the same manner, shear stresses are acting on reduced area. This blockage effect is included in the model using blockage factors β_x and β_y. The blockage factor is defined as the function of the area open for flow through the yz and xz planes respectively.

The drag force, F_d can be expressed by making use of the definition of the drag coefficient, C_d (White, 1991),

$$C_d = \frac{F_d}{\frac{1}{2} \rho v^2 A_p} \tag{2.19}$$

where,

A_p = projected area of the slice of a roughness element penetrating the control volume (m^2). Thus, the drag force on the CV due to a portion of a single element (δy) penetrating the CV is:

$$F_d = \frac{1}{2} \rho v^2(y) C_d d(y) \delta y \tag{2.20}$$

where,

v(y) = velocity in the x-direction at a height y from xz-plane ($m\ s^{-1}$)

d(y) = local roughness diameter at a height y from xz-plane (m)

δ(y) = control volume dimension (m)

The number of roughness elements per unit area of xz-plane is $1/s_x s_z$, where s_z and s_x are the roughness elements spaced in the z- and x- directions, respectively, as shown in Figure 2.2. Therefore, the magnitude of the drag force acting on that portion (δy) of the roughness elements located within a unit area is given by:

$$\frac{1}{s_x s_z} F_d \tag{2.21}$$

Therefore the drag force on control volume is equal to:

$$F_d = \frac{1}{s_x s_z} \frac{1}{2} \rho v^2(y) C_d d(y) \delta y \tag{2.22}$$

The drag force acting over the whole body of the elements situated within a unit area of the surface is:

$$F_d = \int_0^{\infty} \left(\frac{1}{2} \frac{1}{s_x s_z} \rho \, d \, C_d \, V^2 \right) dy \qquad (2.23)$$

where,

V = time mean value of velocity (m s^{-1})

v = velocity component in the x-direction (m s^{-1})

$$or, \; F_d = \frac{1}{2} \frac{1}{s_x s_z} \int_0^{\infty} \left(\rho \, d \, C_d \, v^2 \right) dy \qquad (2.24)$$

The boundary layer conditions for the discrete element approach for rough wall flows are identical to those for smooth wall flows. This is an advantage over the typical equivalent sand grain roughness approach over the interface e_s (roughness)-based models with finite difference method. The wall location (y=0) is the smooth surface on which the roughness elements occur. An exception to this is the case of spherical or other shaped roughness elements packed a dense array. At y=0, all the velocities are zero, and as $y \rightarrow \infty$ $V \rightarrow V_\infty$ where, V_∞ = free stream velocity (m s^{-1}).

The parameters β_x, β_y, and d(y) are determined solely from the roughness element geometry and require no empirical input. For uniform arrays, the cross-sectional diameter, d(y), is the same for all the elements at a given y-location. Determination of d(y) is then a matter of considering the geometry of a single element. β_y is defined from Figure 2.2 as:

$$\beta_y = 1 - \frac{\pi d^2}{4 s_x s_z} \qquad (2.25)$$

where,

d = local roughness diameter (m)

On initial inspection of Figure 2.2, β_x is $(1 - d/s_x)$. However, this is the maximum blockage. A better formulation is obtained by taking an average of the yz-plane blockage over a length corresponding to a multiple of the average x-direction roughness spacing. This average gives:

$$\beta_x = 1 - \frac{\pi d^2}{4 s_x s_z} \qquad (2.26)$$

It is seen that $\beta_x = \beta_y$, which holds for an array of elements with a circular cross-section.

The velocity gradient prevailing within the roughness elements on the wall is given by $\partial V/\partial y$. Hence, the shear stress acting on the wall is $\mu\, \partial V/\partial y$, where μ is the absolute viscosity of the fluid (N s m^{-2}).

Since the β_y fraction of each unit area of the wall is covered by roughness elements, the effective shear stress exerted on these elements due to fluid flow is given by:

$$\beta_y\, \mu\, \frac{\partial V}{\partial y} \qquad (2.27)$$

The wall shear stress is defined as the sum of the shear and drag forces on the wall in the mean flow direction divided by the plane area of the wall. The corresponding coefficient

of friction is then:

$$f = \frac{\left(\beta_y \mu \frac{\partial V}{\partial y} \right)_w + \frac{1}{2} \frac{1}{s_x s_z} \int_0^{\infty} (\rho \, dC_d V^2) dy}{\frac{1}{2} \rho_\infty V_\infty^2} \qquad (2.28)$$

where,

$$\left(\beta_y \mu \frac{\partial V}{\partial y} \right)_w = \textit{the shear stress component} (N \ m^{-2})$$

$$\frac{1}{2} \left(\frac{1}{s_x s_y} \right) \int_0^{\infty} (\rho \, dC_d V^2) dy = \textit{drag components acting on the wall roughness elements} (N \ m^{-2})$$

$$\frac{1}{2} \rho_\infty V_\infty^2 = \textit{total force carried by the fluid}$$

The approach is a theoretical method for defining the coefficient of friction in fundamental fluid mechanics and explains the concept of friction in fluid flows. It is not applied in the present study. This approach is relatively new and is helpful in understanding the concept of friction offered by a rough surface.

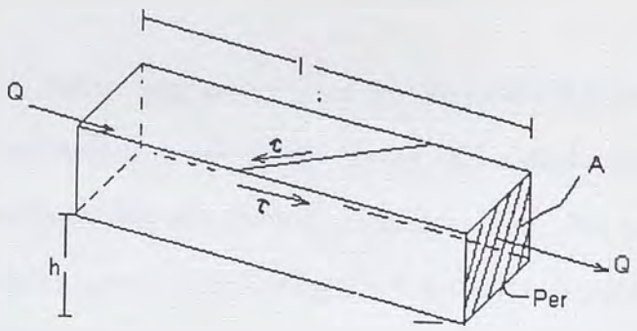

Figure 2.1. Open Channel flow of fluid

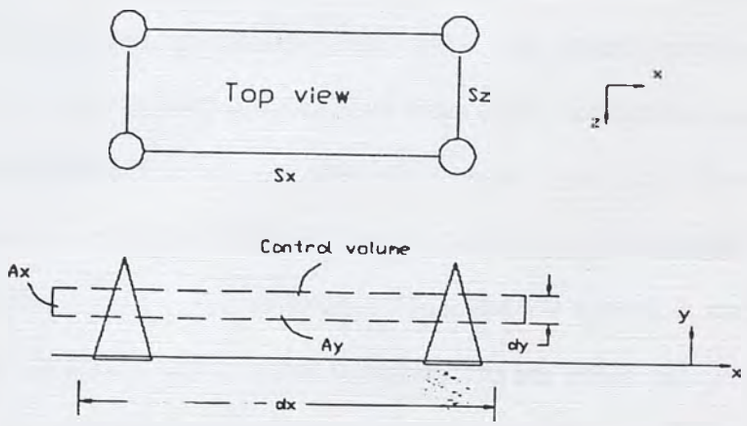

Figure 2.2. Control Volume for Fluid Flow Over a Uniformly Rough Surface

3. FRACTALS

3.1 History

The concept of fractals has been around since the late 1800's. It began with German mathematicians such as Karl Weistrauss and George Cantor, Italian mathematician Giuseppe Peano, and Swedish mathematician Von Koch (La Brecque, 1986). The term fractal was proposed by the french mathematician Benoit Mandelbrot in 1967, to describe this concept. At first, fractals were considered to be mathematical oddities, ie., functions which had no derivatives. It was not until the 1950's that Lewis Richardson discovered an interesting relationship, by measuring a coast line by using a ruler of length, L. This was accomplished by counting the number of times, N, the ruler had to be laid end to end to measure the length of the coastline. It was found that the total length of a coast line, N(L) is proportional to the ruler length, L, raised to a power, or $N(L) = L^{-a}$. The exponent, -a was found to be a characteristic of the coast line measured (Richardson, 1961). An important property of fractals is that of self-similarity. A surface or shape is said to be self-similar when large scale features resemble small scale features. Mandelbrot (1967) states that, typically coastlines are self-similar and fractal. It was determined that the absolute value of the slope of the logarithm of ruler length versus the logarithm of the number of counts is equal to the fractal dimension, D. There are two methods to calculate the fractal dimension of an area or a volume: one is a deterministic method also known as the compass method, and the other is a stochastic method. The latter method of calculating the fractal dimension can use either variography or spectral analysis. Benzer, Jr. (1989), found that the difference between these two methods of calculation is that the deterministic method reflects the shape, while the other depends on statistical properties.

3.2 **Fractal Geometry**

The geometry of nature is so central to the various fields of natural science that there is a tendency to take the geometrical aspects for granted (Feder, 1988). Each field tends to develop concepts (morphology, four-dimensional spaces, texture, conformation and dislocations) used intuitively by the scientists in that field. Traditionally, Euclidean lines, circles, spheres and tetrahedra have served as the basis of the intuitive understanding of the geometry of nature. By definition in loose terms - a fractal is a shape made of parts similar to the whole in some way. This definition contains the essential feature that is emphasized in the analysis of rough surfaces in mine airways. At this point, it is worthwhile to restate that the geometrical characterization of the natural airway roughness, ranging from micro to macro scales, is central to the models that are made in order to understand the interaction between surface roughness and air flow. The following table summarizes some of the major differences between fractals and traditional euclidean shapes.

Table 3.1 Comparison Between Fractal and Euclidean Geometry.

EUCLIDEAN	FRACTAL
Traditional (>200 years)	Modern (≈ 20 years)
Based on characteristic	No specific size or scaling
Suits man-made objects	Appropriate for natural objects
Described by formula	Algorithm (Recursive)

3.2.1 Self-similarity and Fractal Dimension

The property of self-similarity or scaling, is one of the central concepts of fractal geometry. It is connected to the notion of dimension as illustrated in Figure 3.1.

An object normally considered as one-dimensional, a line segment, for example, also possesses a scaling property (Figure 3.1(a)). It can be divided into N identical parts each of which is scaled down by the ratio r = 1/N from the whole. Similarly, a two dimensional object, such as a square area in the plane, can be divided into N self-similar parts each of which is scaled down by a factor $r = 1/\sqrt{N}$ (Figure 3.1(b)). A three-dimensional object like a solid cube may be divided into N smaller cubes each of which is scaled by ratio $r = 1/\sqrt[3]{N}$ (Figure 3.1(c)). With self-similarity, the generalization of fractal dimension is straight forward. A D-dimensional object can be divided into N smaller copies of itself, each of which is scaled down by a factor r where $r = 1/\sqrt[D]{N}$ or:

$$N = \frac{1}{r^D} \tag{3.1}$$

Conversely, given a self-similar object of N parts scaled by ratio r from the whole, it's fractal or similarity dimension is given by:

$$D = \frac{\log (N)}{\log\left(\frac{1}{r}\right)} \tag{3.2}$$

The fractal dimension, unlike the more familiar Euclidean dimension, need not be an integer. A segment of von Koch's curve shown in Figure 3.2 (a), is composed of four sub-segments, each of which is scaled down by a factor 1/3 from it's parent. It's fractal dimension

is F = log(4)/log(3) or about 1.26. This non-integer dimension, greater than one but less than two, reflects the unusual properties of the curve. Any curve fills more of space than a simple line (D = 1), but less than two, ie., a Euclidean area of the plane (D = 2). Mandelbrot gives many variations of the Koch construction and this is presented in Figure 3.3 (Feder, 88). In the Figure 3.2 (b), a segment is replaced by 8 new segments, each 1/4 of the initial line segment length, to yield:

$$D = \frac{\log (8)}{\log (4)} = 1.5$$

In the Figure 3.2 (c), each segment is replaced by 9 new segments with a scaling ratio 1/3 of the original, therefore:

$$D = \frac{\log (9)}{\log (3)} = 2$$

As D increases from 1 to 2, the resulting 'curves' progress from being 'line-like' to filling much of the plane. Indeed, the limit D → 2 gives a Peano or space-filling curve, as shown in figure 3.4. The fractal dimension, D, thus provides a quantitative measure of jaggedness of the curves.

3.2.2 Mathematical Model of Fractional Brownian Motion

One of the most useful mathematical models for the random fractals found in nature (mountain terrains etc.) has been the fractional Brownian motion (fBm) of Mandelbrot and Von Ness. It is an extension of the central concept of Brownian motion that has played an important role in both physics and mathematics.

As can be seen from the sample traces of fBm in Figure 3.5, a fractional Brownian

motion, $V_H(t)$, is a single valued function of one variable, t (usually time, but in this study it stands for asperity height). In appearance, it is reminiscent of the rough surfaces shown. The scaling behavior of the different traces in Figure 3.5 is characterized by the parameter H in the range $0 < H < 1$. When H is close to 0, the traces are roughest while those with H close to 1 are relatively smooth. H relates the typical change in V, $\Delta V = V(t_2) - V(t_1)$ to the time difference $\Delta t = t_2 - t_1$ by the simple law:

$$\Delta V \propto \Delta t^H \tag{3.3}$$

In the usual Brownian or random walk, the sum of independent increments or steps leads to a variation that scales as the square root of the number of steps. Thus H = 0.5 corresponds to a trace of Brownian motion.

3.2.2.1 Self-affinity

The scaling property of fBm represented by equations (10 and 11) (in the next section) is different from the statistical self-similarity of the coastline shown in Figure 3.6. Whereas the self-similar shapes repeat (statistically or exactly) under a magnification, the fBm traces of the curve in Figure 3.3 repeat statistically only when the t and V directions are magnified by different amounts. If t is magnified by a factor r (ie., t= rt), then V must be magnified by a factor r^H (ie., V becomes $r^H V$).

In a random walk over a hilly terrain, when a person takes four times as many steps to go twice as far, the concept of non-uniform scaling is essential . In this scaling scheme, shapes are (statistically) invariant under transformations that scale different coordinates by different amounts. This property is known as self-affinity (Kaye, 1989).

As shown in Figure 3.1, the concept of fractal dimension is strongly established on the self-similar scaling. The extension to self-similar scaling is most important for describing natural objects. It is carried out on the basis of concepts of zerosets and the calculus of fractal dimension (Mandelbrot & Von Ness, 1968).

3.2.2.2 Zerosets

Fractals, like traditional Euclidean shapes, typically reduce their dimensions by one, when intersected by a plane. Thus, the intersection of a solid 3-D sphere with a plane is a 2-D circular area. The intersection of this area with another plane is a 1-D line segment and the intersection with yet another plane is a 0-D point. Similarly, the intersection of a fractal curve in the plane (with fractal dimension $1 < D < 2$) with a straight line is a set of points of dimension (D - 1). By choosing the direction of the intersecting line to eliminate one of the coordinates, it is possible to reduce a self-similar curve to a set of points. The zeroset of fBm is the intersection of the trace of $V_H(t)$ with the t-axis: the set of all points such as at $V_H(t)=0$. The zeroset is a disconnected set of points with topological dimension $D_0 = 1 - H$, that has a value less than 1, but greater than 0. Although the trace of $V_H(t)$ is self-affine, its zeroset is self-similar and different estimates of D_0 yield the same answer. The fractal dimension, $D = D_0 + 1$, of a self-similar fBm is related to the scaling parameter H as $D = 2 - H$.

3.3 **Measurement of Fractal Dimension**

3.3.1 Fractional Brownian Motion: Approximation by Spatial Methods

As described before, fractional Brownian motion is considered to be a phenomenon specified by a random Gaussian distribution. If the process has to be computed for times t,

between 0 and 1, then it starts by setting X(0) = 0, and selecting X(1) as a sample of a Gaussian random variable with a mean 0 and variance σ^2. Then:

$$var\ (X(1) - X(0)) = \sigma^2 \tag{3.4}$$

Therefore:

$$var\ (X(t_2 - X(t_1)) = \sigma^2 \mid t_2 - t_1 \mid \qquad for\ 0 < t_1 < t_2 < 1 \tag{3.5}$$

This can be further written as:

$$var\ (X(t_2) - X(t_1)) = \sigma^2 \mid t_2 - t_1 \mid^{2H} \tag{3.6}$$

where H = 1/2. The generalization to the parameter 0 < H < 1 is called fractional Brownian motion (fBm) (Mandelbrot, 1983). In the case of ordinary Brownian motion, the increments of X are statistically self-similar with parameter H. In other words the following terms,

$$[\ X(t_0 + t) - X(t_0)\ ] \quad and \quad \frac{1}{r^H}[\ X(t_0 + rt) - X(t_0)\ ]$$

have the same finite distribution function for t_0 with any r > 0.

For convenience, consider $t_0 = 0$ and $X(t_0) = 0$, then the two random functions X(t) and $X(rt)/r^H$ are statistically identical. Thus, fractional Brownian motion X(rt) can be properly rescaled by dividing the amplitudes by r^H.

Fractional Brownian motion can be divided into three quite distinct categories:

Category 1: H < 1/2

Category 2: H = 1/2

Category 3: H > 1/2

The case H = 1/2 is ordinary Brownian motion which has independent increments, ie., $X(t_2) - X(t_1)$ and $X(t_3) - X(t_2)$ with $t_1 < t_2 < t_3$ are independent in the sense of probability theory, and their correlation is 0. For H > 1/2, there is a positive correlation between these increments, ie. the group of X is increasing for some t_0, then it tends to continue for $t > t_0$. This means, if X increases for the period t, then it is expected to continue to decrease for a similar period. For H < 1/2 the opposite is true. There is a negative correlation of increments, and the curves seem to oscillate more erratically. This shown in Figure 3.5, where plots of altitude (compared to $V_H(t)$) versus x-position are drawn.

Equation (3.6) can formally be extended to suit approximately parameter $H \neq 1/2$ for fBm. The aim is to describe the fractional Brownian motion in a similar manner to Equation (3.3).

3.4 **Fractional Brownian motion: Approximation by Spectral Analysis**

The spectral analysis method is also known as the Fourier transform of X(t). Since the Fourier transform of X(t) is generally undefined, X(t) is first restricted to a finite interval $0 < t < T$:

$$X(t,T) = X(t) \quad for\ 0 < t < T$$
$$= 0 \qquad\quad otherwise \tag{3.7}$$

thus, the Fourier transform of X(t,T):

$$FT(f,T) = \int_0^T X(t)\, e^{-2\pi i t f}\, dt \qquad (3.8)$$

Now $|FT(f,T)^2|df$ is the contribution of the total energy of X(t,T) from those components with frequencies between f and f+df. The average power of X contained in the interval [0,T] is then given by:

$$\frac{1}{T} \int_{-\infty}^{\infty} |FT(f,T)|^2\, dt$$

and the power spectral density of X(t,T) is:

$$S(f,T) = \frac{1}{T} |FT(f,T)|^2 \qquad (3.9)$$

The spectral density of X is then obtained in the limit as $T \to \infty$:

$$S(f) = \lim_{T \to \infty} \frac{1}{T} |FT(f,T)|^2 \qquad (3.10)$$

The interpretation of S(f) is the following: S(f) df is the average of the contribution to the total power from the components in X(t) with frequencies between f and f + df. S(f) is a non-negative and even function. X(t) is considered as being decomposed into a set with an infinite number of Sine and Cosine terms of frequencies f, whose powers and amplitudes are determined by the spectral density S(f).

At this point, the fundamental property of fBm is: If X(t) denotes fBm with component $0 < H < 1$ then the rescaled random function is:

$$Y(t) = \frac{1}{r^H} X(rt) \tag{3.11}$$

and when r > 0, Equation (3.11) has the same statistical property as X(t). Thus, it also has the same density. From this basic observation, it is possible to determine the fractal dimension as follows.

Consider a case where r > 0,

$$Y(t,T) = Y(t) = \frac{1}{r^H} X(rt) \text{ , } if \quad 0 < t < T \tag{3.12}$$

$$= 0, \qquad otherwise \tag{3.13}$$

and adopt the notation that $FT_x(f,T)$ and $FT_y(f,T)$ are the Fourier transforms of X(t,T) and Y(t,T), and, $S_x(f,T)$ and $S_y(f,T)$ are the spectral densities of X(t,T), Y(t,T).

Computing the Fourier transform of Y(t) using its definition expressed by equation:

$$FT_y(f,T) = \int_0^T Y(t)\, e^{-2\pi i f} dt \tag{3.14}$$

and applying Equation (3.11) yields:

$$FT_y\,(f,T) = \frac{1}{r^H} \int_0^T X(r,t)\, e^{-2\pi i f} dt \tag{3.15}$$

after substituting s for rt or s/r for t, hence, ds/r for dt in the second integral.

Thus:

$$FT_y(f,T) = \frac{1}{r^H}\int_0^T X(s)\, e^{-2\pi i \frac{s}{r} f}\frac{ds}{r} \tag{3.16}$$

Therefore:

$$FT_y = \frac{1}{r^{H+1}}\int_0^T X(s)\, e^{-2\pi i s \frac{f}{r}} ds \tag{3.17}$$

Again from the definition of the Fourier transform given by Equation (3.8), and the left hand side of the equation (3.12), the integral can be expressed as:

$$FT_x\left(\frac{f}{r}, rT\right) = \int_0^T X(s)\, e^{-2\pi i s \frac{f}{r}} ds \tag{3.18}$$

Hence, Equation (3.15) becomes:

$$FT_y = \frac{1}{r^{H+1}} FT_x\left(\frac{f}{r}, rT\right) \tag{3.19}$$

It follows for the spectral density of Y(t,T) that:

$$S_y(f,T) = \frac{1}{r^{2H+1}}\frac{1}{rT}\left| FT_x\left(\frac{f}{r}, rT\right)\right|^2 \tag{3.20}$$

and in the limit as $T \rightarrow \infty$:

$$S_y(f,T) = \frac{1}{r^{2H+1}} S_x\left(\frac{f}{r}\right) \tag{3.21}$$

Since Y is just a rescaled version of X, their spectral densities must coincide, thus:

$$S_x(f,T) = \frac{1}{r^{2H+1}} S_x\left(\frac{f}{r}\right) \tag{3.22}$$

This shows that the characteristic dimension of the spectral function X(t,T) is 2H+1 as opposed to H for the fBm.

3.5 **Surface Roughness Characterization by Fractal Dimension**

Rough surfaces can be characterized by the fractal dimension. This was introduced in Chapter 1. One of the two methods of determining fractal dimension was discussed in the previous section. In this section, determination of the fractal dimension by semi-variography and spectral analysis is discussed. Most mine airways can be better characterized by this dimension along their length rather than their widths, because mine airway roughness is measured from their longitudinal profiles and hence are useful analysis. The rationale behind this particular way of characterization is that the major variations (macro-asperity distribution) in the asperity pattern, exist longitudinally in most mine airways.

The vertical section of a surface can be obtained from any profiler, eg. tunnel profiler (used in mine airways, tunnels, etc.), profilometer (used in laboratory experiments). The surface profile can be analyzed by the fractional Brownian motion approach.

3.5.1 Semi-variogram Technique

With the known surface coordinates, spectral analysis is used for the characterization of the roughness using variograms.

Consider Brown noise. Let y(x) represent the function at 'x'. Let the increment in the function be $y(x_2) - y(x_1)$.

This has a Gaussian distribution, and

$$E\ [(y(x_2) - y(x_1))^2\ ] \propto |x_2 - x_1| \qquad \textbf{(3.23)}$$

A relationship given by Saupe (1987), is as follows:

$$P(f) \propto \frac{1}{f^{\beta}} \qquad \textbf{(3.24)}$$

where, P(f) is a function of f, and ß is the slope which is a constant.

Let ß=2H, then, applying Equation (3.23) results in:

$$E\ [(y(x_2) - y(x_1))^2] \propto (x_2 - x_1)^{2H} \qquad \textbf{(3.25)}$$

Letting $x_2 - x_1 = h_{ij}$, yields:

$$E\ [(y(X_2) - y(X_1))^2] \propto |h_{ij}|^{2H} \qquad \textbf{(3.26)}$$

but, the semi-variogram is defined as:

$$\gamma(h_{ij}) = 1/2\ E\ [((y(x_2) - y(x_1))^2] \qquad \textbf{(3.27)}$$

$$\therefore \quad \gamma(h_{ij}) \propto |h_{ij}|^{2H} \tag{3.28}$$

The slope of the graph Log($\gamma(h_{ij})$) vs. Log(h_{ij}) is 2H.

By comparing this with Brown noise, the relationship that can be obtained is D = 2-Abs(H) (Carr, et al.,1991), where D is the fractal dimension of the profile.

3.5.2 Power Series Technique

This method resolves the stochastic nature of any object, function or process using a power spectrum. Given a function c, the discrete fast Fourier transform C (Press, et al., 1989) is given by:

$$C_K = \sum_{j=0}^{N-1} c_j e^{-2\pi \frac{ijk}{N}}, \; k=0,\; 1,\ldots,\; N-1 \tag{3.29}$$

where N is the sample size, and i and j are the successive samples.

Then the estimate of the power spectrum is defined at N/2 + 1 frequencies as:

$$P(0) = P(f_0) = \frac{1}{N^2}|C_0|^2 \tag{3.30}$$

$$P(f_k) = \frac{1}{N^2}[|C_k|^2 + |C_{N-k}|^2],\; k=1,2,\ldots,(\frac{N}{2}-1) \tag{3.31}$$

$$P(f_c) = P(f_{N/2}) = 1/N^2|C_{N/2}|^2 \tag{3.32}$$

$$f_k = \frac{k}{N\Delta} = 2f_c\frac{k}{N}, \qquad k = 0,1,2,..,\frac{N}{2}$$

where f_k is defined only for the zero and positive frequencies.

Once the power spectrum is calculated, the plot of Log P(f) vs. Log (f) yields a trend. A regression or least square fit is carried out on the curve. Let the slope be ß. When a set of data or a profile is considered, the spectrum is compared to standard White noise and the derived formula for the fractal dimension (Mandelbrot, et al.,1984) is, D = 0.5 (5 - Abs(ß)).

Profiles of natural rock surfaces have spectra with slopes between -2 and -3 corresponding to surface fractal dimensions of 1.5 to 1.0, respectively (Brown, 1987).

Both methods for determining the fractal dimension (variography and power spectrum) are mathematically similar and theoretically give the same results. This can be explained from the relationship given by Saupe (1987) ie., ß = 2H + 1.

In practice, the accuracy of this relationship depends on the window size. The term window size refers to the number of samples used in a calculation and represents the relationship between the spectral estimate P_k at a certain frequency and the actual underlying continuous spectrum P(f) at nearby frequencies. This parameter can be chosen only as a function of powers of 2 due to the limitations in application of fourier transforms. In practice, the window size plays a crucial role (Carr, et al.,1991) in the determination of D, which will vary with different sizes. The optimization of the window size is very important as a compromise between computation time and precision. A large window size provides similar results using either spectral analysis or variography.

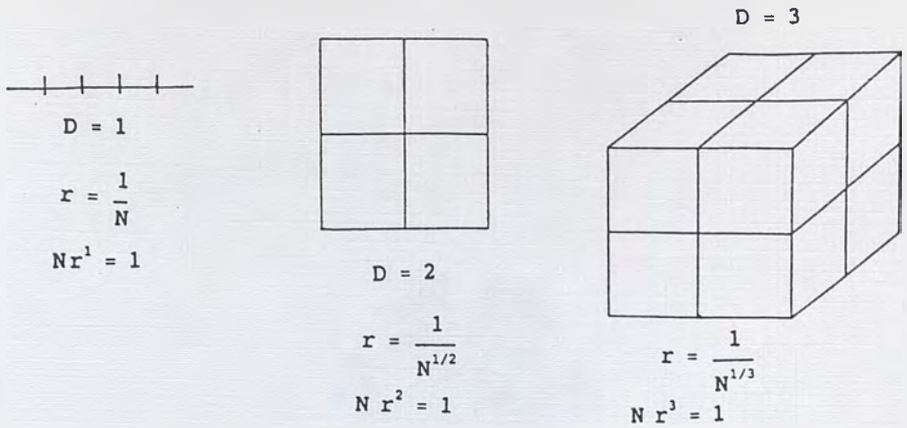

(a) (b) (c)

Figure 3.1. Standard integer dimension figures in terms of self-similarity

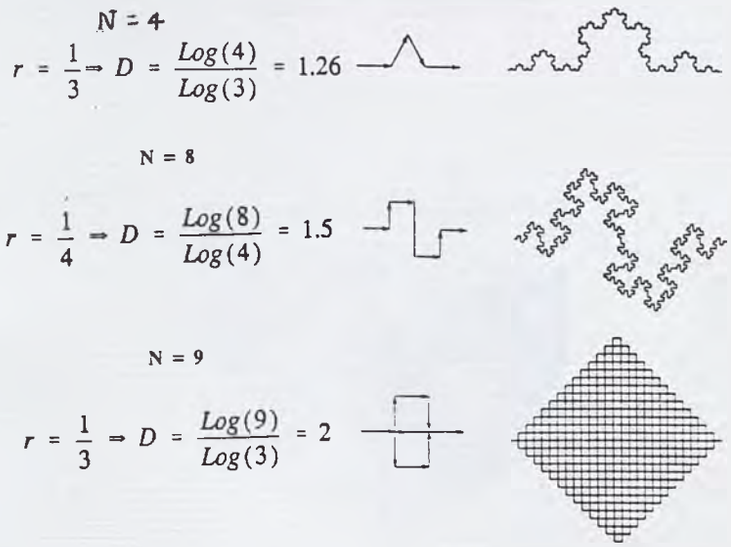

Figure 3.2. Recursive Replacement Procedure for Governing the Von Koch Curve and Variations with Different Fractal Dimensions

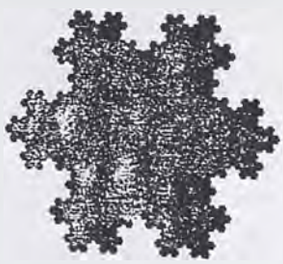

Figure 3.3. Von Koch's Triadic Island: A Variation of Von Koch Construction as Presented in Figure 3.2.

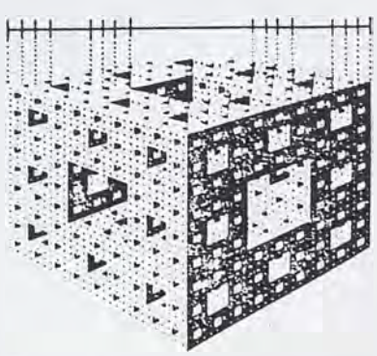

Figure 3.4. A Space filling Sierpinsky Square Curve. (5th Stage).

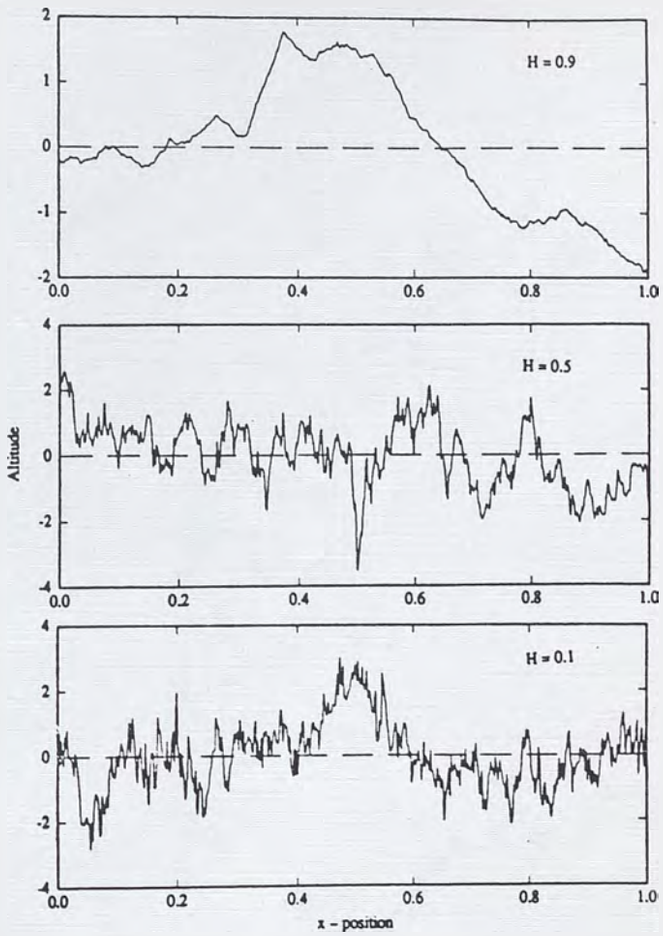

Figure 3.5. Samples of Fractional Brownian Motion Traces (altitude) vs. position for Different H and D (source: Feder, 1988).

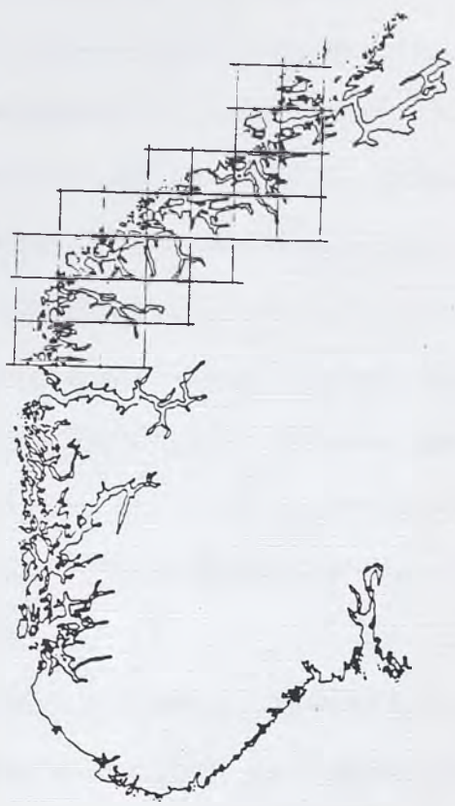

Figure 3.6. The Southern coast of Norway, digitized at 1800 x 1200 pixels. The Grid indicated has a k spacing (source: Feder, 1988).

4. SURFACE ROUGHNESS CHARACTERIZATION FOR AN AIRWAY IN THE SUNSHINE MINE

4.1 Introduction

The flow of air through a bare rock, underground airway is affected by the size and frequency of the micro- and macro-asperities of the rough surface. The focus of this part of the study is to characterize this roughness using the coefficient of friction, the friction factor and the fractal dimension. The rough surfaces were identified by two sets of 177 and 78 transverse profiles measured by a laser profiler along two lengths of an underground airway at the Sunshine Mine, Idaho. Based on the measurements, the friction factor was estimated from Atkinson's equation, the coefficient of friction from the Moody diagram, and the fractal dimension was computed for the airway surface using power series and variography. Significant conclusions are reached relating the effect of error in the measurement of cross-sectional area and perimeter of an underground airway, on the estimated friction factor. The potential role of the fractal dimension as an alternative to the friction factor for characterizing the roughness of a mine airway is discussed.

The roughness of the surface of an airway is described in different ways in the field of fluid dynamics. It is important to characterize the roughness of a surface in order to estimate the energy losses in the flow. The friction factor (k) and coefficient of friction (f) are two parameters frequently used in the field of mine ventilation. The friction factor is calculated from Atkinson's equation, and a standard way of estimating a value for an underground airway is to use McElroy's table (McElroy, 1935). The coefficient of friction is another parameter which can be used to describe the surface roughness of a mine airway. The Moody

diagram which is a function of the ratio of surface asperity to mean hydraulic diameter and the Reynolds number, is used to obtain this parameter.

Recently, the fractal dimension has been proposed to characterize surfaces of rocks and joints. For example, it is being used in the geological sciences for rockmass classification (Carr, 1990), characterization of the joint roughness (Carr & Benzer, 1991), and study of fluid flow through rock joints (Brown, 1987a).

In this paper, a section of a mine ventilation airway at the Sunshine Mine, Idaho, is studied for the determination of the surface roughness parameters and fractal dimension, and a relationship between pressure loss, friction factor and fractal dimension is discussed.

4.2 **Rough Surface Data and Measurements**

A set of data describing the surface of an underground airway was obtained using an Amberg Measuring Technique (AMT) 2000 tunnel laser profiler (Calizaya, et al.,1991). An illustration explaining the construction of the profiler is shown in Figure 4.1 The survey was performed in a fan drift located on the 3100 level at the Sunshine Mine, Idaho. The layout of the fan drift and the location of the test sections are shown in Figure 4.2. Two sections of this drift, 35.2 and 15.4 meters in length, were laser surveyed to obtain 177 and 78 transverse profiles respectively. A pressure and quantity survey was carried out in the former section and this was used for the calculation of k.

The tunnel profiler, was used to map the airway surface in the test sections. Each point on the transverse profile is represented by two parameters: a vertical angle and a radial distance. The profiles were taken every 20 centimeters over the test lengths in the airway. A schematic of the installation of the profiler and the angular positions of the longitudinal pro-

files are shown in Figures 4.3 and 4.4 respectively. For comparison purposes, the cross section was measured manually at approximately 5 meter intervals in both the test sections. Figures 4.5 and 4.6 show the isometric view of Sections I and II respectively. F1 to F8 are the positions where manual measurements were made in Section I. Manual measurements are numbered C1 to C4 for the 15.4-meter test section. Tables 4.1 and 4.2 compare the cross section-areas and perimeters measured manually and by the laser profiler. The percentage differences are calculated with respect to the laser measurements. Figure 4.7 shows a typical method of estimating the cross-sectional area and perimeter of an airway. In practice, it is customary to average a few measurements and take the calculated area and perimeter as a representative value of the airway. It can be seen from Tables 4.1 and 4.2, that the manual method of measurement over-estimates an irregular profile's area and perimeter. Appendix A lists the cross-sectional area and perimeter of each transverse profile measured by the AMT 2000 laser profiler for both the sections.

Longitudinal profiles from -30^0 to 210^0 to the horizontal were plotted for each test section from the laser profiler data. These are shown in Figures 4.8 and 4.9 for the two test sections. These longitudinal profiles are used to compute the coefficient of friction and the fractal numbers. The data describing the longitudinal profiles are listed in Appendix B.

4.3 **Friction Factor and Coefficient of Friction**

An important objective of this research is to compare the estimated airway values of k and f obtained when area and perimeter are measured using either conventional (hand taping) or laser techniques.

The friction factor, or Atkinson's k factor, is an empirical factor used to predict

pressure drops in mine airways. Atkinson's equation is used to calculate this factor. As discussed in Chapter 2, the relationship between Darcy's coefficient of friction and Atkinson's friction factor is given by:

$$f = \frac{2k}{\rho} \tag{4.1}$$

where, ρ is the local air density (kg/m^3).

For standard air conditions (ρ = 1.2 kg/m^3) this equation yields f = 1.667 k.

Alternatively, f can be determined from the Moody diagram based on two parameters: the surface roughness, characterized by the asperity height to hydraulic diameter ratio, and the Reynolds number. Both f and k were calculated using the following airway conditions in the test section I:

Pressure drop, [Δp] = 11.45 Pa

Quantity of air, [Q] = 27.4 m^3/s.

Airway length, [l] = 35.2 m

4.3.1 Friction Factor

Based on Atkinson's equation, this factor is given by:

$$k = \frac{\Delta p\, A^3}{Q^2 Per\, l} \frac{\rho}{\rho_{std}} \tag{4.2}$$

The elevation of the drift (3100 level) is slightly below sea level, hence the term ρ/ρ_{std} reduces to unity. Using the average area (A) and perimeter (Per) from the 177 transverse laser profiles, namely 6.614 m^2 and 9.955 m, this equation yields k = 0.0126 kg/m^3.

The best estimate of the actual rubbing surface area ('Per .*l*' in Equation 4.2) can be obtained from the laser profiler data. This was determined using the SURFER computer software package. The input for the software is the x,y & z coordinates of the surface in ASCII format. Once the xyz coordinates are input, a surface model is formulated. Using surface interpolation, an (inverse distance squared weighing was used), coordinates are calculated at the grid intersections and using a contouring technique the surface area is computed. The surface contour plots of both the airway sections are shown in Figures 4.10 and 4.11. For the 35.2 m length of the drift, the rubbing surface area was computed to be equal to 396.72 m^2. Considering this a true Per.*l*, the best estimate of the perimeter is equal to 11.27 m which yields a *k* factor equal to 0.0111 kg/m^3 when an average drift cross-sectional area of 6.614 m^2 is used. This is 11.9% less than the *k* factor calculated from the average of the 177 profiles. Table 4.3 shows the table of rubbing surface areas computed from the 3-D mapping of the airway surfaces of the two test sections and by conventional estimates of surface area.

The k value of 0.0111 kg/m^3 is compared in Table 4.4 with the estimated friction factors obtained using each of the eight manual-measurements as representative of the average airway dimensions. It is typical in normal ventilation practice to take only one manual-measurement in such a short length of airway. It can be seen that if any of the eight *k* values, based on the manual measurements, are used to estimate the *k* value for the airway, a considerable error would occur, typically overestimating the *k* value.

4.3.2 Coefficient of Friction

In this case, the coefficient of friction, *f*, was determined based on the following

parameters: mean asperity height to hydraulic diameter ratio and Reynolds number. The longitudinal profiles produced from laser data were used to determine the asperity height. The asperity heights of each longitudinal profile from the base-line of the laser profiler is listed in Appendix B. The average asperity height of a test section, e, was determined by normalizing to the minimum value and averaging the asperity heights of the nine longitudinal profiles. For example, the profile which is inclined 150^0 to the positive x-axis from Section I, has a minimum asperity height of 0.733 meters, and this was subtracted from all the values in order to obtain the real or reduced asperity heights. The mean of these values gives the mean asperity height of a profile. For this profile the mean value is 0.2216 meters.

Table 4.1. Comparison of Area and Perimeter Using Manual and Laser Profiling Methods for Section I.

Station	Area (m^2)		% Diff.	Perimeter (m)		% Diff.
	Manual	Laser		Manual	Laser	
F1	6.917	6.726	2.84	10.526	10.091	4.31
F2	7.800	7.879	-1.00	11.176	10.669	4.75
F3	7.756	7.480	3.69	11.158	10.408	7.21
F4	6.821	6.812	0.13	10.448	10.131	3.13
F5	6.778	7.084	-4.32	10.426	10.590	-1.55
F6	5.700	5.566	2.41	9.552	9.219	3.61
F7	7.499	7.381	1.60	10.954	10.561	3.72
F8	6.753	6.587	2.52	10.408	10.278	1.27
F_{Ave}*	7.004	6.939	0.94	10.581	10.243	3.30

*Average area and perimeter from 177 profiles are 6.614 m^2 and 9.955 m respectively.

Table 4.2. Comparison of Area and Perimeter Using Manual and Laser Profiling Methods for Section II.

Station	Area (m^2)		% Diff.	Perimeter (m)		% Diff.
	Manual	Laser		Manual	Laser	
C1	6.097	6.588	7.45	9.878	9.714	1.69
C2	6.477	6.299	2.82	10.184	9.677	5.24
C3	5.796	5.397	7.39	9.632	9.064	6.27
C4	6.948	6.973	-0.36	10.544	9.868	6.85
C_{Ave}*	6.328	6.314	0.22	10.060	9.581	5.00

*Average area and perimeter from 78 profiles are 6.252 m^2 and 9.666 m respectively.

Table 4.3. Comparison of the Estimated Rubbing Surface Areas.

Test section	3-D Contouring (m^2)	Laser Profiles (m^2)	Hand Measurements (m^2)
Section I	396.72	350.416	372.45
Section II	189.57	148.86	154.92

Table 4.4. Estimation and Comparison of the Friction Factors using Manual Measurement and Laser Profiling.

Station	k_{manual}	k_{laser}	% Difference
F1	0.0136	0.0111	22.5
F2	0.0184	0.0111	65.8
F3	0.0181	0.0111	63.1
F4	0.0132	0.0111	18.9
F5	0.0129	0.0111	16.2
F6	0.0084	0.0111	-24.3
F7	0.0167	0.0111	50.5
F8	0.0128	0.0111	15.3
F_{ave}	0.0141	0.0111	27.0
Average of 177 profiles	0.0126	0.0111	13.5

The mean asperity height of the nine profiles was taken and averaged to get a representative asperity height of the section. Three quarters of this quantity represents the true asperity height, which was 0.2439. This is because the floor of the drift was assumed to have a linear profile with a zero asperity height. The hydraulic diameter, d, was determined by dividing four times the area by the perimeter.

4.3.2a. Test Section I:

Based on the best estimate of area and perimeter, the average hydraulic diameter was calculated to be 2.348 meters. The e/d ratio from these parameters was found to be 0.1039. The Reynolds number was calculated from the equation Re = 67,280 dv (Hartman, 1982). For v = 4.143 m/sec and d = 2.348 meters, this number was estimated to be 654,500.

For these values, using the Moody Diagram (McPherson, 1993) the coefficient of friction was calculated to be 0.026.

In developed turbulent flow, this coefficient can also be obtained from Von Karman's equation (Equation 2.17):

$$\sqrt{f} = 2.276 - 4 \log_{10} (e/d) \qquad \textbf{(4.3)}$$

which yields a value of 0.0259.

Table 4.5 shows, using the manual measurements, the estimates of the coefficient of friction determined from the Moody diagram or Von Karman's equation (which yield the same values), and compares them with the best estimate of f calculated above.

4.3.2b. Test Section II:

The best estimate of the rubbing surface area for this section was 189.57 m^2, and from this the equivalent perimeter for the 15.4 m length of airway was calculated to be 12.309 m. The mean hydraulic diameter of the airway using an average area of 6.252 m^2 determined from the 78 profiles, is 2.032 m. From the nine longitudinal profiles obtained, the true asperity height was calculated to be 0.1643 m. From this the e/d ratio is equal to 0.0809. The value of f from Von Karman's equation is 0.0226. Table 5.6 shows a comparison of coefficients of

friction calculated from the manual and laser measurements. The error between the estimated *f* value for the airway, obtained from a single manual measurement, and the best estimate of *f*, is considerably less than the obtained error for the *k* values in section I. Instead of the large overestimation of *k*, Tables 5.5 and 5.6 show a small underestimation of the *f* value. It can be seen that the average % difference between the f values is greater in Table 5.6. This might be due to a lower e/d ratio for test section II. The result of lower e/d ratios is from the over estimation of d from the manual measurements. This further demonstrates the inaccuracy of the typical manual method of estimating airways cross-section parameters.

4.4 **Fractal Dimension**

There are two methods to estimate the fractal dimension for any set of data. One of these is based on the measurement process called the divider or compass technique (Mandelbrot,1967). The other is based on stochastic notions, namely: variography and the power spectrum. The fractal dimension, D, can be determined by the formula (Carr & Benzer, 1991):

$$D = 2 - Abs(H) \tag{4.4}$$

where, H is the slope of the regression fit of the logarithm of semi-variogram on the y axis and logarithm of lag distance on the x axis. If β is the slope of the log-log plot of the power series versus frequency of the same data, its relationship with H was given by Saupe (1987):

$$\beta = 2H + 1 \tag{4.5}$$

Table 4.5. Estimation and Comparison of the Coefficients of Friction Using Manual Measurement and Laser Profiling for Section I.

Station	d	e/d	Re	f_{manual}	f_{laser}	% Diff.
F1	2.629	0.0928	732800	0.02437	0.026	-6.1
F2	2.794	0.0873	778800	0.02358	0.026	-9.1
F3	2.780	0.0880	774900	0.02368	0.026	-8.7
F4	2.611	0.0934	727800	0.02445	0.026	-5.8
F5	2.600	0.0938	724700	0.02451	0.026	-5.5
F6	2.387	0.1022	665400	0.02570	0.026	-1.0
F7	2.740	0.0891	763750	0.02384	0.026	-8.1
F8	2.586	0.0943	720800	0.02458	0.026	-5.3
F_{ave}	2.640	0.0921	735900	0.02427	0.026	-6.5
Average of 177 profiles	2.658	0.0918	740900	0.0245	0.026	-5.6

This relationship was derived from the basic fBm and spectral functions. Using the above relationship in Equation (4.4), the following equation can be obtained:

$$D = 2.5 - Abs\left(\frac{\beta}{2}\right) \qquad \textbf{(4.6)}$$

where, ß is the slope of the regression fit of the logarithm of power values on the y axis to

the logarithm of the frequency on the x axis (Mandelbrot, 1984). Both methods for determining the fractal dimension (variography and power spectrum) are mathematically

Table 4.6. Estimation and Comparison of the Coefficients of Friction Using Manual Measurement and Laser Profiling for Section II.

Station	d	e/d	f_{manual}	f_{laser}	% Diff
C1	2.469	0.0666	0.02051	0.0226	- 9.25
C2	2.544	0.0646	0.02020	0.0226	-10.62
C3	2.407	0.0683	0.02077	0.0226	- 8.1
C4	2.636	0.0624	0.01986	0.0226	-12.12
C_{ave}	2.4006	0.0685	0.02080	0.0226	-7.96
Average of 78 profiles	2.517	0.0635	0.0200	0.0226	-11.5

similar and, theoretically, give the same results.

In practice, the accuracy of this relationship depends on the window size. The term window size refers to the number samples used in a calculation and represents the relationship

between the spectral estimate at a certain frequency and the actual underlying continuous spectrum at nearby frequencies. This parameter can be chosen as function of powers of 2. The window size plays a crucial role (Huang, et al., 1992, Carr & Benzer, 1991) in the determination of D, which will vary with different sizes. The optimization of the window size is very important as a compromise between computation time and precision for a given data. Window size is nothing but the number of points describing the surface profile or a function. The larger the window size, the more accurate are the results (Konduri, et al., 1992). This is clearly demonstrated in the Power series section of this chapter.

4.4.1 Section I

4.4.1a. Semi-Variogram:

Table 4.7 shows the estimated fractal numbers for the nine profiles investigated. The experimental semi-variogram shown in Figure 4.12 is for the profile at -30^0 to the horizontal. This method has the added advantage over the power spectrum method to compute D, ie., the semi-variograms allow the trend of the data to be observed. The semi-variogram shown in Figure 4.12 shows a period variation for every 10 lag intervals (2 m). This is up to point A in the figure. From point B in the figure the $\gamma(h)$ value oscillates around a downward tending axis, which is due to a small departure of the baseline of the profiler from the center of the mine drift. However, the semi-variogram needs only to be considered up to its sill value in order to compute D (Huang, et al., 1992, Carr, 1992). Figure 4.13 shows the linear part of the semi-variogram of a profile and Figure 4.14 shows the log-log plot of the same values. The fractal dimensions in this table indicate some uniformity in the variation of the surface profiles along the drift. The last three profiles have significantly lower fractal numbers and

these differences can be observed in the corresponding longitudinal profiles (Figure 4. 8).

4.4.1b. Power Spectrum:

Spectral analysis was carried out on all of the nine profiles using a code written in Fortran called FRACTAL which uses fast fourier transform (Press, et al., 1989). The plot of the logarithm of the spectral numbers (P_f) and frequency (f) for a profile is shown in Figure 4.15. The profiles of the power spectrum showed spikes in the low frequency region corresponding to high power values. These can be interpreted as infrequently occurring large asperities. These were neglected in the slope computations of the spectrum. The influence of these spikes can be considerable, and it was observed that elimination of such points from the power series gave consistent values for the fractal number. In the evaluation, a window of size 128 was used. Results are tabulated in Table 4.7, which show a good comparison to those obtained using the semi-variogram method.

4.4.2 Section II

In this section the nine profiles were analyzed in a similar fashion to obtain the fractal numbers. The results are shown in Table 4.8. From this table, it can be observed that the differences between the fractal dimensions of corresponding profiles are quite high. This is due to two reasons, firstly, the relative variation in the profiles is much higher in Section II than in Section I. Secondly, since there were only 78 profiles measured in this section and a window size of 64 was used in the power series for the analysis, the fractal dimension results are less reliable.

All the semi-variograms and power series plots of the longitudinal profiles of each section

are shown in Appendix C.

Table 4.7. Fractal Dimensions for Different Profiles in Section I.

Angular Position	Semi-Variography		Spectral Analysis	
	2H	D	β	D
-30^0	-0.698	1.651	-1.63	1.685
0^0	-0.822	1.589	-1.49	1.755
30^0	-0.874	1.563	-1.66	1.670
60^0	-0.808	1.596	-1.71	1.645
90^0	-0.572	1.714	-1.50	1.750
120^0	-0.782	1.609	-1.76	1.620
150^0	-1.39	1.305	-2.27	1.365
180^0	-1.04	1.480	-2.18	1.410
210^0	-1.05	1.475	-2.19	1.405

Table 4.8. Fractal Dimensions for Section II.

Angular Position	Semi-Variography		Spectral Analysis	
	2H	D	β	D
-30^0	-0.666	1.667	-1.59	1.705
0^0	-0.702	1.649	-1.53	1.735
30^0	-0.752	1.624	-1.31	1.845
60^0	-0.956	1.522	-2.23	1.385
90^0	-0.808	1.596	-1.79	1.605
120^0	-1.31	1.345	-2.72	1.140
150^0	-0.71	1.645	-1.47	1.765
180^0	-0.526	1.737	-1.01	1.995
210^0	-0.39	1.805	-1.23	1.885

4.5 **Discussion**

It is clear that the laser profiler results give a more accurate measurement of the area and perimeter at a particular cross section in a mine airway, than does the standard manual taping method. The difference does not appear to be that significant when comparing values at the same location (Tables 4.1 & 4.2). However, the ability of the laser profiler to measure many more cross sections accurately, makes it possible to estimate overall measurements of rubbing surface and cross-sectional areas for a length of an airway, which is much more

accurate than that obtained by the typical methods currently in use.

The k value, obtained using all the laser profiles (177 cross sections) to provide the best estimates of actual rubbing surface and cross-sectional areas for the test section, was considerably lower than those determined from manual measurements. The differences ranged from +65% to -24% (Table 4.4), where most of the differences show that the estimated k values from the manual readings were too high.

It is interesting to observe that the difference between the respective values of f is considerably less than that for k and is in the opposite direction i.e. the manual measurements underestimate the f values (compare Tables 4.4, 4.5 and 4.6). This is primarily due to the use of area and perimeter in the respective equations to determine f and k. If laser profiles are not available, these results indicate that using the f value computed from Equation 4.3, and back calculating k value from Equation 4.1 will result in a closer estimate of the actual value of k, than directly using Equation 4.2. These results indicate that the published k factors, to date, may be too high. It is recommended that mines requiring accurate k or f values for future ventilation planning, at least consider renting a laser profiler to accurately measure airway profiles during a pressure quantity survey.

The fractal numbers obtained from both the variogram and the power series are found to be within a smaller range for Section I than for Section II. The fractal numbers obtained from variography are more consistent with each other than are the results obtained from spectral analysis. The larger the window width, the more consistent are the results. The variogram results are believed to be more accurate, not just because the values are more consistent with each other, but because all the data are used when the variograms are

calculated. In the power spectrum method, due to the restrictions of the Fast Fourier series, for Section I, out of 177 observations, only 128 were used. Additional information that can be obtained from the semi-variogram is periodic variation, which is observed every 2 meters, coinciding with the length of a development round at the Sunshine Mine.

The fractal dimension reflects the self similarity of a profile or a surface. The results tabulated for the fractal dimension show that there is a sudden drop in the values from the profile at 150^0 to 210^0 angular position for Section I. This reveals that the jaggedness in these profiles is very low and shows higher self-similarity. Similarly, the profiles at angles 180^0 and 210^0 for Section II have very high fractal numbers. This is not obvious from visual inspection of these profiles. Thus fractal dimension can be considered as a very useful tool in finding such properties in the surfaces both at micro- and macro-scopic levels. It shows the potential of fractal analysis in defining roughness geometry of rough surfaces. This study has been conducted in order to investigate the applicability of fractal analysis in surface roughness characterization of mine airways, as an alternative to e/d ratio. The discussion in the final chapter includes the drawbacks and merits more in detail.

The results obtained in this study shows some agreement with those generated by Banik (1993) at the laboratory level, it is clear that two sets of readings are not sufficient to establish any conclusive relationship on this matter. One of the reasons for such a difference could be because of the method of calculation of fractal dimension, scale used and profile interval. Similar work has been conducted by Jeffery and Durucan (1993) in an attempt to correlate conventional macro surface roughness parameters with the fractal dimension. As described in Chapter I, it has to be realized that the fractal dimension needs serious modifications and has limitations when applied to profiles that are less random, sinusoidal, and have flow

reversals. Therefore, it is recommended that the study be repeated at many different mines, for a variety of surface roughnesses and flow rates, in order to determine a relationship between pressure loss and fractal dimension.

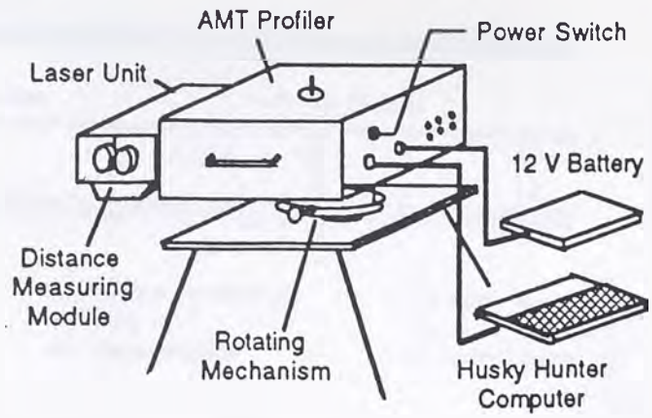

Figure 4.1. AMT 2000 Profiler and Construction

Figure 4.2. Layout of the Mine Drift in the Sunshine Mine.

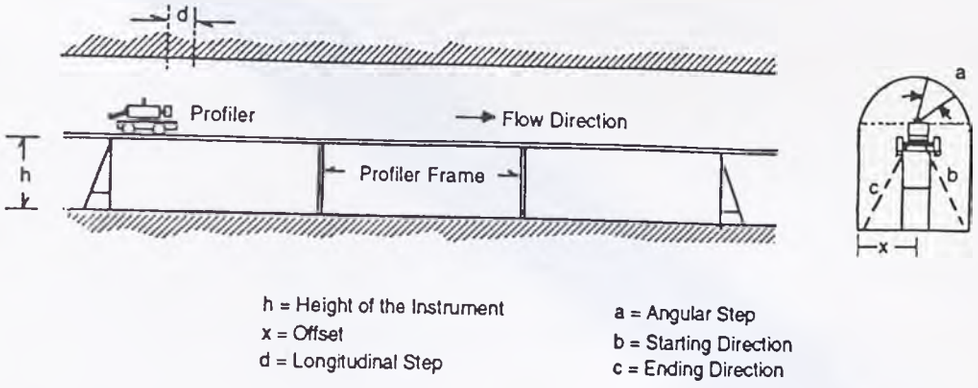

Figure 4.3. Schematic Drawing of Installation of AMT Profiler.

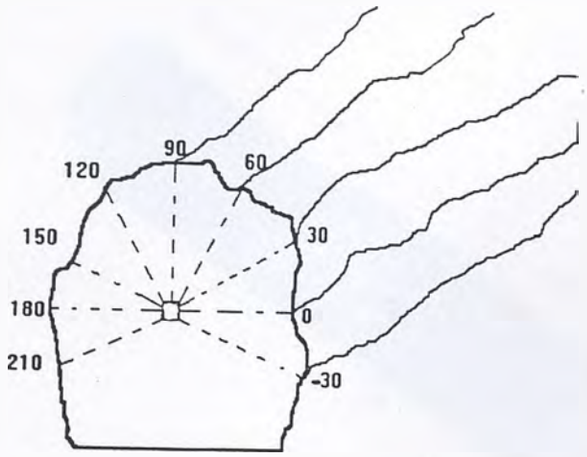

Figure 4.4. Drawing Indicating the Positions of the Longitudinal profiles.

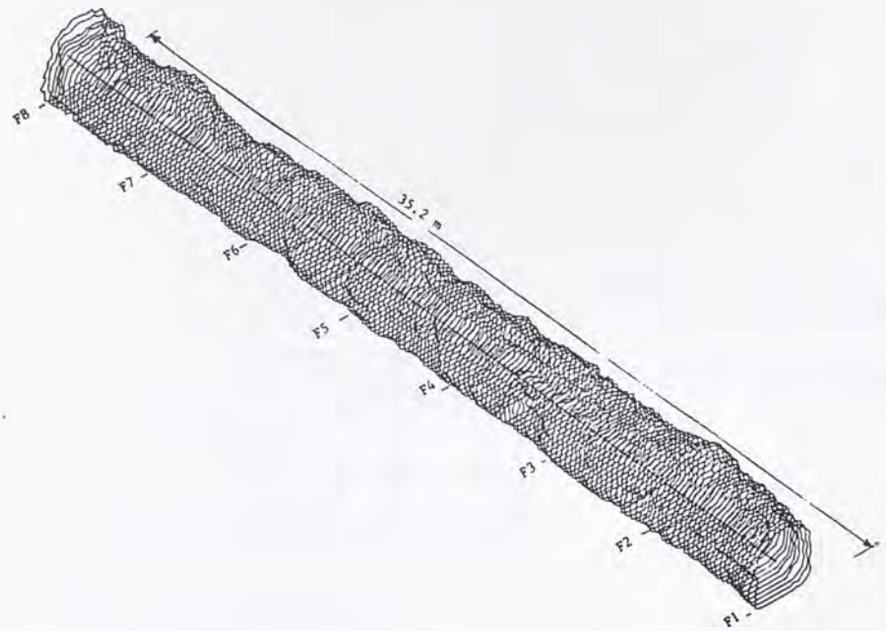

Figure 4.5. Isometric View of the Test Section I (35.2 m Long)

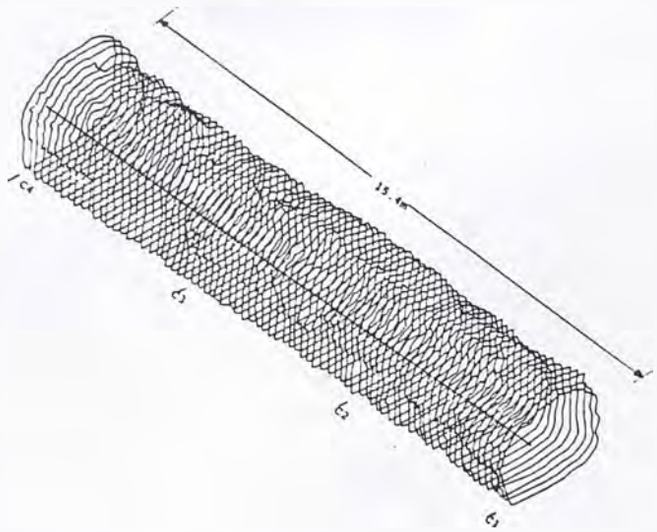

Figure 4.6. Isometric View of the Test Section II (15.4 m Long)

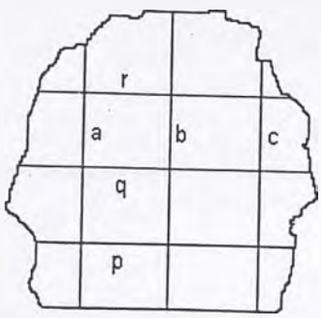

$w = (p + q + r)/3$ = width

$h = (a + b + c)/3$ = height

area = h . w

perimeter = 2 (h + w)

Figure 4.7. Typical Method of Estimating Area and Perimeter of a Cross-section from Hand Measurements.

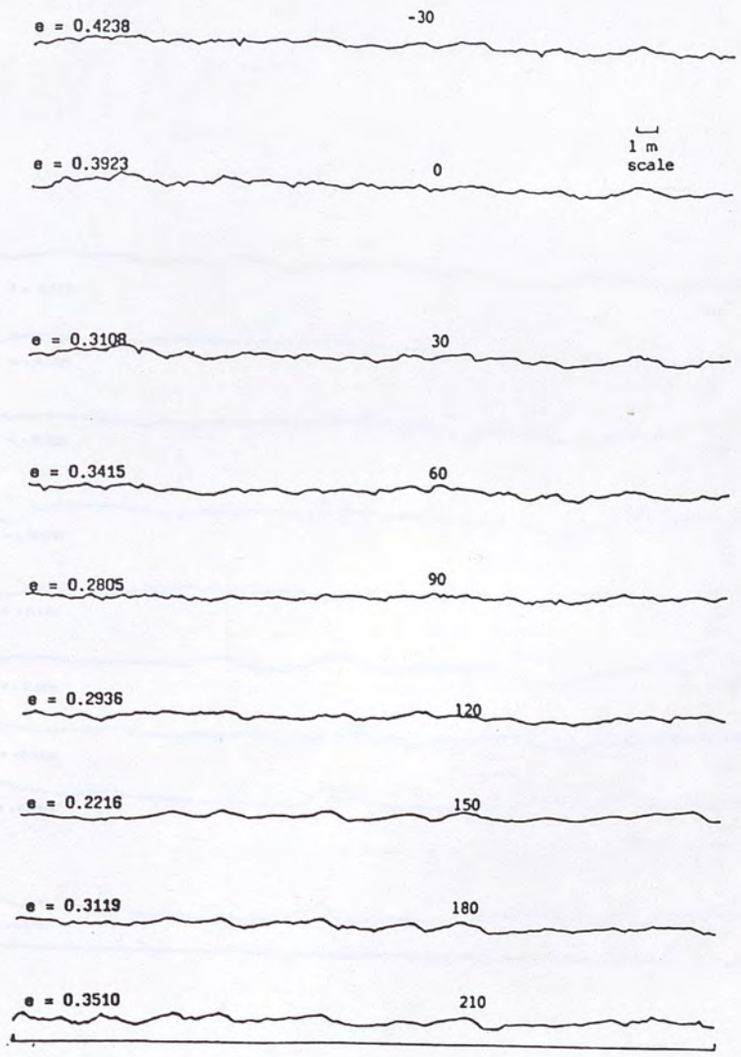

Figure 4.8. Longitudinal Profiles of Section I at Various Angular Positions.

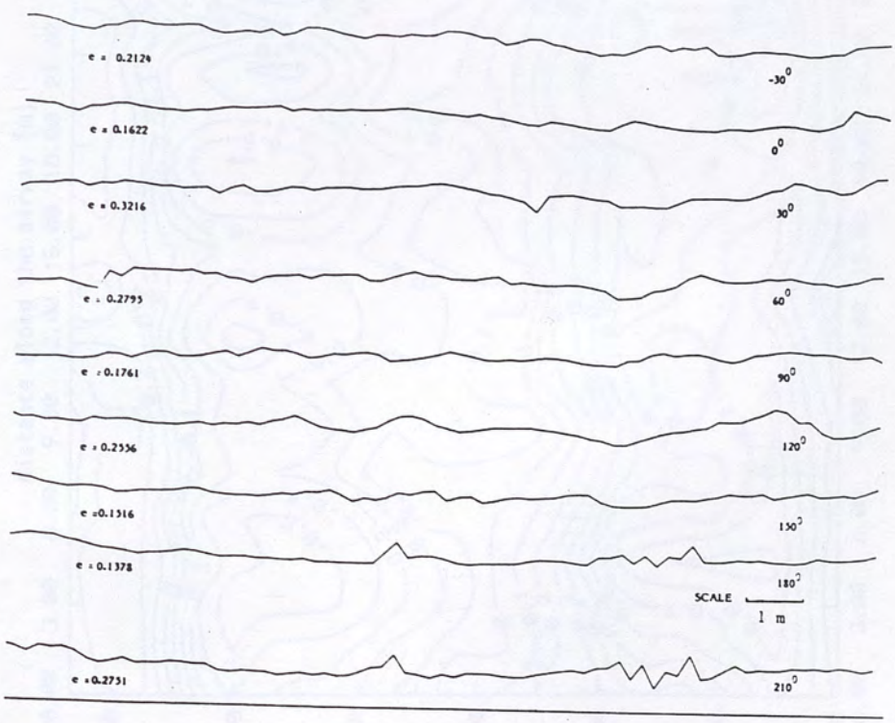

Figure 4.9. Longitudinal Profiles of Section II at Various Angular Positions.

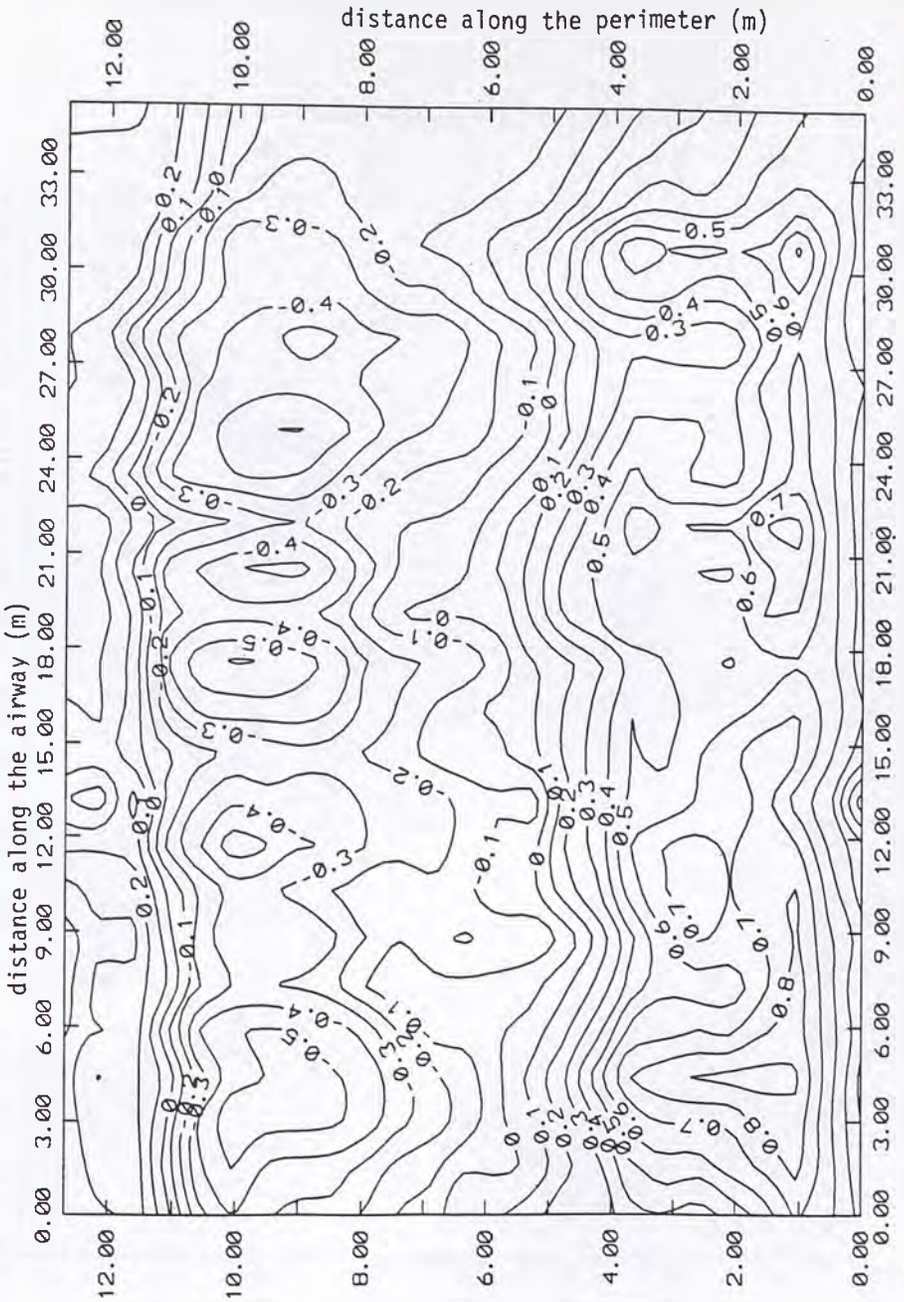

Figure 4.10. Contour Plot of the Airway Surface of Section I.

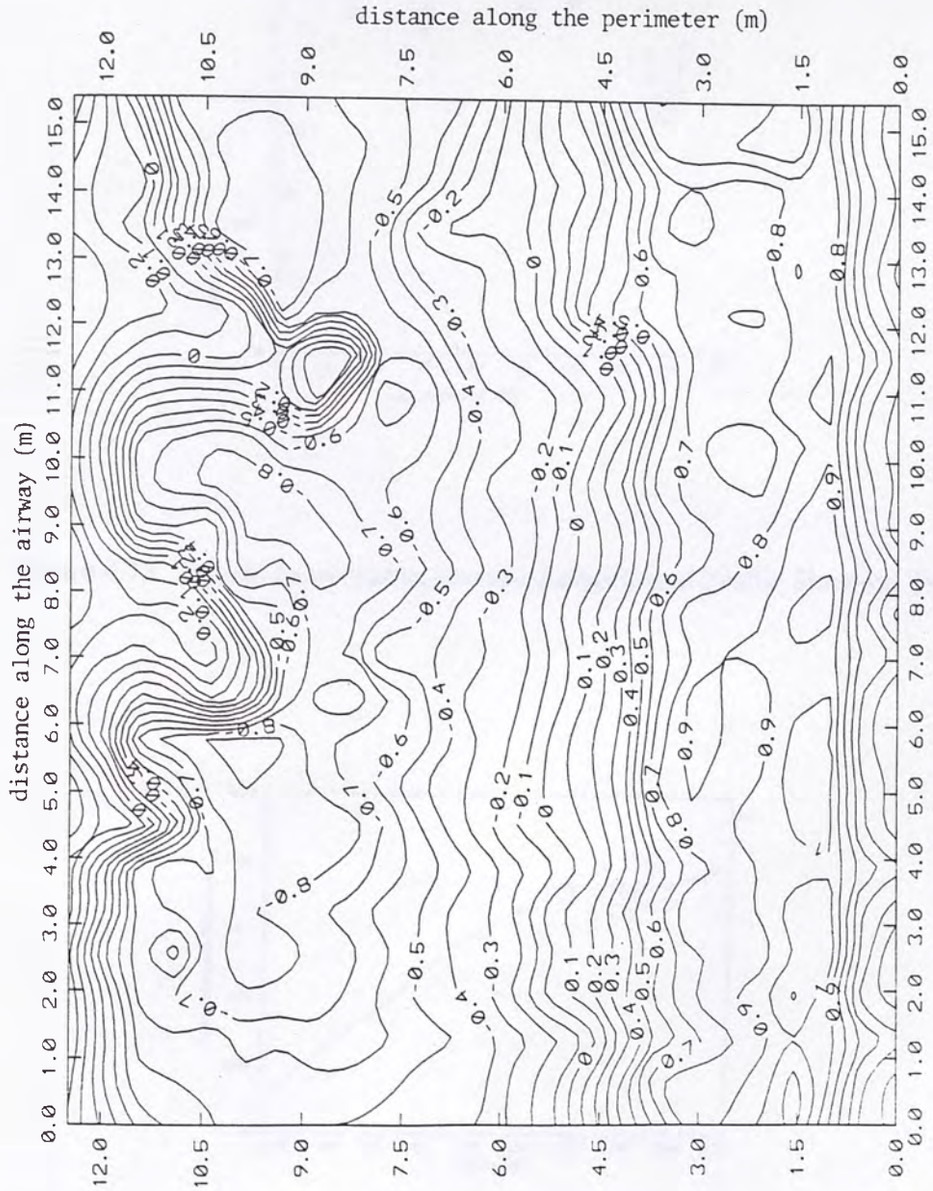

Figure 4.11. Contour Plot of Airway Surface of Section II.

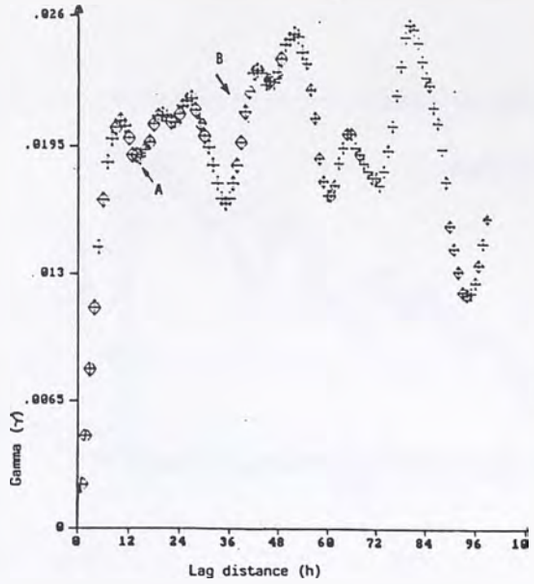

Figure 4.12. Typical Semi-Variogram of a Longitudinal Profile Showing Trend.

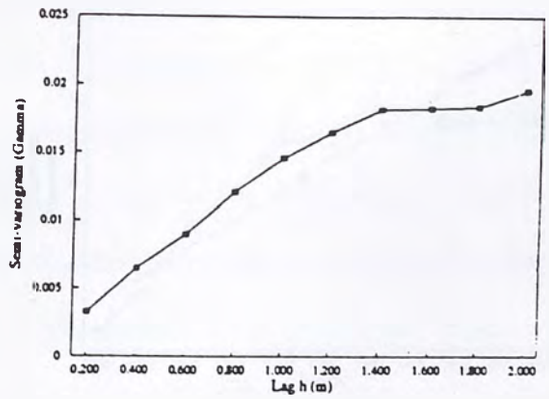

Figure 4.13. Plot of Semi-Variogram of -30^0 Longitudinal Profile of Section I.

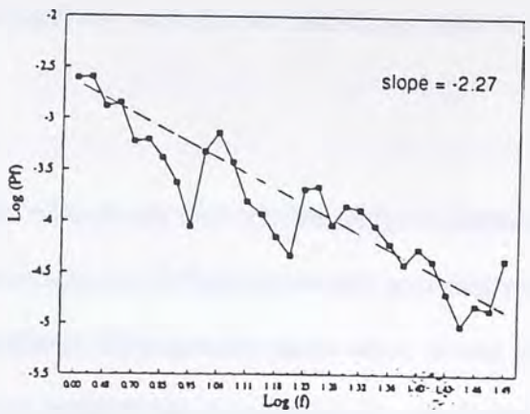

Figure 4.14. Log-Log Plot for the Semi-Variogram in Figure 4.10.

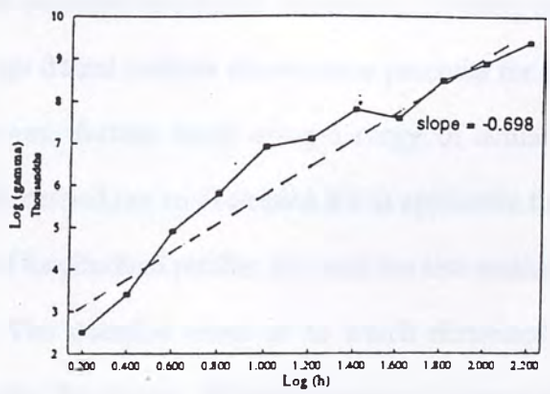

Figure 4.15. Log-Log Plot of Power Series of the Profile shown in Figure 4.12.

5. ANALYSIS OF AIR FLOW OVER A WAVY WALL

5.1 Background

In Chapter 4 a typical mine airway was considered for 3-dimensional surface mapping, in order to characterize its roughness in three commonly accepted ways. It can be observed from the results that significant discrepancies occur when airway geometry measurement techniques change. From the results of the computations for calculating k (friction factor) and f (coefficient of friction), it was concluded that, their estimates are dependant upon the precision of the airflow measurements and parameters describing the airway geometry. Similarly other parameters such as profiling interval and airway sinuosity play a significant role when fractal dimension analysis is carried out. Periodic variations in the longitudinal profiles of both the test sections of the mine airway can be observed from visual inspection. Based on the fractal analysis it was found that the statistical/spatial variations in the profiles can be determined and quantified as a fractal dimension (D) using spectral analysis and semi-variography. Although fractal analysis shows some potential for characterizing the macro-roughness of an airway, further work using a range of actual mine airways and flow conditions needs to be carried out to determine if it is applicable for use in mine ventilation.

In the analysis of longitudinal profiles for both the test sections, the fractal dimensions varied significantly. The question arises as to which dimension should be chosen as a representative value for the airway. Although, semi-variograms of all the profiles of each section indicate a regular variation (around 2 m), the fractal values of some profiles failed to show such behavior. In spectral analysis the plot showed a dominant frequency of 1.3 on a logarithmic scale ($\log_{10}$), therefore, the corresponding wavelength is around 1.77 m over the

35.2 m length of the airway. In fractal analysis it is important to choose the interval length for profiling. Huang, et al., (1992) suggested that the profiling interval must be smaller or equal to a critical length called, the "crossover length", which varies from profile to profile. Further work is needed to establish the critical interval lengths for profiling in different mine airways with respect to determining the fractal dimension. As the fractal dimension failed to recognize the directional bias in an airway, further research is needed to quantify and characterize the large scale roughness of mine airways.

The effect of large scale periodic variations or waviness on the frictional pressure drop in mine airways was suspected by Danko and Cifka (1984). In order to simulate such roughness, a fully equipped wind tunnel that simulates typical mine airway macro-roughness was constructed in the ventilation laboratory of the Mackay School of Mines. The aim was to investigate the effect of surface waviness on the frictional pressure drop in airways, and this is explained in detail and the results are presented in this chapter.

5.2 **Introduction**

A mine tunnel can be considered as a rough duct, with the typically high Reynolds number of ventilating air reflected in a proportionally thin laminar boundary layer. The first systematic investigation of duct roughness was carried out by D'arcy (1858) followed by Nikuradse (Nikuradse, 1950), Moody (Moody, 1944), and Von Karman (Von Karman, 1939). The models proposed are widely used in the field of fluid mechanics by engineers, but are principally based on the uniform sand or artificial mechanical roughness of surfaces. In practice, mine airways have very irregular and large scale roughness present, where the conventional models have severe limitations. This is primarily due either to the drill and blast

pattern in cyclic mining operations (Danko & Mousset-Jones, 1988, and Konduri, et al., 1992) or to the use of continuous mining machines (Jeffery & Durucan, 1993).

A few studies have been conducted to analyze the flow over such large scale roughenings (Calizaya, et al., 1991, and Danko & Mousset-Jones, 1988). In the field of gas dynamics this problem was approached and analyzed as flow over wavy walls (John, 1984, Panton, R.L., 1984) with some necessary assumptions. Figure 5.1 shows the schematic of a two-dimensional wave shaped wall. However, this does not apply well to mine ventilation, as the assumptions made are not appropriate for underground mine airflow.

5.3 **Simulation of Mine Air Flow**

A study was carried out in the laboratory using a scaled model of a mine airway and a precise instrumentation set-up, in order to measure and analyze the flow conditions in the model. The construction of the model and instrumentation set-up are explained in the following section. Appendix D includes photographs illustrating the construction of the wind tunnel.

5.3.1 Construction of Wind Tunnel

A wavy-walled wind tunnel had been designed and was built in the ventilation laboratory of Mackay School of Mines. Figure 5.2 shows an assembly stage of the model. A schematic view of the model is shown in Figure 5.3. The author's involvement in the project was to complete the construction of the tunnel, implementing the instrumentation for the airflow measurement, and connecting the fan to the wind tunnel.

A self standing steel frame was assembled to support the model drift. The four legs of

the main frame rests on the ground. The main frame consists of two individual moving frames with which the waviness of the roof and floor of the mine drift can be changed. The two moving frames are connected to the main frame by twelve (6 in bottom, 6 in top) threaded iron rods (spindles). The spindles have right handed threads and are fixed to the stationary middle frame. The rotation of the spindles moves the frames in opposite directions (upward/downward). A drawing illustrating the working principle for changing the waviness of the drift surface and construction is shown in Figure 5.4. The frames support the roof and floor of the model using plastic fiber rods of 0.64 cm (3/4 in.) diameter.

The roof and the floor of the model tunnel are made of flexible electronic circuit boards sections welded together. The side walls are two rigid plexi-glass pieces that are clamped tightly against the roof and floor by threaded bars, to prevent air leakage. They can be unclasped from the roof and floor of the model when it is necessary to change the wave amplitude. The adjustable roof and floor are supported by plastic fibre rods attached to the main steel frame. A view showing these details is given in Figure 5.5. The design dimensions of the airway is 4.8 m long, 10 cm high and 46 cm wide. The wind tunnel's length decreases by a very small amount as the amplitude of the waves increase. Some overlap was provided at the ends of model to compensate for this. This wind tunnel is used for simulating developed turbulent flow with Reynolds numbers ranging from 30,000 to 400,000 (Konduri, 1992). The surface of the model drift is very smooth and special care was taken in the construction process so that there are no surface discontinuities and projections in the flow path. This was intended in order to minimize the effect of surface friction (micro-asperities) on pressure drop when compared to the waviness. A drawing showing a pictorial view with details is given in Figure 5.6.

5.3.2 Instrumentation

In order to measure the changes in static and velocity pressures at various points along the test section, it was decided to build a moving platform inside the model that can hold a pitot tube. The design constraints for the platform were: a) minimum flow resistance to avoid major upstream disturbance, b) precisely controlled movement from the outside, and, c) minimum vibration in high velocity airflow so as not to effect the mounted instrumentation and to withstand transverse eddies due to surface waviness (Danko, 1993). An engineering drawing showing all the construction details of the platform is given in Figure 5.7.

A steel frame of 3.5 mm thickness, 35 cm long with 4 wheels, was assembled and mounted inside the tunnel, with its wheels resting on the side walls. The side walls are provided with aluminum guides (1 cm dia., 2.4 m long cylindrical rods). The guides were chosen so that they would allow uniform flow within the test length. The pitot tube was carefully mounted on the moving platform (cart). It was adjusted so that its tip projects 15 cm (6 in.) upstream from the platform and is positioned in the centerline (23 cm from the side wall, 5 cm from roof/floor) of the tunnel. The pitot tube was connected by flexible rubber tubing and was hooked to Betz manometer located outside the tunnel. The Betz manometer is a simple and precise instrument used to measure differential pressure with an accuracy of 0.2 mm water gage. The platform was connected to a wire loop to assist in its movement inside the tunnel. This wire loop passes over four pulleys located outside of the tunnel. The movement of the wire from the outside changes the position of the pitot tube. The drawing explaining the wire loop arrangement is shown in Figure 5.8. Every effort was taken to minimize the localized movement of the pitot tube, and the kinking of the manometer tubes, before sealing the tunnel for experimentation. Photographs of the arrangement are shown in

Appendix D.

5.3.3 Flow Conditions and Testing

The model tunnel was connected to a 5 hp, variable pitch, axial flow exhaust fan with the help of an aluminum expansion box and a wooden duct. The air inlet end of the wind tunnel was assembled with a parabola shaped bell to minimize shock loss and eliminate flow separation in the test section. The intended test section (2 m) is located near the outlet end of the model drift. The fan curves and air leakage was checked to determine the maximum range of Reynolds number. The fan was fixed at a 13.8^0 pitch for satisfactory flow conditions (static pressure and velocity). For precise flow measurements, 5 cm was chosen as the measurement interval for the flow parameters. Leakages areas were detected in the early tests by computing and checking the quantity flowing along the test section length after precisely measuring the cross-sectional area and air velocities at close intervals. The air quantity flowing through the section is expected to be constant (continuity principle - incompressible flow). Leakage spots can be detected at points of increase in mean airflow. The joints of the side walls and the roof and the floor were completely sealed using insulation tape for each change in wave amplitude, therefore, effectively eliminating most leakage. The average cross-sectional area and perimeter of the test section (when not wavy) are 0.04408 m^2 and 1.1085 m, respectively. The mean hydraulic diameter ($d = 4A/Per$) of the tunnel is 0.1591 m (remains constant for all waviness settings).

However, due to the presence of the aluminum expansion box at the end of the drift (see Figure 5.6), which connects to the fan, the last 10 cm of the test section showed very high centerline static pressure and air velocity. This was probably caused by the formation of

a vena-contracta, flow constriction due to change of cross-sectional area, close to the exit. Owing to this, the last 25 cm of the test section was eliminated from flow measurement. The tunnel connection and taping are flexible enough so that, the increase in waviness does not effect the length of the test section. From the initial testing it was concluded that within the limits of the fan capacity, three high velocities can be achieved for conducting experiments at 5 m/sec velocity intervals. The three maximum or centerline velocities were decided to be 21 m/sec, 26 m/sec and 31 m/sec. For the calculation purposes the representative velocity of the air stream is taken as (Hartman, 1982):

$$v_{ave} = 0.8\, v_{max} \qquad (5.1)$$

This was confirmed by measuring the velocity profile across the width of the model drift in the test section. A typical velocity pressure profile across the width of the model drift is shown in Figure 5.9.

5.3.4 Experimental Procedure and Flow Measurements

In order to know the macro roughness or waviness of the wind tunnel when it was adjusted for waviness, the pitch of the threaded screws was calculated (the threaded screws control the wave amplitude). This was verified over a range of waviness adjustments by actually measuring the waviness of the roof and floor with the help of a vernier scale. Sample readings are given as follows:

From the threaded screws:

10 pitches = 18.54 mm (screw 1)

10 pitches = 18.56 mm (screw 2)

10 pitches = 18.35 mm (screw 3)

15 pitches = 27.46 mm (screw 4)

20 pitches = 36.44 mm (screw 5)

10 pitches = 18.55 mm (screw 6)

Average pitch = 1.842 mm

(6 screws were selected at random, three from floor and three from roof)

From actual waviness of the model:

2 pitches = 3.7 mm

2 pitches = 3.75 mm

2 pitches = 3.6 mm

2 pitches = 3.73 mm

(these were measured at various points on the model for a set wave amplitude)

Average pitch = 1.8475 mm

This confirmed that the waviness set through the threaded screws, (spindles that control the movement of the frames) were exactly represented as waviness in the model drift (see Figure 5.4). Hence, it was decided that the increment in waviness can be set more easily by rotating the screws by a fixed number of turns. A half rotation of each screw gives a waviness of 1 pitch to the tunnel, i.e., the waviness is considered as double the wave amplitude. This is shown in Figure 5.10, and is because the mean roughness in an airway is defined as the average of the roughness above the minimum value (see Chapter 4, on the method of calculation of mean asperity height). For each specific waviness the fan was set at three

different velocities. For each velocity static pressure and velocity pressure were measured at 5 cm intervals in the test section of 1.70 m in length (35 readings), which includes four complete waves of the airway (Each wave length is roughly 42.5 cm). A drawing showing these details is given in Figure 5.11. The wave length of the model drift remained approximately constant for all wave amplitudes. For this reason the total length of the model reduces with increasing waviness. A sample plot of static pressure and velocity for a particular waviness along the test section, is shown in Figure 5.12. The periodic change in the respective flow parameters are self explanatory for a wavy wall. The upstream drop in the static pressure can be observed due the effect of the waviness.

At higher velocities, as the waviness increased, the fluctuation/pulsations in the airflow and range of measured values increased. High velocity ranges can be observed in the plots of the velocity at different waviness shown in Appendix E. The higher the waviness of the wall, the higher the velocity range in the flow along the length of the test section. The pulsations are probably due to the development of eddies in the flow. The strength of these transverse eddies increases with wave amplitude and airflow velocity. In the low settings of waviness fluctuations in the static pressure were not present, but were persistent at higher wave amplitudes. A reason for such high differences in velocities at high wave amplitudes is due to large areal changes in the airway cross-section along the length. Appendix E includes plots of static pressure and velocity at each point for each waviness setting.

5.4 **Flow Parameter Computations**

5.4.1 Static and Velocity Pressures

The Betz manometer measures the gage pressure (static pressure and velocity pressure,

which is the difference between the total and static pressures in the flow zone) in millimeters of water gage. Then the pressure drop, P (Pa) is calculated as:

$$P = \rho_l g h_l \tag{5.2}$$

where,

ρ_l = density of water (Kg/m^3) = 1000 Kg/m^3

g = acceleration due to gravity (m/s^2) = 9.81 m/s^2

h_l = height of the liquid column (m)

This formula is also used for calculating barometric pressure. A barometer is used to measure the ambient atmospheric pressure in order to calculate the density of ambient air.

5.4.2 Air Density

$$\rho = \frac{P_a}{R_u T} \tag{5.3}$$

The air density, ρ can be approximated by the formula:

where,

P_a = Ambient atmospheric pressure (Pa)

T = Dry bulb temperature (K)

R_u = Universal Gas constant (J/Kg.K) = 287.045 J/Kg.K

During the laboratory experimentation period there was not a significant variation in the dry bulb temperatures (20.7~22^{0}C). The laboratory wet bulb temperature ($\approx$13.8^{0}C)

practically had no significant impact on the air density. This was calculated and checked as shown in the example below:

Eg. $t_d = 21^0C$ $t_{wet} = 13.8^0C$ $P_a = 85650$ Pa

($T_{wet} = t_{wet} + 273.13$ K, $T_d = t_d + 273.13$ K)

Relative humidity (Hartman, 1983) = 56%

Specific humidity = 8.725×10^{-3} Kg/Kg Dry air

Dry air density = $P_a/RT_d = 1.022$ Kg/m^3

Moist air density (Hartman, 1983) = 1.036 Kg/m^3

For all practical purposes, the density was calculated from only the dry bulb temperature, and occasionally checked for accuracy using the dry and wet bulb temperatures. In all the calculations there were no large differences. The air density was calculated separately for each temperature reading, and used in subsequent calculations for Re and v.

5.4.3 Air Velocity

The following equation is used to calculate air velocity:

$$v = \sqrt{\frac{2P_v}{\rho}} \qquad (5.4)$$

where, P_v = velocity pressure (Pa).

5.4.4 Absolute Viscosity

The absolute viscosity, μ of a fluid is a function of room temperature, T. The viscosity

of a gas is given by the Sutherland law (White, 1991):

$$\frac{\mu}{\mu_0} \approx \left(\frac{T}{T_0}\right)^{3/2} \frac{T_0+S}{T+S} \qquad (5.5)$$

where,

μ_0 = Reference viscosity (Pa. s)

T_0 = Reference temperature (K)

S = Constant fit to data ≈ 111 K for air

The reference viscosity at 273 K is 1.716×10^{-5}. In the laboratory conditions, μ was calculated to be on average 1.817×10^{-5} Pa. s. Sample calculations and viscosity values for the laboratory temperatures are shown in Appendix F.

5.4.5 Reynolds Number

Reynolds number was calculated from:

$$Re = \frac{\rho v d}{\mu} \qquad (5.6)$$

The temperature corrected viscosity (μ), air density (ρ), air velocity (v) and hydraulic diameter (d = 0.159 m) calculated from Equations 5.9, 5.10 & 5.11 were used to determine the flow parameter.

5.5 Data Analysis and Results

Appendix G shows complete list of measured data in the wind tunnel at 8 different

values of waviness (0 - 7), and 3 velocities at each waviness. The three average velocities at which measurements were made were 17.5 m/s, 21.94 m/s and 26.84 m/s. The mean range of Reynolds numbers for these velocities are approximately 150,500, 190,000 and 230,800, respectively.

From Darcy's law (Equation 2.9):

$$\Delta p = 4f\frac{l}{d}\frac{\rho v^2}{2}$$

In this equation, for the given experimental set-up, f has to be determined and is expected to vary from one waviness to another. The change in f causes change in the pressure loss, Δp. From the above equation, f is given by:

$$f = \left(\frac{\Delta p}{l}\right)\left(\frac{1}{v^2}\right)\left(\frac{d}{2\rho}\right) \qquad (5.7)$$

where, $\Delta p/l$ = pressure gradient (Pa/m).

This means, f is proportional to the pressure gradient and inversely proportional to the square of the velocity. The term $d/2\rho$ is a constant for all waviness. The pressure gradient is obtained by performing a regression on the static pressure points. The slope of the regression curve is the pressure drop per unit length of the test section.

For each Re, the frictional pressure drop per unit length per square of the velocity, and the coefficient of friction, are listed in Tables 5.1, 5.2 and 5.3. In the calculations the first four points and last two points in the test section are neglected in order to use untruncated periods and eliminate any kind of bias in the average value (Danko, 1993). The value e is the waviness

of the wall in meters. It can be seen from Tables 5.1, 5.2 and 5.3, there is an increasing trend in the rate of pressure drop per unit length per square of the velocity in the flow as the waviness of the surface increases. The coefficients of friction for a straight wall (zero waviness) obeys the Moody diagram, which is decreasing for increasing Re. Surprisingly, the *f* values of higher waviness do not show this trend. The combined graph, *f* versus waviness (e/d, where e is the waviness) is shown in Figure 5.13.

The increase in the waviness has caused an increase in the flow resistance, and hence the coefficient of friction. This kind of roughness is quite different from the uniform sand roughness, both theoretically and practically. This is proved by these experimental results; hence, the coefficient of friction with increasing $e/d_{waviness}$ does not decrease with increasing Re, which is opposite to the Moody diagram.

The increase in the *f* with waviness can be explained in the following two ways, a) increase in the rubbing surface area, and b) a reduction of the effective hydraulic diameter due to constriction by eddies. However, this study suggests that in typical mine airways, eg. Sunshine Mine, where it is common to observe such periodic areal changes, it would be useful to consider surface sinuosity when calculating the static (frictional) pressure drop. The plot (graph) Figure 5.13 can be used to predict the additional pressure drop due to waviness. In addition, the e/d used in this case should not be confused with the e/d used conventionally. For this reason it is suggested to use the roughness parameter $e/d_{waviness}$ in the nomenclature describing a tunnel geometry. Further work needs to be carried out on similar models by superimposing uniform micro-surface roughness elements in order to study their combined effect on pressure losses, followed by additional measurements in mine airways.

Table 5.1 Comparison of the Pressure Drop and Coefficient of Friction at Different Waviness for Re averaging 150,500

Waviness	Velocity	Regression equation of the Static Pressure	$\Delta p/l/v^2$	f
e	v	$\Delta p = ml + c$ *		
$(x10^{-3})$			$(x10^{-3})$	$(x10^{3})$
(m)	(m/s)	(Pa)	Pa. s^2/m^3	
0	17.07	15.3 l + 254	52.51	4.09
1.85	17.03	15.7 l + 264	54.13	4.22
3.7	17.25	16.5 l + 262	55.45	4.32
5.55	17.12	20.8 l + 260	70.98	5.53
7.4	17.80	24.8 l + 272	78.26	6.10
9.25	17.11	24.03 l + 269	82.09	6.40
11.1	17.99	30.3 l + 306	93.60	7.30
12.95	18.624	38.2 l + 323	110.13	8.59

* m (slope) and c are the constants in the regression equation

Table 5.2 Comparison of the Pressure Drop and Coefficient of Friction at Different Waviness for Re averaging 190,000

Waviness	Velocity	Regression equation of the Static Pressure	$\Delta p/l/v^2$	f
e	v	$\Delta p = ml + c$ *		
($x10^{-3}$)			($x10^{-3}$)	($x10^{-3}$)
(m)	(m/s	(Pa)	Pa. s^2/m^3	
0	21.39	20.2 l + 400	44.16	3.44
1.85	22.01	29.0 l + 417	59.88	4.66
3.7	22.06	29.3 l + 416	60.24	4.70
5.55	22.40	37.3 l + 452	74.33	5.80
7.4	21.96	42.6 l + 422	88.38	6.89
9.25	22.20	44.2 l + 441	89.65	6.99
11.1	21.68	47.9 l + 486	101.92	7.95
12.95	21.854	55.6 l + 466	116.42	9.08

* m (slope) and c are the constants in the regression equation

Table 5.3 Comparison of the Pressure Drop and Coefficient of Friction at Different Waviness for Re averaging 230,800

Waviness	Velocity	Regression equation of the Static Pressure	$\Delta p/l/v^2$	f
e	v	$\Delta p = ml + c$ *		
$(x10^{-3})$			$(x10^{-3})$	$(x10^{-3})$
(m)	(m/s)	(Pa)	Pa. s^2/m^3	
0	25.67	27.5 l + 598	41.73	3.25
1.85	26.05	31.3 l + 591	46.18	3.60
3.7	26.47	33.0 l + 609	47.10	3.67
5.55	26.66	48.9 l + 647	68.83	5.37
7.4	26.98	54.5 l + 692	74.87	5.84
9.25	26.98	58.2 l + 644	79.97	6.24
11.1	28.18	71.3 l + 702	89.77	7.00
12.95	27.753	81.9 l + 707	106.33	8.29

* m (slope) and c are the constants in the regression equation

$$y_b = A \sin \frac{2\pi x}{\lambda}$$

A - wave amplitude (m)

y_b - y-coordinate on the wall (m)

x - x-position on the wall (m)

λ - wave length (m)

Figure 5.1. Two Dimensional Wave Shaped Wall

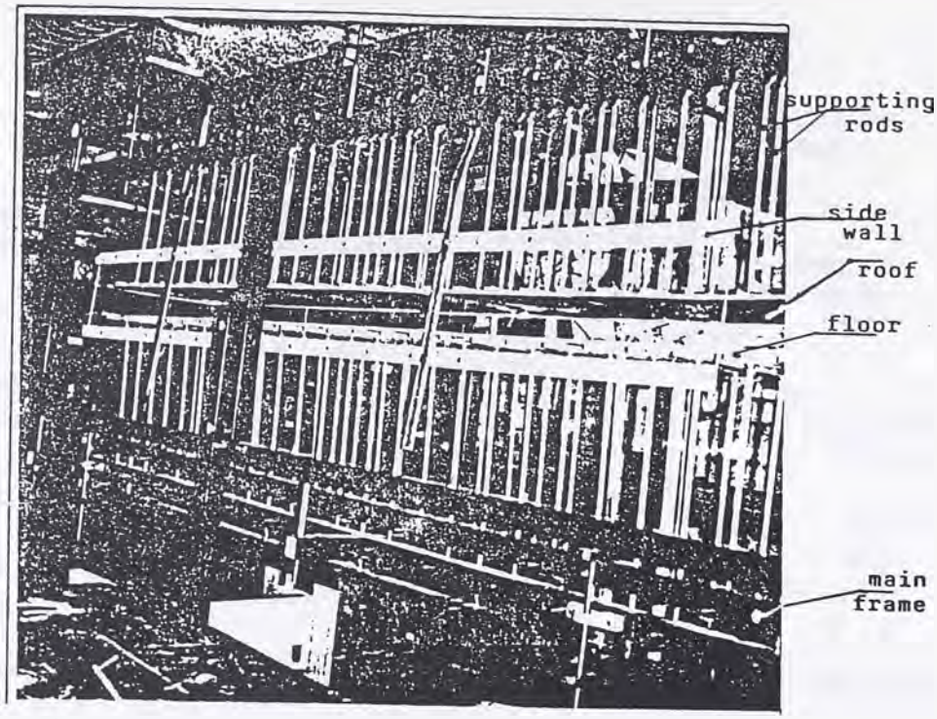

Figure 5.2. Picture of the Wind Tunnel Explaining its Construction

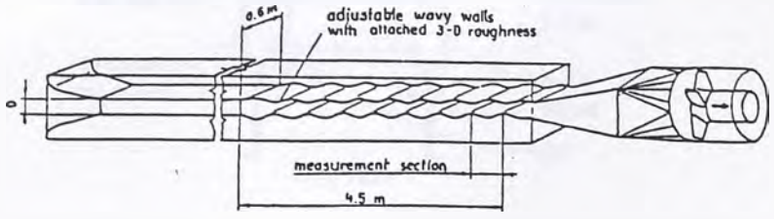

Figure 5.3. Schematic of the Wind Tunnel Including the Fan and General Setup (Danko & Mousset-Jones, 1988)

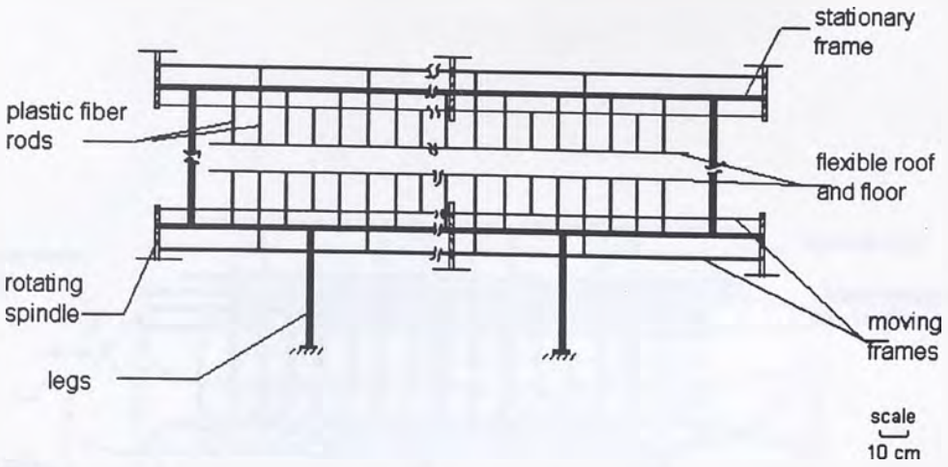

Figure 5.4. Drawing of the main Frame Showing the Working Principle of the Wavy Wall

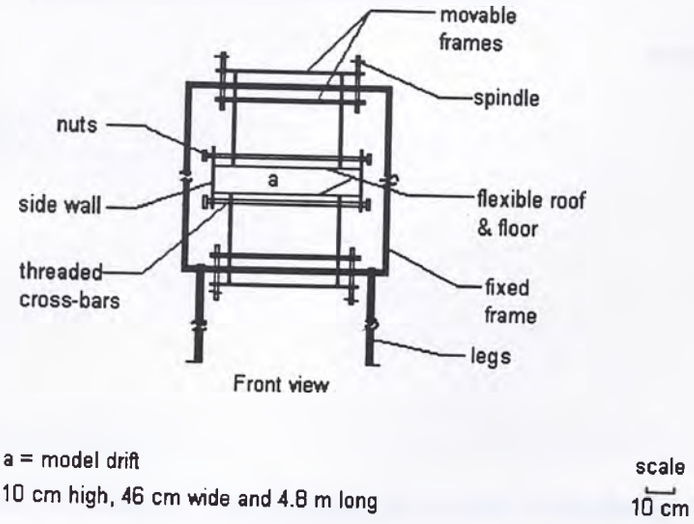

Figure 5.5. A View Showing the Cross Bars Connecting the Side Walls to Clamp the Roof and Floor

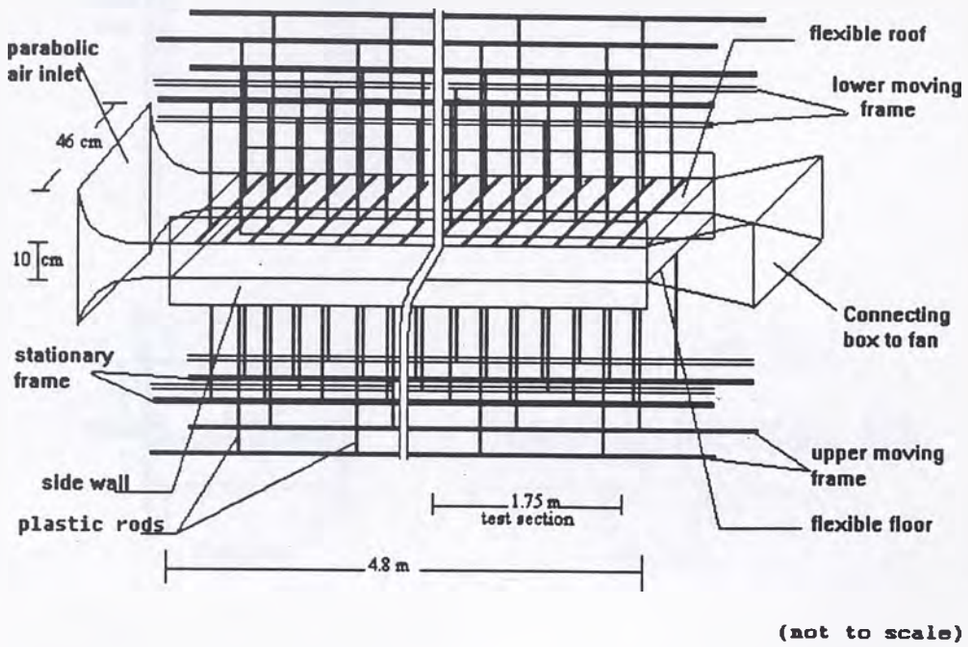

Figure 5.6. Pictorial View Showing the Details of the Model Drift

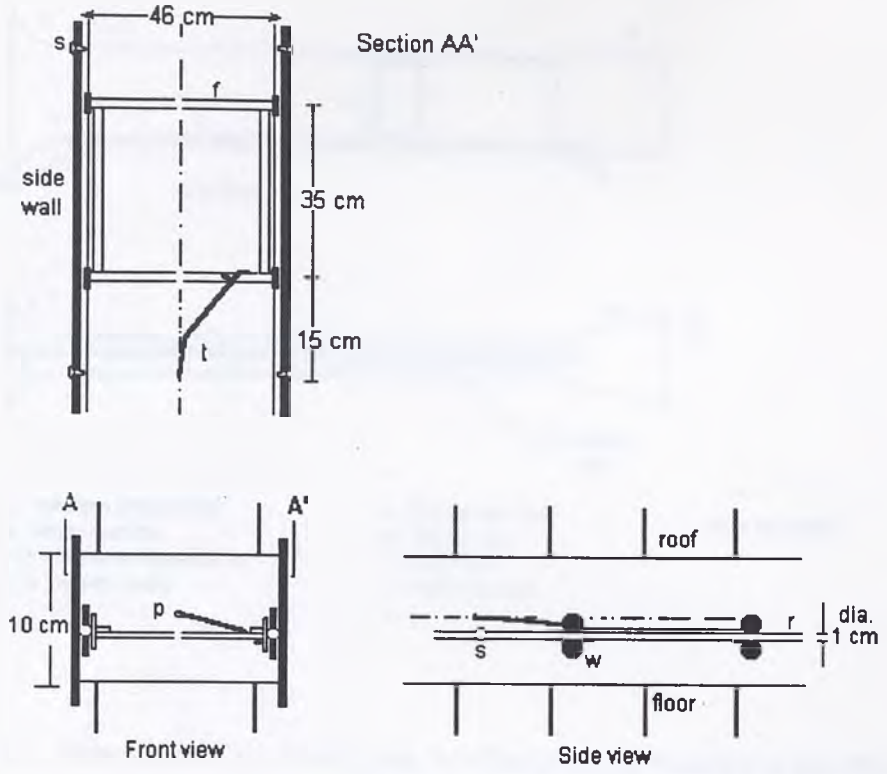

f - metal frame
r - 2m long aluminum rod
w - plastic wheels attached

t - pitot tube
p - measurement point
s - screws that support rod

Figure 5.7. Engineering Drawing of the Construction of the Platform that Accommodates Flow Measurement Instrumentation

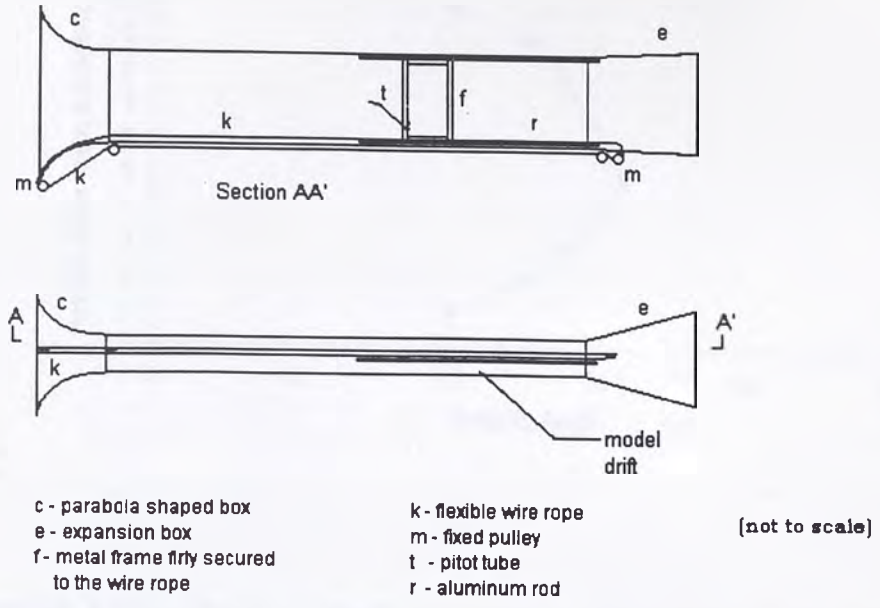

Figure 5.8. Schematic of the Wire Loop for Changing the Position of the Pitot Tube

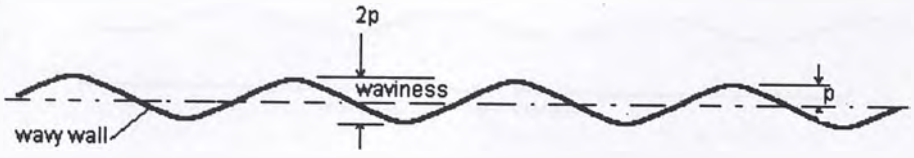

p = screw x number of turns

Figure 5.9. Waviness Notation in Relation to the Screw Pitch (p)

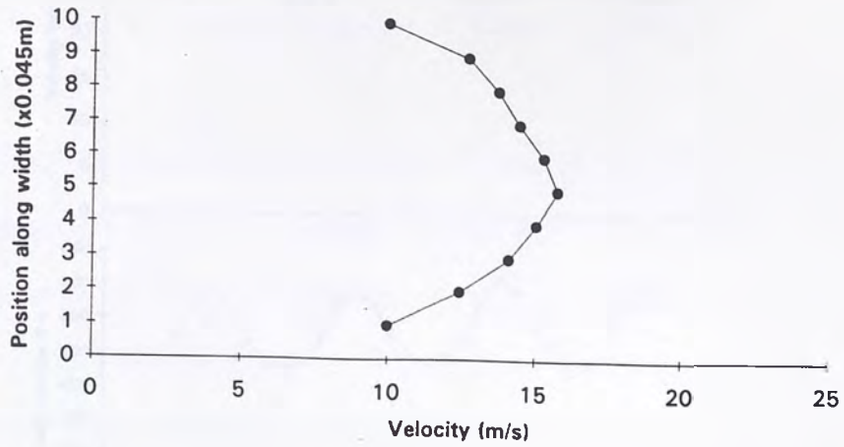

Figure 5.10. A Plot of Velocity Profile Measured at a Cross-Section in the Test Section

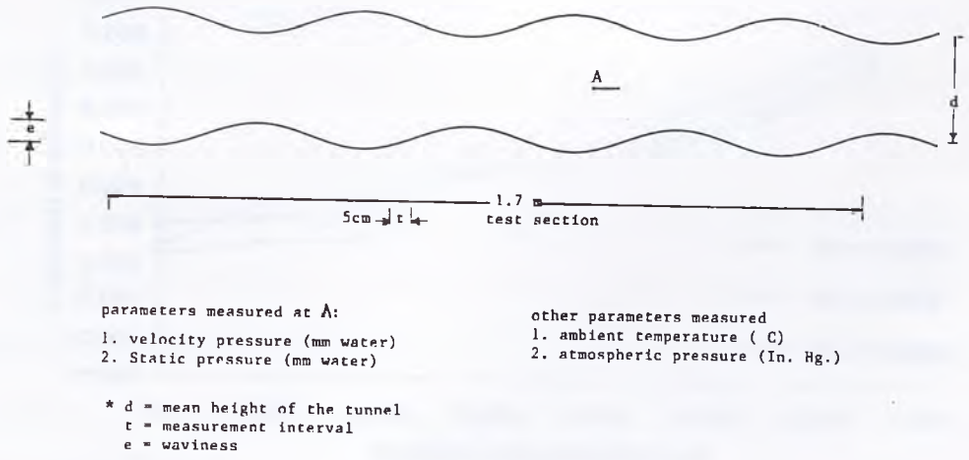

Figure 5.11. Illustration of the Wavy wall and the Flow Parameters Measured

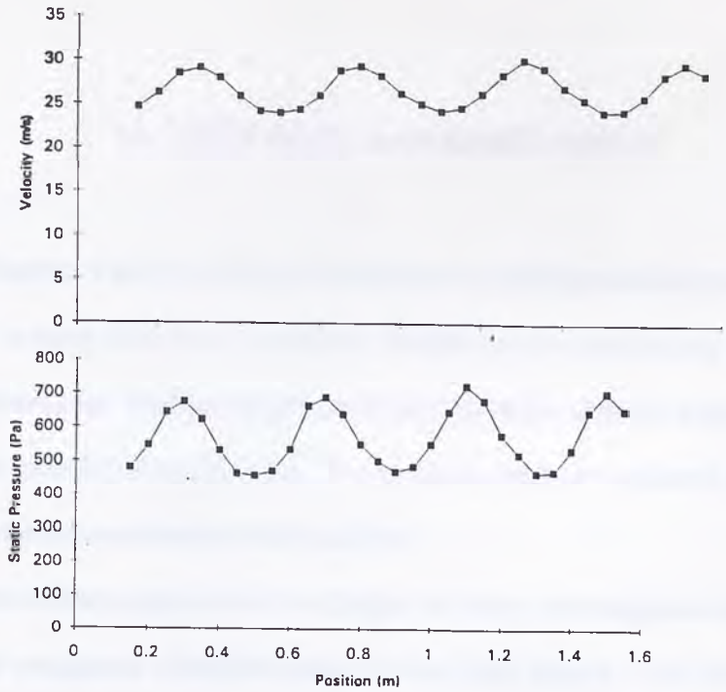

Figure 5.12. Sample Plot of Static Pressure and Velocity Along the Test Section

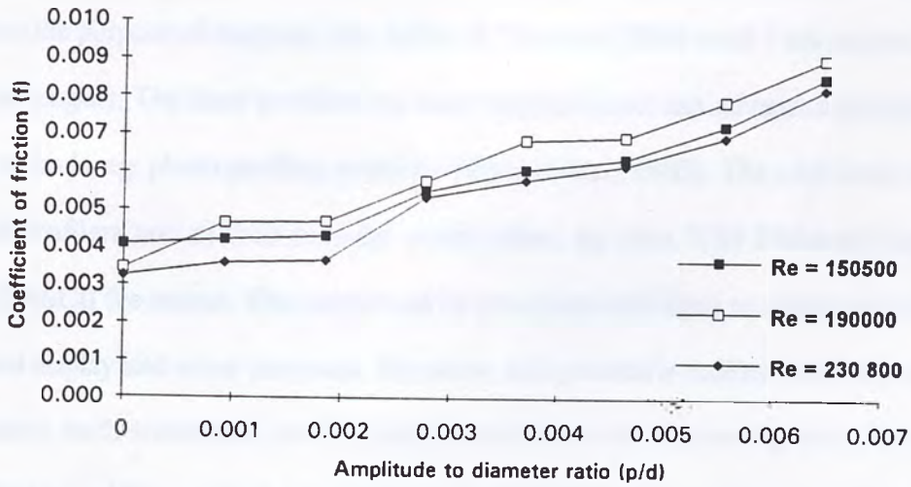

Figure 5.13. Plot of Coefficient of Friction (f) versus p/d (Waviness) at different Re

6. DISCUSSION AND CONCLUSIONS

In Chapters 4 and 5, a detailed analysis of an underground mine airway surface and airflow over a wavy wall were presented. Studies on the mine airway have shown some interesting results for surface roughness characterization. Fractal analysis of the surface profiles gave speculative conclusions. The previous chapter concluded by highlighting the importance of macro-waviness in mine airflow.

A non-contact measurement technique has many advantages in mine airway surface mapping and roughness characterization. It has been shown that this type of distance measurement technique can be used to generate three dimensional representations of mine workings. The AMT 2000 laser profiler helps to visualize the mine drift surface and has the flexibility to generate longitudinal profiles at any desired angular position. A 2-D laser profiler allows surface mapping at any desired resolution. The measurement interval can be optimized based on the purpose of mapping, (eg. Jeffery & Durucan (1993) used 1 cm interval to survey a 4.5 m length). The laser profilers are more sophisticated and advanced compared to the other methods, eg. photo profiling technique (Gangal, et al., 1985). The additional advantages in such profilers are: a) their modular construction, eg. uses Wild Distomat range finding laser, b) ASCII file output. The output can be processed and input to computer software for graphical display and other purposes. However, this process is tedious and time consuming. Processing each transverse profile's radial coordinates by converting them into cartesian coordinates, adding a third coordinate to each point and combining all the profiles to represent a 3-D surface takes considerable time. A profiler having the capability of generating output that can be directly used as input for graphical display/CAD software, eg. AutoCAD,

SURFER, is needed for extensive use in industry. The AMT 3000 is the next generation tunnel profiler and produces a 3-D profile.

For experimental purpose, the true surface area of the airway, Section I (length, 35.2 m) was used for calculating the *k* factor. It was found that there is the potential for a considerable error involved in the calculated *k* values using manual estimates of the area and perimeter of cross-sections (Table 4.4). The calculated *k* value from the average area and perimeter of all laser profiles has the lowest deviation (13.5%) from the one calculated from the rubbing surface area. This further suggests that the established McElroy's tables of k values used by practicing ventilation engineers needs to be revised as they were determined from hand measurements. Another reason for the revision of McElroy's tables is the change (increase) in size (cross-sectional area) of the openings from the 1930s through the 1990s. Therefore, a relative decrease in the ratio of mean roughness to hydraulic diameter significantly changes the airway roughness.

The calculations of *f* values resulted in a relatively smaller error. In all the calculations, the mean asperity height, e was used from the laser profiler data. Hydraulic diameter was the variable in each calculation of the airway section. For both the test sections (Table 4.5 & 4.6) the error in calculated *f* values are within a range of -1 to -12.1%. All the manual measurements resulted in a very close estimate of *f* value. This means that the accuracy of *f* is more dependant on e than d. A comparison of these tables also show that the *f* value is highly sensitive to the e/d ratio. Section II (length, 15.4 m) has a relatively smaller e/d ratio resulting in a higher percentage variation in the *f* values.

All the longitudinal profiles were analyzed using the two techniques; Variography and Power Series. A check was made on the validity of these two techniques. The results of the

variography are more consistent and the process illustrates a very important nature of an airway, ie. regular variation/periodicity in the airway (approximately 2m). The results of the power series often tend to yield either too high or low values (Tables 4.7 & 4.8). The spectral analysis also reveals some important information about the surface profiles. Closer examination of the plots can help in finding out about obstructions, if any, in the profiling process (section 4.4.1b). Such values need to be omitted from the calculations. It is recommended that variography is used rather than a power series. A semi-variogram uses the entire data set whereas, due to the limitations of the application of fast fourier series, only the highest second power (2^n) of data points can be used in a power series.

A typical mine airway shows considerable variation in the cross-sectional area along its length. Such macro variations can be seen in longitudinal profiles. The use of fractal analysis was not very successful in characterizing such roughness in both the test sections. The fractal dimensions of some profiles have shown a remarkable difference from others, for a given test section. Banik, et al. (1993), using laboratory experimental data, obtained a relationship between *f* and D showing the potential of the fractal dimension as an alternative for the conventional roughness descriptor *f*. The results of the fractal analysis of longitudinal profiles of the Sunshine Mine airway showed a deviation of up to 70% from each other. The results of the research of Huang, et al. (1992) on the fractal geometry of rock profiles and the science of self-affine (statistically self-similar) fractals show that D is highly dependant upon the profiling interval. It was also suggested that smaller interval lengths give more accurate results. Other conventional methods describing the surface roughness of underground airways are using root mean square (RMS) and center line average (CLA) of the roughnesses. Jeffery & Durucan (1993) have used 1 cm profiling interval in an airway and attempted to correlate

D with parameters Root Mean Squared value (RMS) and Center Line Average (CLA) roughness. No significant results were obtained in their analysis. Further research is needed at many different mines, for a variety of surface roughness and flow rates, in order to determine if there is a possible relationship between the fractal dimension and any of the conventional roughness parameters or the pressure loss in a mine airway. However, it appears from this investigation that a relationship exists between conventional roughness and fractal dimension of an airway.

The use of fractals raises many questions regarding their application in characterizing surface roughness in fluid flow. A fractal is not sensitive to the directional bias, of the roughness, which is the opposite to the *f* value. It cannot show a significant difference in the dimensions of the profiles which have the same frequency but different amplitudes, as it more describes a scale dependant property. Alternatively, Jeffery and Durucan (1993) attempted to characterize the macro roughness of airways with the parameters, RMS and CLA roughnesses parallel to the fractal dimension. Their study indicated that these two parameters also varied with the trace length. Hence, it difficult to conclude on the use of the fractal dimension for the description of macro-roughness in mine airways, as its precision is dependant on sample interval. For this reason, in the study described in the last chapter, large airway surface roughness (macro-asperities) was compared to waviness, and its effect on air flow was investigated.

Airway sinuosity in mine airways is caused by either cyclic mining operations (drilling and blasting in conventional mining) or continuous mining (road header developed airways). During the ventilation planning phase of a mine, the pressure loss calculations are carried out using friction factors determined from previously existing airways. It was found that the

calculated pressure loss is frequently inaccurate. One of the reasons could be accuracy of the *k* value, another is the lack of information on pressure loss due to areal variations or waviness of a mine airway, which is often ignored. To date, no one has investigated the effect airway surface waviness has on the air pressure loss in mines. From the experiments conducted, it was found that there is a considerable pressure loss in airways caused by surface waviness. This type of roughness is quite different from the uniform surface roughness (micro/sand roughness) of airways (Figure 5.14). The roughness exhibited results in areal variations and development of eddies in the flow path. This means, that the combined effect of these two roughnesses is the factor that is causing the uncertainty in the pressure loss estimation in mine ventilation practice. From these laboratory experimental results it is not reasonable to draw a general relationship between the waviness and pressure loss. However, this gives a guideline for considering the airway waviness as a standard roughness descriptor for estimating the pressure loss in mine airways. It is recommended to carry out further research on similar lines in different flow conditions and underground mine airways.

3-D velocity measurements in a number of cross-sections along the length of the test section of the existing wavy wall model, is recommended for further study. The study of 3-D velocity profiles in the transverse sections will help in understanding the phenomenon of the development of eddy currents in the flow regime and the effective/hydraulic diameter of the section. The study on the effect of waviness using the same model but without any areal variations, on the frictional pressure drop, could provide results which will assist in the better understanding of flow over wavy walls.

To summarize, the highlights of the research project are the following:

i. Laser profiling is very useful for the visualization of drift surfaces and airway roughness characterization.

ii. Manual estimation of area and perimeter can lead to an erroneous calculation of the friction factor.

iii. It is time to consider updating and reviewing the McElroy tables of friction factors in order for the values to be more representative of modern underground development methods.

iv. Calculation of coefficient of friction using mean asperity height to hydraulic diameter ratio gives reasonably accurate results, independent of the two cross-sectional parameter measurement techniques mentioned.

v. Fractals reflect the random roughness property in surface profiles, but there are problems when applied to profiles that are less random, sinusoidal, and have flow reversals.

vi. Variography is advantageous to use for computing the fractal dimension of a profile.

vii. Surface waviness of airways cause considerable pressure loss in airways. For a normal airway, it can be up to 70-80 Pa/m, for Re values around 250,000.

viii. Waviness in a mine airway is a major contributing factor to pressure loss.

ix. The combined effect of uniform roughness and waviness is one of the causes for uncertainty in the frictional pressure drop estimation in mine airways.

The following are suggestions for future research work:

i. Fractals need more in-depth understanding for their sensible application mine ventilation.

ii. 3-D velocity profile measurements at various cross-sections along the length in the existing wavy wall model could be very useful in better understanding of the flow phenomenon and

the effective hydraulic diameter.

iii. Further study on the effect of waviness can be carried out using the same experimental set-up by adding small scale roughness, and altering the waviness when roof and the floor are in phase with each other.

iv. Further study on the effect of waviness needs to be carried out in the laboratory under controlled conditions in order to see if a relationship to static pressure drop can be established, which, if this proves this to be the case, can be verified by in-situ mine measurements.

7. REFERENCES

Banik, J., 1990. Airflow Characteristics Over Rough Surfaces. Master's Thesis. Department of Material Science and Mineral Engineering, University of California, Berkeley. 120 p.

Banik, J., McPherson, M. J., Calizaya, F., & Mousset-Jones, P., 1993, The Application of Fractal Analysis to Mine Airways. Proceedings of the 6th U.S. Mine Ventilation Symposium. SME, Littleton, CO. pp 125-130.

Barnes, R. J., & Rellier, F., 1989, Adjustment of Mine Ventilation System Parameters. Proceedings of the 4th U.S. Mine Ventilation Symposium. SME, Littleton, CO. pp 113-122.

Benzer, Jr., W. B., 1989, On the Use of the Variogram for the Estimation of Rock Surface Profile Fractal Dimension. Master's Thesis, Department of Geological Engineering, University of Nevada, Reno. 170 p.

Brown, S. R., 1987, Fluid Flow through Rock Joints: The Effect of Surface Roughness. Journal Geophysical Research. Vol. 92. pp 1337-1347.

Calizaya, F., You. K., McPherson, M. J., Danko, G., & Mousset-Jones, P., 1991, The Flow of Air Over Rough Surfaces In Simulated Mine Openings. Proceedings of 5th U.S. Mine Ventilation Symposium. S.M.E., Littleton, CO. pp. 447-457.

Calizaya, F., McPherson M. J., & Mousset-Jones, P., 1990. The Effect of Flow Direction on Friction Factor in Simulated Mine Openings. Proceedings of the 8th Annual Workshop. Generic Mineral Technology Center for Mine System Design and Ground Control. University of Nevada, Reno. 12 p.

Carr, J. R. 1990. Surface Roughness Characterization of Rockmasses Using The Fractal Dimension and the Variogram. Department Of Army Technical Report, REMR-GF143.

Carr, J. R. & Benzer, W. B. 1991, On the Practice of Fractal Dimension. Mathematical Geology, Vol 23, No. 7, pp. 945-958.

Carr, J. R., & Warriner, J. B., 1989, Relationship between Fractal Dimension and Joint Roughness Coefficient. Bulletin of Association of Engineering Geologists. Vol. XXVI, No. 2. pp 253-263.

Carr, J. R., & Warriner, J. B., 1987, Rockmass Classification using Fractal Dimension. Proceedings of 28th U.S. Symposium on Rock Mechanics. Balkema, Rotterdam. pp 73-80.

Daily, J. W., & Harleman, D. R. F., 1966, Fluid Dynamics. Addison-Wesley Publishing Company, Inc. 454 p.

Danko, G., 1993, Personnel Communication.

Danko, G., & Cifka, I., 1984, Measurement of the Convective Heat Transfer Coefficient on Naturally Rough Tunnel Surfaces. Proceedings of the III International Mine Ventilation Congress. Harrogate, England. pp 375-380.

Danko, G., & Mousset-Jones, P., 1988, Heat, Mass and Impulse Transport Analyses for Underground Airways. Proceedings of 4th International Mine Ventilation Congress. Brisbane, Australia. pp 237-247.

Davies, J. T., 1972, Turbulence Phenomena. Academic Press, New York. 412 p.

Feder, J., 1988, Fractals. Plenum Press, New York. 283 p.

Hartman, H. L., 1987, Introductory Mining Engineering. John-Wiley & Sons, Inc., New York. 633 p.

Hartman, H. L., 1982, Mine Ventilation and Air Conditioning. Second Edition, John Wiley & Sons, New York. 791 p.

Huang, S. L., Oelfke, S. M., & Speck, R. C., 1992, Applicability of Fractal Characterization and Modelling to Rock Joint Profiles. International Journal of Rock Mechanics, Mining Sciences and Geomechanics, Vol 29, No 2. pp. 89-98.

John, J. E. A., 1984, Gas Dynamics. Alan & Bacon, Inc., Boston. 426 p.

Jeffery, A. J., & Durucan, S., 1993, The Measurement and Characterization of Tunnel Roughness with Respect to Ventilation and Heat Flow Theory. Proceedings of the 6th US Mine Ventilation Symposium. SME, Littleton, CO. pp. 131-136.

Kaye, B. H., 1989, A Random Walk Through Fractal Dimensions. VCH Publishers, New York.

Kharkar, R., Stefanko, R., & Ramani, R. V., 1973, Analyses of Leakage and Friction Factor in Coal Mine Ventilation Systems. Special Research Report, No. SR-99 PA, Department of Commerce, Harrisburg, Pennsylvania, 73 p.

Konduri, I. M., 1992, Study of Airflow Over Natural Rough Surfaces. Masters Thesis Proposal (Unpublished). 10 p.

Konduri, I. M., 1991, Numerical Modelling of Mine Pollutants in Mine Airways. Master's Thesis. Department of Mining Engineering. Banaras Hindu University. Varanasi, India.

Konduri, I. M., Calizaya, F., Mousset-Jones, P., Danko, G., & McPherson., M. J., 1993, Surface Roughness Characterization for a Mine Airway in the Sunshine Mine. Proceedings of the 6th U.S. Mine Ventilation Symposium. SME, Littleton, CO. pp 137-143.

Konduri, I. M. Calizaya, F. Mousset-Jones, P. Danko, G. & McPherson, M. J. 1992, Surface Roughness Characterization for a Mine Airway in the Sunshine Mine. Proceedings of 10th

Workshop of the Generic Mineral Research Center for Mine Systems Design and Ground Control, Moscow, Idaho. 12 p.

Gangal, M. K., Notley, K. R., & Archibald, J. F., 1985, Analysis of Friction Factors in Mine Ventilation Systems. Proceedings of the 2nd U.S. Mine Ventilation Symposium. Balkema, Rotterdam. pp 707-713.

La Brecque, M., 1986, Fractal Applications, Mosaic, Vol. 17, No. 4. pp 34-38.

Mandelbrot, B. B., 1984, Fractals in Physics: Squig Clusters, Diffusions, Fractal Measures, and the Unicity of Fractal Dimensionality. Journal of Statistical Physics, Vol. 34. pp 895-930.

Mandelbrot, B. B., 1983, The Fractal Geometry of the Nature. W.H. Freeman Company, San Francisco. 468 p.

Mandelbrot, B. B., Passoja, D. E., & Paullay, A. J., 1984, Fractal Character of Fracture Surfaces of Metals. Nature, v. 308, pp. 721-722.

Mandelbrot, B. B., 1967, How Long Is the Coast of Great Britain? Statistical Self-Similarity and the Fractal Dimension. Science, v. 156, pp. 636-638.

Mandelbrot, B. B., Von Ness, J. W., 1968, Fractional Brownian Motion. Fractional Noises. and Applications. SIAM Review, Vol. 10, 4. pp 422-437.

McElroy, G. E. 1935, Engineering Factors in Ventilation of Metal Mines. Bureau of Mines Bulletin, No.: 385, p. 43.

McPherson, M. J., 1993, Mine Ventilation and Subsurface Environmental Engineering. Chapman & Hall, London. 900 p.

McPherson, M. J., 1988, An Analysis of Resistance and Airflow Characteristics of Mine Shafts. Proceedings of 4th International Mine Ventilation Congress, Brisbane, Australia. pp 55-92.

McPherson, M. J., 1987, The Resistance to Airflow of Mine Shafts. Proceedings of the 3rd U.S. Mine Ventilation Symposium, SME, Littleton, CO. pp 465-477.

Moody, L. F., 1944, Friction Factors for Pipe Flow. Transactions, ASME, Vol. 66. pp 135-176.

Moody, L. F., 1944, Friction Factors for Pipe Flow. Transactions, ASME, Vol. 66. pp 671-677.

Notley, K. R., 1985, A Study to Determine Friction Factors of Mine Airways, The Canada Center for Mineral and Energy Technology Report, Report No. OST84-00243, Department of Mining Engineering, Queens University, Canada. 95 p.

Nikuradse, J., 1950, Law of Flow in Rough Pipes. NACA Technical Memorandum. No. 1292.

Nikuradse, J., 1933, Stromungsgesetze in Rauhen Rohren. Ver. Dtsch. Ing. Forschungsh, Vol. 361.

Panton, R. L., 1984, Incompressible Flow. John Wiley & Sons, New York. 780 p.

Press, W. H., Flannery, B. R., Teukolsky, S.A., & Vetterling, W. T., 1989, Numerical Recipes: The Art of Scientific Computing (FORTRAN Version). Cambridge University Press, New York. pp. 381-429.

Rahim, M. O., Patnaik, N. K., 1976, Determination of the Frictional Coefficient of Mine Airways with Varied Lining and Support Systems. Journal of Mines, Metals and Fuels. Vol. 7. pp 222-229.

Richardson, L. F., 1961, The Problem of Contiguity, General Systems Yearbook, Vol. 6. pp 139-187.

Shames, I. H., 1984, Mechanics of Fluids. Second Edition, McGraw-Hill Book Company, New York. 692 p.

Suape, D., 1987, Algorithms for Random Fractals, Course Notes for Course 15: Fractals:

Introduction, Basics and Perspectives: given at SIGGRAPH '87', Anaheim, California (U.S.A.), July 27-31.

Taylor, R. P., Coleman, H. W., & Hodge, B. K., 1984, A Discrete Element Prediction Approach for Turbulent Flow Over Rough Surfaces. Report TDF-84-1, Mechanical and Nuclear Engineering Department, Mississippi State University.

Thakur, P. C., 1979, Methane Drainage and Transport in Consol Mines. Pittsburgh Mining Institute Annual Meeting, Pittsburgh, Nov. 8-9.

Von Karman, Th., 1939, Analogy Between Fluid Friction and Heat Transfer. Transactions, ASME, Vol. 61. pp. 705-710.

Wala, A. M., 1991. Studies of Friction Factors for Kentucky's Coal Mines. Proceedings of 5th U.S. Mine Ventilation Symposium. S.M.E., Littleton, CO. pp. 675-684.

White, F. M., 1991, Viscous Fluid Flow. McGraw-Hill, Inc. 614 p.

White, R.J., 1982, Physical Parameters and the Friction Factor of Mine Airways. Ph.D. Dissertation, University of Idaho, Moscow. pp 58-125.

APPENDIX A

Estimates of Cross-sectional Area and Perimeter from Laser Profiling
(Each profile is taken at 0.2 m interval along the base line)

TEST SECTION I (177 profiles)			TEST SECTION II (78 profiles)		
Profile Number	Area (m^2)	Perimeter Number (m)	Profile Area	Perimeter (m^2)	(m)
1	10.091	7.726	1	9.714	6.588
2	10.312	6.954	2	9.838	6.627
3	10.502	7.075	3	9.983	6.62
4	10.251	6.863	4	10.158	6.474
5	10.471	6.867	5	9.769	6.527
6	10.005	6.762	6	9.653	6.425
7	10.137	6.833	7	9.64	6.321
8	10.283	6.874	8	9.534	6.281
9	10.505	6.94	9	9.805	6.249
10	10.229	6.735	10	9.792	6.368
11	9.989	6.878	11	9.817	6.404
12	9.973	6.8	12	9.685	6.173
13	10.047	6.932	13	9.571	6.251
14	10.21	6.878	14	9.782	6.292
15	10.232	6.92	15	9.707	6.285
16	10.057	6.793	16	9.899	6.434
17	9.967	6.834	17	9.795	6.489
18	10.2	6.854	18	9.756	6.462
19	9.87	6.809	19	9.695	6.292
20	9.81	6.668	20	9.566	6.398
21	10.351	7.205	21	9.538	6.293
22	10.384	7.565	22	9.643	6.21

Profile Number	Area (m^2)	Perimeter Number (m)	Profile Area	Perimeter (m^2)	(m)
23	10.668	7.767	23	9.728	6.327
24	10.605	7.846	24	9.561	6.339
25	10.669	7.879	25	9.735	6.386
26	10.792	7.983	26	9.917	6.484
27	10.618	7.841	27	9.677	6.299
28	10.326	7.408	28	9.845	6.225
29	10.165	7.086	29	9.859	6.254
30	10.147	6.851	30	9.707	6.261
31	10.186	6.723	31	9.67	6.219
32	10.221	6.814	32	9.576	6.229
33	10.107	6.834	33	9.574	6.241
34	9.959	6.78	34	9.68	6.357
35	9.926	6.569	35	9.627	6.428
36	10.218	6.996	36	9.739	6.434
37	10.375	7.279	37	9.854	6.435
38	10.398	7.363	38	9.775	6.403
39	10.606	7.318	39	9.555	6.315
40	10.574	7.328	40	9.54	6.237
41	10.385	7.215	41	9.613	6.194
42	9.989	6.869	42	9.37	6.099
43	10	6.738	43	9.561	6.107
44	10.269	6.74	44	9.307	5.972
45	10.263	6.702	45	9.296	5.947
46	10.265	6.76	46	9.563	5.963
47	10.275	6.892	47	9.386	5.906
48	10.276	7.091	48	9.406	5.95
49	10.345	7.321	49	9.577	5.923

Profile Number	Area (m^2)	Perimeter Number (m)	Profile Area	/Perimeter (m^2)	(m)
50	10.408	7.48	50	9.392	5.708
51	10.621	7.704	51	9.318	5.558
52	10.848	7.532	52	9.015	5.492
53	10.633	7.474	53	9.064	5.397
54	10.345	7.063	54	9.134	5.442
55	9.836	6.59	55	9.344	5.524
56	10.121	6.632	56	9.18	5.558
57	9.748	6.445	57	9.21	5.491
58	9.828	6.471	58	9.254	5.701
59	9.819	6.62	59	9.547	5.966
60	10.008	6.716	60	9.706	6.112
61	9.879	6.755	61	9.738	6.183
62	9.96	6.778	62	9.738	6.171
63	9.771	6.783	63	9.669	6.248
64	10.046	6.784	64	9.657	6.297
65	9.863	6.73	65	9.632	6.353
66	9.744	6.497	66	9.921	6.619
67	9.602	6.414	67	10.02	6.54
68	9.795	6.595	68	10.051	6.572
69	9.931	6.551	69	9.928	6.497
70	10.108	6.744	70	9.705	6.326
71	10.131	6.812	71	9.708	6.294
72	9.829	6.822	72	9.666	6.306
73	10.273	6.874	73	9.983	6.674
74	10.19	6.938	74	10.342	6.917
75	10.327	6.879	75	10.16	7.065
76	10.075	7.082	76	10.261	7.012
77	10.226	7.1	77	9.868	6.979

Profile Number	Area (m^2)	Perimeter Number (m)	Profile Area	/Perimeter (m^2)	(m)
78	10.234	6.95	78	9.671	6.276
79	10.145	6.917			
80	9.772	6.697			
81	9.743	6.555			
82	9.73	6.467			
83	9.778	6.339			
84	9.711	6.357			
85	9.723	6.369			
86	9.556	6.199			
87	9.165	5.882			
88	9.293	5.757			
89	9.617	5.969			
90	9.543	6.016			
91	9.594	5.934			
92	9.532	6.111			
93	9.78	6.348			
94	9.908	6.602			
95	10.218	6.897			
96	10.59	7.084			
97	10.604	7.272			
98	10.701	7.395			
99	10.608	7.319			
100	10.1	6.981			
101	9.917	6.67			
102	9.913	6.6			
103	9.87	6.556			
104	9.907	6.411			

Profile Number	Area (m^2)	Perimeter Number (m)
105	10.236	6.558
106	10.135	6.794
107	10.172	6.923
108	10.371	7.236
109	10.295	7.282
110	10.271	7.381
111	10.417	7.199
112	10.514	7.499
113	10.494	7.453
114	10.213	7.326
115	10.128	6.932
116	9.812	6.605
117	9.493	6.274
118	9.23	6.011
119	9.165	5.802
120	9.189	5.751
121	9.219	5.566
122	9.257	5.672
123	9.335	5.844
124	9.526	5.902
125	9.225	5.764
126	9.013	5.63
127	9.073	5.613
128	9.254	5.618
129	9.074	5.477
130	9.299	5.887
131	9.414	6.035
132	9.342	6.054
133	9.45	6.106

Profile Number	Area (m^2)	Perimeter (m)
134	9.398	6.186
135	9.571	5.94
136	9.004	5.595
137	8.775	5.242
138	8.91	5.174
139	9.054	5.086
140	8.686	5.165
141	8.99	5.343
142	9.129	5.355
143	9.058	5.476
144	9.08	5.584
145	9.162	5.666
146	9.312	6.012
147	9.563	6.245
148	9.569	6.431
149	9.807	6.654
150	10.089	7.097
151	10.561	7.381
152	10.622	7.462
153	10.639	7.511
154	10.608	7.389
155	10.537	7.224
156	10.566	7.182
157	10.372	7.13
158	10.284	7.009
159	10.27	7.083
160	10.099	6.923
161	9.993	6.631
162	9.908	6.559

Profile Number	Area (m^2)	Perimeter (m)
163	9.666	6.393
164	9.529	6.193
165	9.717	6.387
166	9.8	6.449
167	9.988	6.408
168	9.499	6.421
169	9.702	6.463
170	9.82	6.559
171	9.961	6.839
172	10.3	6.971
173	10.097	6.622
174	9.953	6.265
175	9.842	6.002
176	9.933	6.311
177	10.278	6.587

APPENDIX B

Longitudinal Profiles of the test sections in the Mine Drift in Sunshine Mine
(Radial distance from the base line of the laser profiler in meters)

TEST SECTION I

Position	Angular Position (Degree)								
(m)	-30^0	0^0	30^0	60^0	90^0	120^0	150^0	180^0	210^0
0	1.546	1.288	1.045	1.757	1.516	1.431	1.096	1.039	1.085
0.2	1.521	1.279	1.129	1.884	1.534	1.416	1.127	0.994	1.35
0.4	1.513	1.363	1.103	1.944	1.549	1.373	1.137	1.035	1.467
0.6	1.544	1.282	1.071	1.872	1.59	1.39	1.27	1.03	1.299
0.8	1.545	1.27	1.068	1.878	1.559	1.16	1.16	1.041	1.206
1	1.564	1.243	1.027	1.969	1.514	1.297	1.105	1.043	1.154
1.2	1.726	1.189	1.023	2.036	1.539	1.315	1.071	1.014	1.079
1.4	1.769	1.19	1.008	2.038	1.697	1.307	1.104	0.969	1.168
1.6	1.984	1.23	1.025	2.124	1.737	1.279	1.094	0.936	1.072
1.8	2.021	1.152	1.003	2.08	1.699	1.26	1.112	0.906	1.097
2	1.89	1.092	0.98	2.055	1.733	1.347	1.02	0.874	1.184
2.2	1.83	1.08	0.827	1.966	1.824	1.356	0.959	0.87	1.219
2.4	1.856	1.099	0.794	2.118	1.869	1.375	1.025	0.86	1.122
2.6	1.911	1.089	0.839	2.22	1.765	1.383	1.032	0.892	1.046
2.8	1.907	1.088	0.959	2.22	1.761	1.425	1.081	0.868	0.918
3	1.924	1.242	0.863	2.223	1.777	1.393	1.035	0.81	0.961
3.2	2.002	1.234	0.857	2.161	1.821	1.306	0.97	0.773	0.865
3.4	1.964	1.11	0.915	2.1	1.778	1.287	0.919	0.767	0.985
3.6	1.934	1.062	0.848	2.186	1.789	1.255	0.887	0.748	0.962
3.8	1.839	0.965	0.87	2.058	1.773	1.192	0.809	0.774	1.126
4	1.964	1.126	0.899	2.221	1.946	1.324	0.882	0.815	1.186

Position	Angular Position (Degree)								
(m)	-30^0	0^0	30^0	60^0	90^0	120^0	150^0	180^0	210^0
4.2	2.117	1.041	0.866	2.225	1.975	1.365	0.956	0.762	1.371
4.4	2.27	1.103	0.974	2.223	2.025	1.401	0.969	0.863	1.268
4.6	2.214	1.144	0.963	2.205	2.06	1.43	1.09	0.857	1.121
4.8	2.167	1.209	0.826	2.243	2.043	1.44	1.101	0.842	1.117
5	2.168	1.137	0.875	2.254	2.028	1.475	1.128	0.899	1.184
5.2	2.1	1.132	0.823	2.296	1.929	1.358	1.104	0.804	1.059
5.4	2.08	1.173	0.826	2.193	1.686	1.279	1.153	0.837	0.979
5.6	1.907	1.157	0.799	2.088	1.921	1.464	1.148	0.847	0.928
5.8	1.902	1.22	0.925	1.996	1.871	1.293	1.154	0.873	0.896
6	1.808	1.158	0.953	1.993	1.82	1.29	1.199	0.89	0.909
6.2	1.886	1.193	0.89	2.022	1.693	1.216	1.19	0.92	0.961
6.4	1.744	1.214	0.926	2.019	1.612	1.143	1.164	0.947	1.025
6.6	1.635	1.13	0.945	1.933	1.551	1.134	1.173	0.994	1.067
6.8	1.689	1.096	0.99	2.045	1.469	1.202	1.283	1.018	1.194
7	1.689	1.061	1.033	2.064	1.579	1.234	1.263	1.083	1.224
7.2	1.79	1.182	1.099	2.08	1.601	1.234	1.255	1.113	1.309
7.4	1.794	1.184	1.186	2.093	1.615	1.222	1.226	1.169	1.336
7.6	1.636	1.116	1.18	2.007	1.681	1.183	1.202	1.173	1.372
7.8	1.816	1.126	1.162	2.083	1.819	1.153	1.192	1.133	1.424
8	1.838	1.029	1.1	1.953	1.736	1.12	1.2	1.091	1.394
8.2	1.845	0.985	1.064	1.88	1.606	1.073	1.142	1.048	1.345
8.4	1.809	1.077	0.999	2.013	1.562	1.049	1.16	0.991	1.165
8.6	1.772	1.04	1.02	1.998	1.48	1.039	1.172	0.945	1.188
8.8	1.823	0.974	0.984	2.121	1.429	0.998	1.25	0.92	1.228
9	1.774	1.037	1.021	1.998	1.479	1.037	1.17	0.942	1.187
9.2	1.859	0.948	1.017	2.132	1.445	1.002	1.211	0.925	1.268
9.4	2.049	1.036	1.067	2.03	1.523	1.063	1.196	0.973	1.294
9.6	2.168	1.048	1.07	2.042	1.548	1.12	1.172	1.088	1.344

Position	Angular Position (Degree)								
(m)	-30^0	0^0	30^0	60^0	90^0	120^0	150^0	180^0	210^0
9.8	2.079	1.082	1.126	2.055	1.654	1.141	1.205	1.141	1.347
10	2.003	1.166	1.151	2.157	1.561	1.246	1.239	1.236	1.399
10.2	2.03	1.203	1.246	1.852	1.63	1.284	1.264	1.226	1.489
10.4	1.949	1.137	1.165	2.166	1.67	1.299	1.215	1.122	1.384
10.6	1.847	1.074	1.076	2.001	1.785	1.228	1.17	1.1	1.334
10.8	1.817	1.108	0.929	1.998	1.784	1.128	0.969	1.041	1.161
11	1.934	1.076	0.833	1.956	1.762	1.242	0.96	0.992	1.069
11.2	1.935	1.081	0.836	1.957	1.73	1.271	0.937	0.939	1.063
11.4	1.93	1.062	0.75	1.948	1.759	1.255	1.019	0.861	1.029
11.6	1.964	1.079	0.846	2.027	1.765	1.273	1.018	0.894	1.125
11.8	1.987	1.084	0.839	2.061	1.718	1.316	1.07	0.903	1.136
12.2	1.918	1.142	0.885	2.047	1.695	1.332	1.061	0.903	1.104
12.4	1.879	1.09	0.943	2.112	1.666	1.342	1.04	0.939	1.066
12.6	1.848	1.127	0.978	2.123	1.655	1.34	1.053	0.979	1.182
12.8	1.873	1.101	1.009	2.055	1.641	1.225	1.044	0.981	1.237
13	1.76	1.084	1.08	1.974	1.685	1.188	1.03	0.977	1.191
13.2	1.665	1.063	1.126	1.998	1.602	1.133	1.05	0.976	1.163
13.4	1.851	1.027	1.084	2.014	1.572	1.103	0.991	0.973	1.208
13.6	1.872	0.997	1.102	2.029	1.698	1.102	0.948	0.926	1.209
13.8	1.787	1.104	1.096	2.075	1.748	1.218	0.998	0.91	1.277
14	1.902	1.065	1.022	2.163	1.699	1.302	0.96	0.944	1.257
14.2	1.933	1.107	1.084	2.142	1.746	1.326	0.978	0.968	1.235
14.4	1.822	1.077	1.129	2.125	1.636	1.342	0.992	0.968	1.278
14.6	1.91	1.053	1.08	2.093	1.573	1.315	1.037	0.983	1.329
14.8	1.795	1.218	1.143	2.125	1.591	1.182	1.168	1.024	1.359
15	1.794	1.28	1.215	2.028	1.564	1.251	1.14	1.125	1.365
15.2	1.767	1.267	1.248	1.988	1.565	1.314	1.174	1.184	1.375
15.4	1.735	1.151	1.256	1.905	1.501	1.286	1.109	1.186	1.407

Position	Angular Position (Degree)								
(m)	-30^0	0^0	30^0	60^0	90^0	120^0	150^0	180^0	210^0
15.6	1.648	1.194	1.161	1.811	1.512	1.365	1.114	1.195	1.303
15.8	1.658	1.184	0.988	1.852	1.601	1.356	1.131	1.121	1.154
16	1.685	1.203	0.893	1.802	1.643	1.371	1.231	0.994	1.057
16.2	1.769	1.224	0.757	1.811	1.65	1.338	1.172	0.861	1.088
16.4	1.877	1.21	0.925	1.856	1.625	1.267	1.093	0.756	1.009
16.6	1.896	1.186	0.824	1.89	1.599	1.278	0.935	0.733	0.933
16.8	1.751	1.177	0.874	1.906	1.677	1.291	1.006	0.784	0.925
17	1.864	1.135	0.896	1.902	1.619	1.269	0.933	0.78	0.888
17.2	1.75	1.04	0.786	1.858	1.492	1.179	1.02	0.784	0.871
17.4	1.651	1.073	0.782	1.831	1.433	1.145	1.059	0.764	0.882
17.6	1.713	1.06	0.776	1.765	1.508	1.387	1.049	0.783	0.894
17.8	1.757	1.055	0.781	1.768	1.55	1.339	1.026	0.813	0.905
18	1.671	0.984	0.667	1.796	1.579	1.307	1.062	0.833	0.915
18.2	1.739	1.186	0.824	1.828	1.589	1.307	1.003	0.873	0.963
18.4	1.711	1.161	0.834	1.837	1.639	1.43	1.067	0.885	0.954
18.6	1.72	1.19	0.929	1.94	1.824	1.452	1.099	0.959	0.935
18.8	1.772	1.204	0.948	1.96	1.859	1.486	1.161	0.989	1.017
19	1.717	1.228	0.999	1.98	1.751	1.533	1.196	1.016	1.083
19.2	1.733	1.196	1.029	2.043	1.834	1.56	1.229	1.043	1.137
19.4	1.892	1.202	1.059	2.025	1.801	1.542	1.277	1.054	1.125
19.6	1.782	1.159	1.104	2.042	1.774	1.432	1.36	1.056	1.122
19.8	1.7	1.137	1.126	1.919	1.643	1.376	1.39	1.045	1.09
20	1.538	1.183	1.124	1.848	1.65	1.313	1.308	0.999	1.094
20.2	1.673	1.236	0.974	1.805	1.634	1.336	1.375	0.945	1.052
20.4	1.662	1.344	0.873	1.867	1.713	1.596	1.222	0.895	1.014
20.6	1.604	1.376	0.718	1.929	1.791	1.639	1.143	0.753	0.952
20.8	1.682	1.176	0.798	1.955	1.835	1.641	1.106	0.764	0.998
21	1.736	1.301	0.805	1.998	1.846	1.569	1.152	0.787	1.069

Position	Angular Position (Degree)								
(m)	-30^0	0^0	30^0	60^0	90^0	120^0	150^0	180^0	210^0
21.2	1.709	1.174	0.899	2.037	1.888	1.452	1.164	0.829	1.154
21.4	1.817	1.251	0.921	2.158	2.872	1.447	1.204	0.943	1.182
21.6	1.832	1.157	1.015	2.111	1.9	1.516	1.198	1.031	1.207
21.8	1.808	1.231	1.006	2.081	1.922	1.454	1.195	1.076	1.258
22	1.857	1.252	1.121	2.089	1.954	1.453	1.129	1.094	1.286
22.2	1.85	1.287	1.207	2.099	1.897	1.422	1.155	1.16	1.296
22.4	1.779	1.15	1.236	2.118	1.607	1.422	1.128	1.157	1.341
22.6	1.833	1.178	1.209	2.14	1.647	1.388	1.166	1.131	1.374
22.8	1.779	1.142	1.113	1.969	1.674	1.362	1.123	1.074	1.366
23	1.699	1.057	1.082	1.804	1.73	1.317	1.022	1.062	1.302
23.2	1.668	1.074	1.052	1.757	1.76	1.226	0.987	0.93	1.205
23.4	1.554	1.088	0.998	1.756	1.722	1.244	1.017	0.923	1.048
23.6	1.595	1.056	0.823	1.739	1.741	1.359	1.071	0.905	0.862
23.8	1.534	1.102	0.701	1.775	1.74	1.358	1.069	0.823	0.821
24	1.541	1.081	0.711	1.797	1.765	1.289	1.077	0.821	0.832
24.2	1.526	1.185	0.727	1.712	1.761	1.395	1.08	0.805	0.814
24.4	1.581	1.14	0.724	1.852	1.755	1.309	1.107	0.774	0.82
24.6	1.696	1.123	0.749	1.879	1.736	1.278	1.075	0.744	0.911
24.8	1.659	1.058	0.762	1.804	1.566	1.134	1.021	0.801	1.063
25	1.586	0.961	0.823	1.773	1.545	1.06	0.948	0.757	1.026
25.2	1.572	0.883	0.825	1.787	1.539	1.042	0.92	0.756	1.047
25.4	1.575	0.939	0.781	1.763	1.5	1.04	0.856	0.757	1.068
25.6	1.532	0.862	0.816	1.516	1.543	1.104	0.852	0.789	1.072
25.8	1.585	1.002	0.823	1.831	1.644	1.181	0.827	0.816	1.082
26	1.593	0.963	0.9	1.818	1.613	1.309	0.896	0.855	1.071
26.2	1.558	0.99	0.86	1.912	1.596	1.168	0.94	0.883	1.044
26.4	1.629	1.015	0.898	1.88	1.598	1.311	0.936	0.909	1.071
26.6	1.659	1.022	0.904	1.978	1.561	1.333	0.956	0.932	1.08

Position	Angular Position (Degree)								
(m)	-30^0	0^0	30^0	60^0	90^0	120^0	150^0	180^0	210^0
26.8	1.671	0.842	1.025	1.777	1.46	1.37	0.948	0.925	1.098
27	1.556	1.079	0.968	1.831	1.373	1.143	0.88	0.903	1.069
27.2	1.452	0.922	0.998	1.727	1.381	1.043	0.9	0.859	1.036
27.4	1.511	0.876	0.914	1.728	1.408	1.028	0.883	0.834	1.032
27.6	1.352	0.859	0.936	1.603	1.45	1.039	0.81	0.806	1.077
27.8	1.353	0.916	0.896	1.629	1.478	0.953	0.8	0.784	1.093
28	1.455	0.92	0.894	1.717	1.494	1.065	0.872	0.753	1.136
28.2	1.372	0.982	0.826	1.648	1.522	1.189	0.903	0.762	1.145
28.4	1.398	0.992	0.925	1.683	1.548	1.323	0.882	0.783	1.173
28.6	1.424	1.073	0.928	1.702	1.568	1.243	0.893	0.822	1.125
28.8	1.404	0.979	0.954	1.738	1.58	1.228	0.932	0.862	1.146
29	1.431	1.085	0.952	1.832	1.599	1.281	0.939	0.893	1.221
29.2	1.585	1.047	1.014	1.786	1.675	1.297	1.032	0.921	1.264
29.4	1.531	1.174	1.02	1.794	1.688	1.383	1.044	0.966	1.277
29.6	1.585	1.19	1.018	1.808	1.74	1.394	1.035	1.001	1.311
29.8	1.679	1.222	1.044	1.849	1.793	1.395	1.161	1.023	1.342
30	1.738	1.298	1.074	2.02	1.801	1.489	1.187	1.023	1.377
30.2	1.8	1.335	1.126	1.994	1.846	1.549	1.137	1.027	1.414
30.4	1.926	1.227	1.059	2.053	1.995	1.507	1.103	0.994	1.349
30.6	1.932	1.199	0.984	2.16	1.981	1.534	1.061	0.955	1.28
30.8	1.915	1.217	0.932	2.172	2.035	1.48	1.214	0.96	1.18
31	1.825	1.178	1.081	2.05	1.842	1.489	1.205	0.99	1.179
31.2	1.87	1.243	1.004	1.977	1.911	1.392	1.182	1.028	1.377
31.4	1.712	1.147	1.01	1.88	1.81	1.324	1.217	1.076	1.348
31.6	1.699	1.218	1.056	1.901	1.807	1.278	1.249	1.107	1.319
31.8	1.606	1.104	1.068	1.86	1.768	1.27	1.214	1.124	1.41
32	1.556	1.043	1.132	1.828	1.561	1.234	1.149	1.176	1.384
32.2	1.473	1.078	1.213	1.835	1.503	1.194	1.126	1.176	1.595

Position	Angular Position (Degree)								
(m)	-30^0	0^0	30^0	60^0	90^0	120^0	150^0	180^0	210^0
32.4	1.431	1.077	1.145	1.744	1.502	1.216	1.059	1.17	1.493
32.6	1.446	1.138	1.163	1.623	1.486	1.18	1.004	1.141	1.418
32.8	1.511	1.068	1.141	1.698	1.466	1.226	1.251	1.146	1.449
33	1.524	1.053	1.196	1.729	1.469	1.169	1.277	1.183	1.386
33.2	1.576	1.162	1.147	1.683	1.544	1.203	1.213	1.2	1.337
33.4	1.485	1.165	1.168	1.688	1.584	1.175	1.237	1.208	1.307
33.6	1.529	1.193	1.161	1.626	1.565	1.25	1.264	1.233	1.272
33.8	1.485	1.208	1.142	1.701	1.547	1.259	1.239	1.259	1.273
34	1.606	1.191	1.201	1.87	1.739	1.411	1.262	1.278	1.295
34.2	1.66	1.137	1.156	1.866	1.868	1.365	1.31	1.204	1.303
34.4	1.7	1.086	1.059	1.76	1.797	1.3	1.306	1.09	1.285
34.6	1.723	1.036	1	1.589	1.812	1.317	1.277	0.943	1.436
34.8	1.671	1.018	0.873	1.757	1.831	1.262	1.207	0.804	1.158
35	1.591	1.143	0.97	1.704	1.816	1.413	1.155	0.77	1.156
35.2	1.671	1.204	0.873	1.729	1.867	1.446	1.08	0.792	1.126

TEST SECTION II

Position	Angular Position (Degree)								
(m)	-30^0	0^0	30^0	60^0	90^0	120^0	150^0	180^0	210^0
0	2.343	2.048	1.78	1.271	0.945	0.695	0.606	0.453	0.606
0.2	2.444	2.045	1.654	1.058	0.81	0.837	0.819	0.878	1.003
0.4	2.493	2.071	1.631	1.074	0.791	0.849	0.813	0.784	0.962
0.6	2.509	2.068	1.715	1.093	0.785	0.764	0.776	0.806	0.908
0.8	2.48	2.052	1.731	1.086	0.785	0.778	0.748	0.843	0.829
1	2.435	2.042	1.738	1.096	0.795	0.726	0.688	0.822	0.932
1.2	2.363	1.978	1.773	1.121	0.799	0.74	0.659	0.814	0.899
1.4	2.325	1.934	1.771	1.068	0.77	0.711	0.626	0.747	0.915
1.6	2.297	2.015	1.694	1.013	0.774	0.703	0.645	0.71	0.851
1.8	2.371	2.023	1.754	0.976	0.805	0.785	0.645	0.654	0.726
2	2.379	2.072	1.748	1.28	0.875	0.758	0.616	0.609	0.668
2.2	2.445	2.081	1.798	1.19	0.866	0.772	0.556	0.596	0.706
2.4	2.452	2.043	1.777	1.342	0.809	0.775	0.565	0.566	0.76
2.6	2.411	2.017	1.758	1.325	0.88	0.735	0.594	0.523	0.683
2.8	2.401	1.994	1.727	1.328	0.929	0.713	0.599	0.545	0.694
3	2.41	1.995	1.734	1.327	0.922	0.713	0.602	0.552	0.692
3.2	2.427	1.976	1.702	1.308	0.855	0.704	0.611	0.574	0.722
3.4	2.426	2	1.716	1.338	0.853	0.73	0.649	0.607	0.711
3.6	2.338	2.003	1.726	1.271	0.877	0.752	0.654	0.586	0.684
3.8	2.296	2.037	1.624	1.291	0.925	0.709	0.588	0.542	0.686
4	2.322	2.061	1.725	1.221	0.961	0.742	0.568	0.505	0.589
4.2	2.343	2.053	1.776	1.207	0.876	0.734	0.557	0.518	0.568
4.4	2.317	2.064	1.678	1.147	0.956	0.771	0.562	0.524	0.595
4.6	2.38	2.08	1.676	1.23	1.032	0.733	0.547	0.5	0.581
4.8	2.281	2.1	1.715	1.269	0.988	0.795	0.574	0.502	0.578

Position	Angular Position (Degree)								
(m)	-30^0	0^0	30^0	60^0	90^0	120^0	150^0	180^0	210^0
5	2.328	2.026	1.768	1.273	0.995	0.826	0.602	0.488	0.528
5.2	2.42	2.065	1.767	1.293	0.944	0.893	0.584	0.483	0.556
5.4	2.425	2.046	1.721	1.235	0.876	0.81	0.64	0.509	0.573
5.6	2.391	2.064	1.77	1.307	0.907	0.723	0.635	0.463	0.536
5.8	2.335	2.053	1.777	1.3	0.958	0.688	0.679	0.466	0.572
6	2.302	2.073	1.785	1.316	0.95	0.672	0.594	0.456	0.53
6.2	2.269	2.066	1.762	1.318	0.98	0.642	0.492	0.457	0.546
6.4	2.336	2.073	1.769	1.225	0.993	0.693	0.553	0.458	0.607
6.6	2.334	2.079	1.777	1.222	0.956	0.727	0.52	0.459	0.676
6.8	2.315	2.101	1.813	1.283	0.853	0.834	0.566	0.63	0.694
7	2.362	2.113	1.827	1.343	0.876	0.916	0.652	0.814	0.895
7.2	2.343	2.09	1.832	1.397	0.895	0.931	0.62	0.549	0.599
7.4	2.356	2.067	1.868	1.331	0.933	0.884	0.675	0.585	0.568
7.6	2.428	2.039	1.883	1.332	0.975	0.781	0.694	0.584	0.518
7.8	2.43	2.026	1.853	1.28	1.033	0.733	0.529	0.537	0.585
8	2.399	2.004	1.816	1.274	0.989	0.678	0.589	0.476	0.535
8.2	2.343	2.048	1.78	1.271	0.945	0.695	0.606	0.453	0.606
8.4	2.337	2.001	1.728	1.305	0.898	0.728	0.5	0.469	0.605
8.6	2.234	1.983	1.71	1.33	0.894	0.756	0.532	0.473	0.604
8.8	2.278	1.943	1.659	1.213	0.914	0.754	0.583	0.478	0.571
9	2.338	1.896	1.604	1.238	0.902	0.76	0.604	0.477	0.559
9.2	2.332	1.881	1.436	1.215	0.926	0.764	0.588	0.524	0.569
9.4	2.256	1.957	1.712	1.195	0.956	0.74	0.604	0.552	0.618
9.6	2.23	1.938	1.728	1.202	0.948	0.722	0.615	0.55	0.649
9.8	2.17	1.909	1.737	1.215	0.925	0.692	0.66	0.546	0.679
10	2.152	1.874	1.7	1.206	0.883	0.666	0.68	0.515	0.7
10.2	2.093	1.847	1.667	1.17	0.862	0.61	0.675	0.49	0.663
10.4	2.128	1.836	1.655	1.126	0.856	0.585	0.552	0.619	0.744

Position	Angular Position (Degree)								
(m)	-30^0	0^0	30^0	60^0	90^0	120^0	150^0	180^0	210^0
10.6	2.113	1.927	1.556	0.996	0.846	0.519	0.493	0.62	0.754
10.8	2.188	2.004	1.561	1.01	0.942	0.518	0.48	0.677	0.87
11	2.264	1.972	1.569	1.033	0.948	0.582	0.486	0.526	0.565
11.2	2.291	1.925	1.552	1.136	1.044	0.643	0.499	0.664	0.82
11.4	2.203	1.897	1.555	1.168	1.087	0.704	0.556	0.488	0.419
11.6	2.26	1.869	1.639	1.231	1.04	0.75	0.61	0.658	0.705
11.8	2.232	1.856	1.715	1.363	1.069	0.768	0.616	0.626	0.636
12	2.283	1.851	1.72	1.439	1.08	0.809	0.608	0.947	1.2
12.2	2.141	1.844	1.724	1.381	1.041	0.834	0.646	0.578	0.578
12.4	2.133	1.885	1.725	1.332	0.986	0.94	0.673	0.569	0.617
12.6	2.152	1.887	1.709	1.316	0.954	0.934	0.726	0.581	0.721
12.8	2.201	1.871	1.73	1.326	1	0.941	0.705	0.612	1.05
13	2.212	1.903	1.793	1.347	1.081	1.013	0.706	0.6	0.716
13.2	2.197	1.935	1.868	1.393	1.097	1.074	0.743	0.614	0.748
13.4	2.189	1.951	1.894	1.381	1.133	1.166	0.654	0.584	0.736
13.6	2.16	1.944	2.007	1.409	1.15	1.123	0.695	0.578	0.741
13.8	2.133	1.906	1.981	1.368	1.138	0.955	0.727	0.566	0.781
14	2.143	1.884	1.909	1.332	1.108	0.962	0.76	0.584	0.772
14.2	2.184	1.928	1.902	1.336	1.116	0.786	0.696	0.659	0.788
14.4	2.192	2.001	1.836	1.295	1.099	0.703	0.711	0.623	0.758
14.6	2.296	2.231	1.867	1.329	1.054	0.709	0.733	0.622	0.8
14.8	2.329	2.161	1.983	1.372	1.061	0.736	0.706	0.636	0.774
15	2.339	2.148	2.085	1.441	1.092	0.83	0.77	0.657	0.735
15.2	2.354	2.092	2.1	1.455	1.002	0.895	0.842	0.714	0.782
15.4	2.318	2.086	2.109	1.411	0.945	0.74	0.705	0.742	0.799

APPENDIX C

Plot of Semi-variogram

Logarithmic Plot of Semi-variogram

-30 degrees, Section I

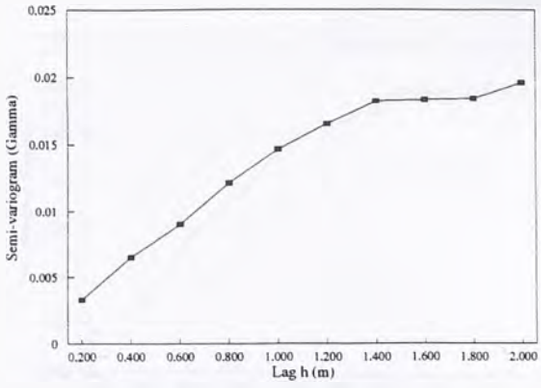

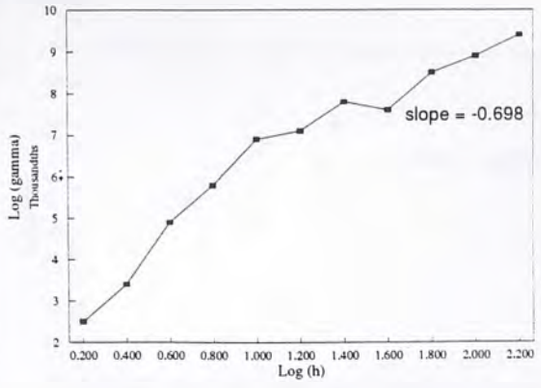

0 degree, Section I

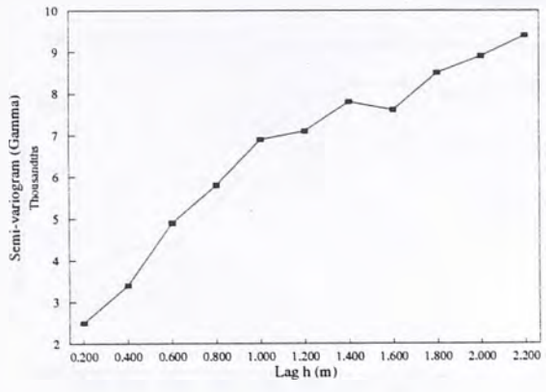

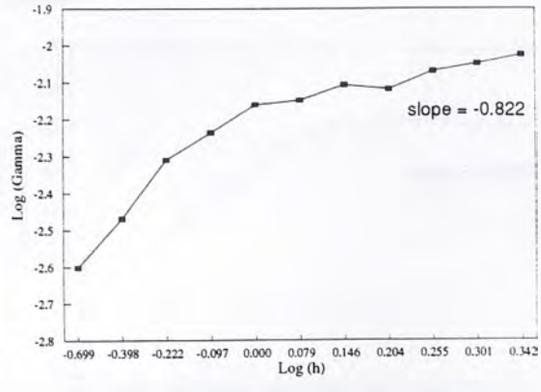

30 degrees, Secion I

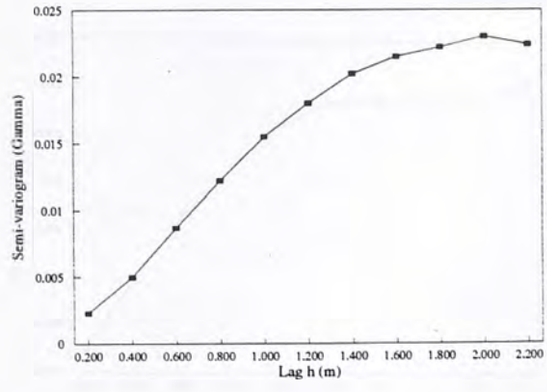

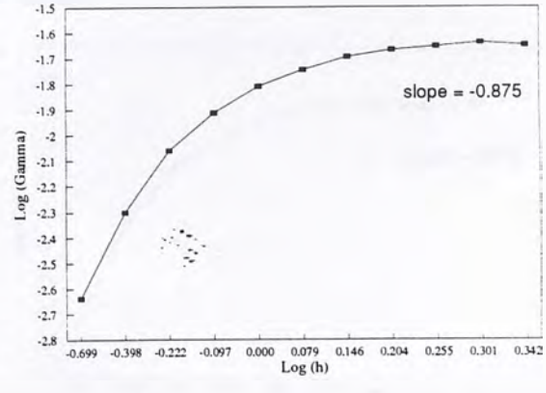

Plot of Semi-variogram

Logarithmic Plot of Sem-variogram

60 degrees, Section I

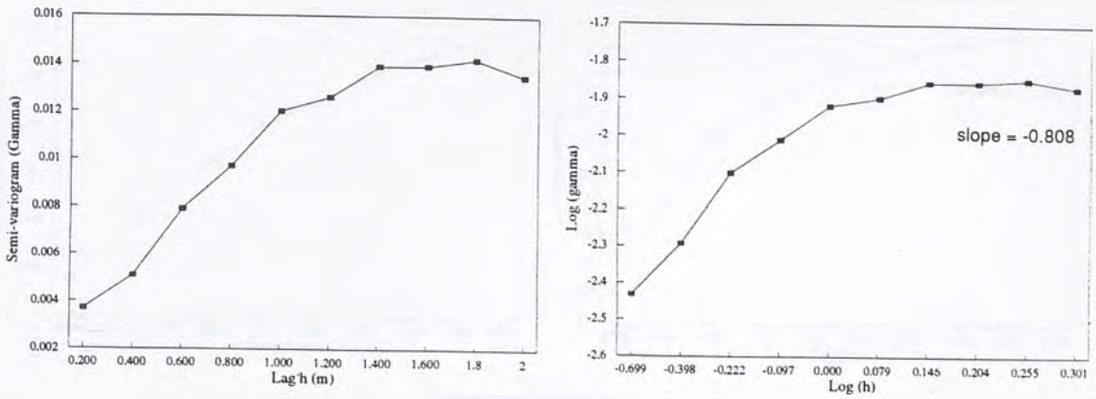

90 degree, Section I

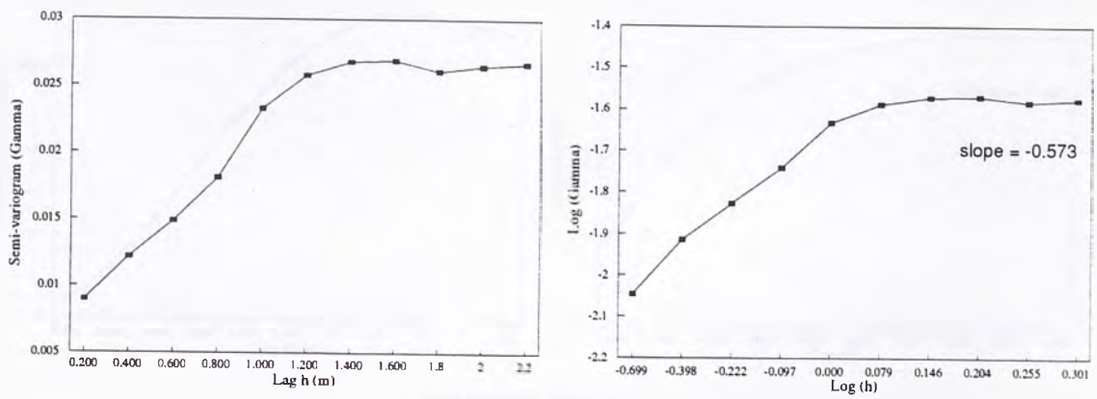

120 degrees, Secion I

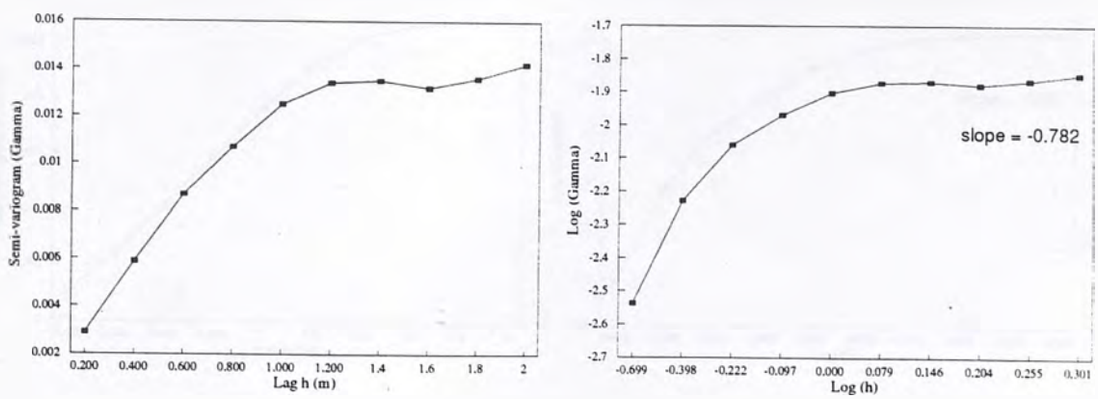

Plot of Semi-variogram

Logarithmic Plot of Sem-variogram

150 degrees, Section I

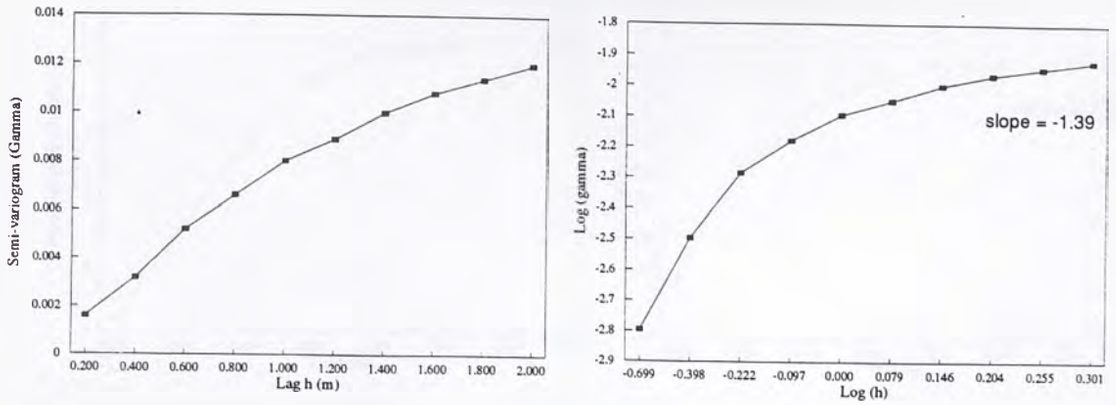

180 degree, Section I

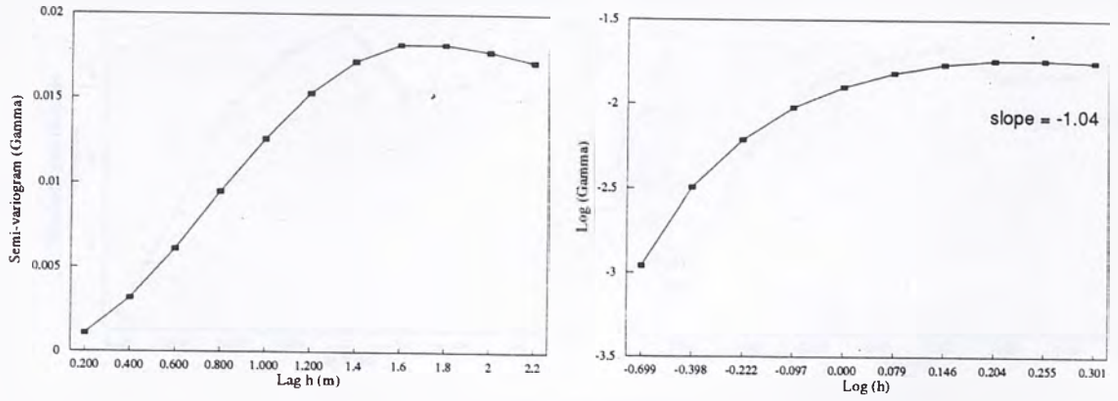

210 degrees, Secion I

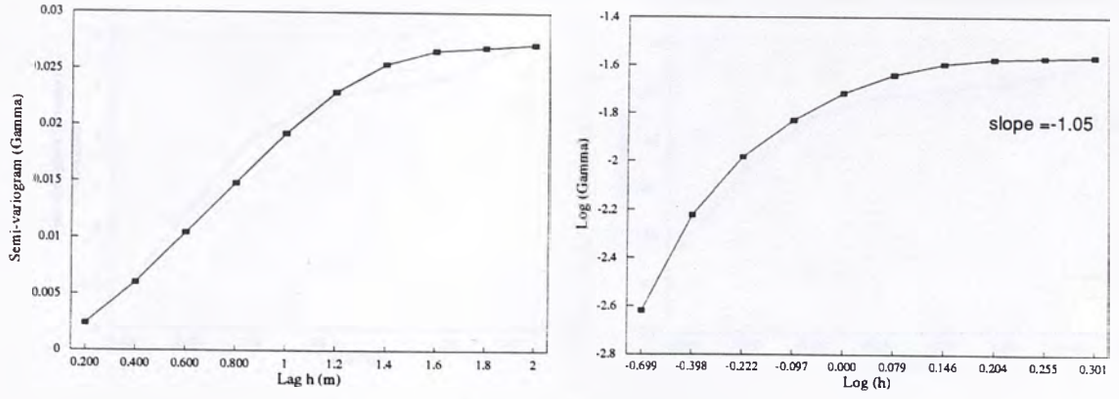

Plot of Semi-variogram

Logarithmic Plot of Sem-variogram

-30 degrees, Section II

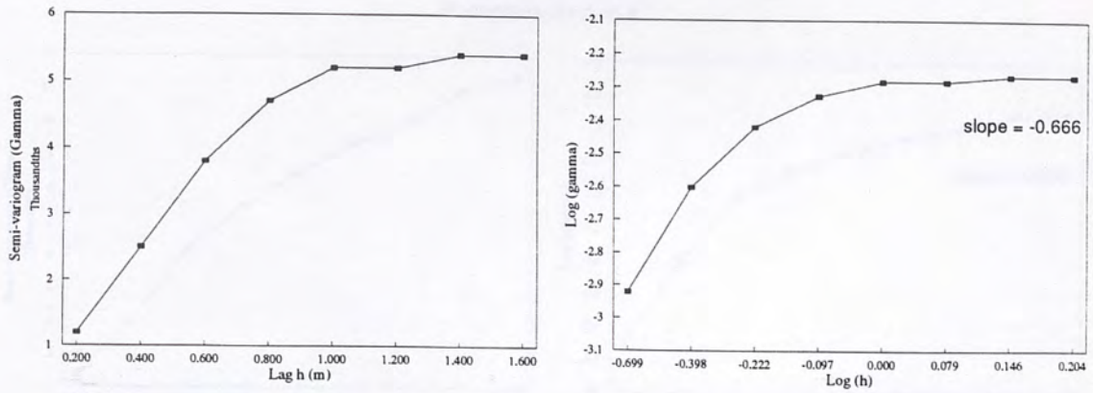

0 degree, Section II

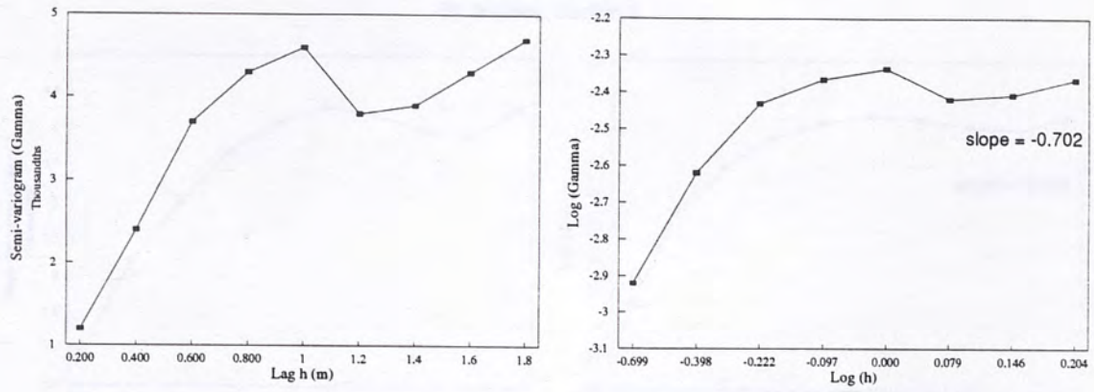

30 degrees, Secion II

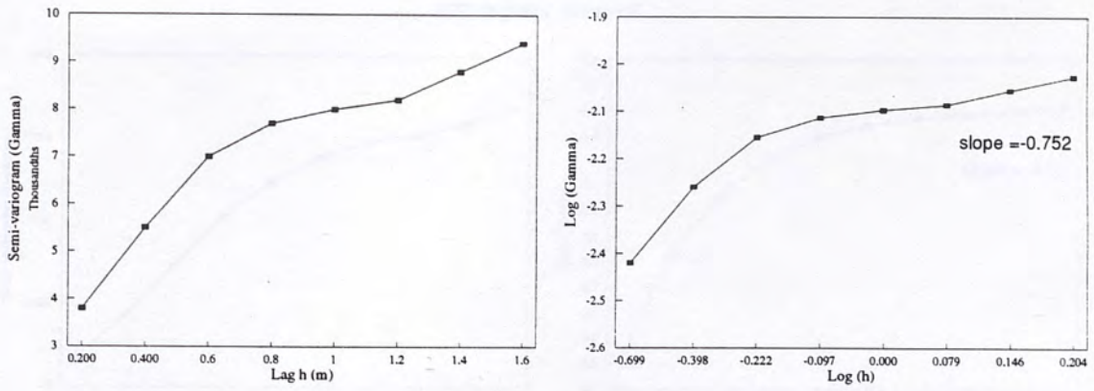

Plot of Semi-variogram

Logarithmic Plot of Sem-variogram

60 degrees, Section II

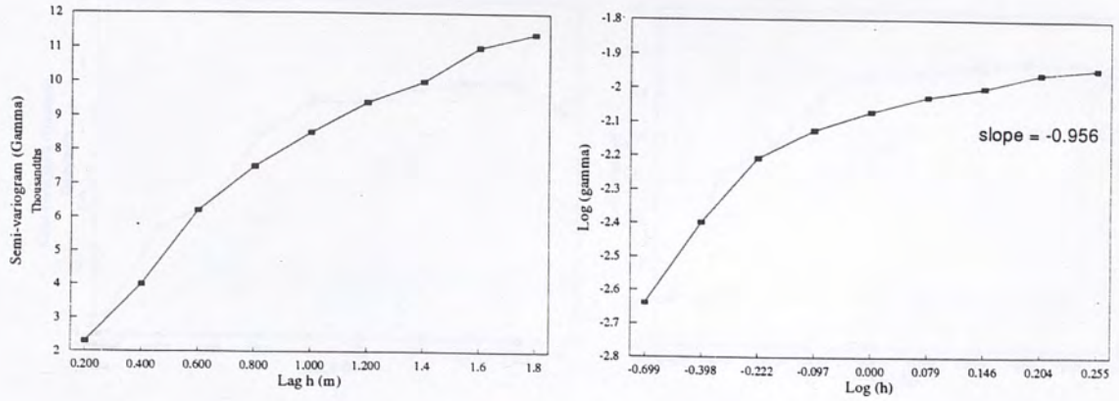

90 degrees, Section II

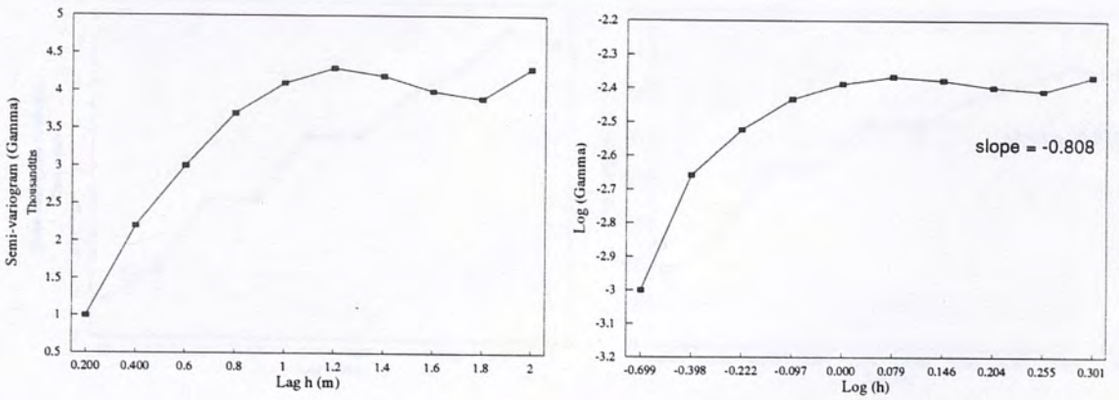

120 degrees, Secion II

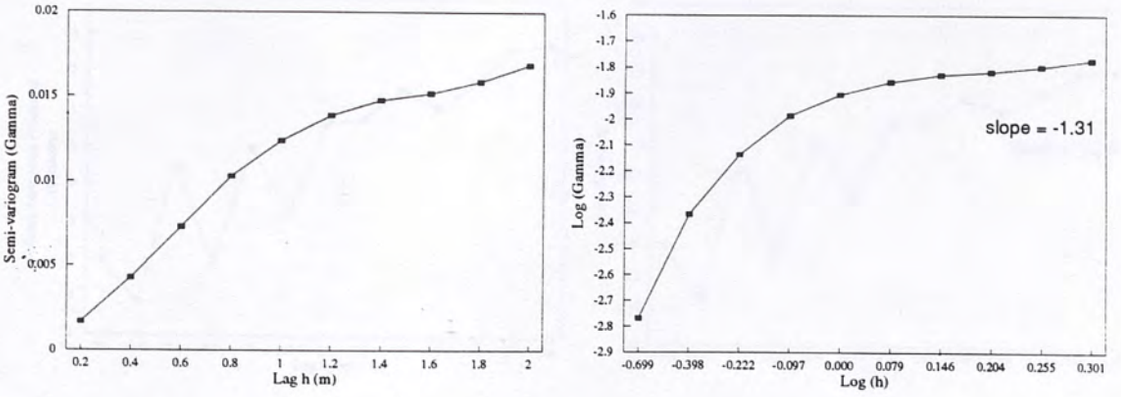

Plot of Semi-variogram

Logarithmic Plot of Sem-variogram

150 degrees, Section II

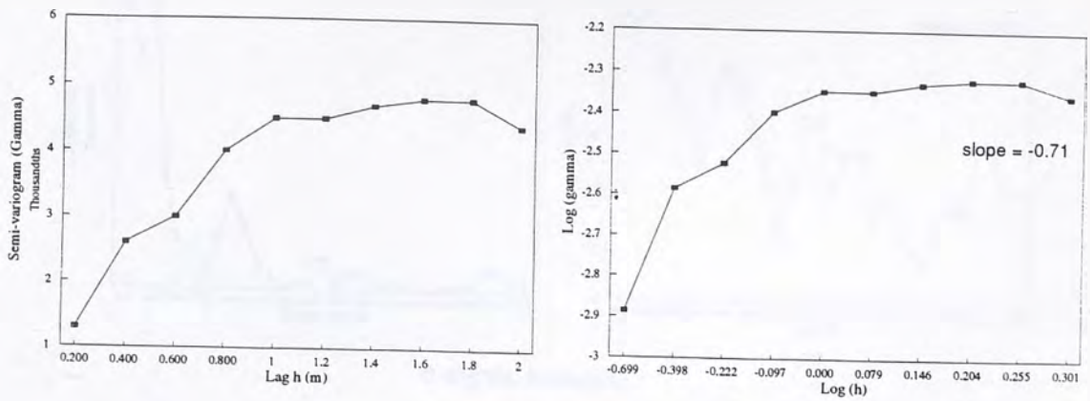

180 degrees, Section II

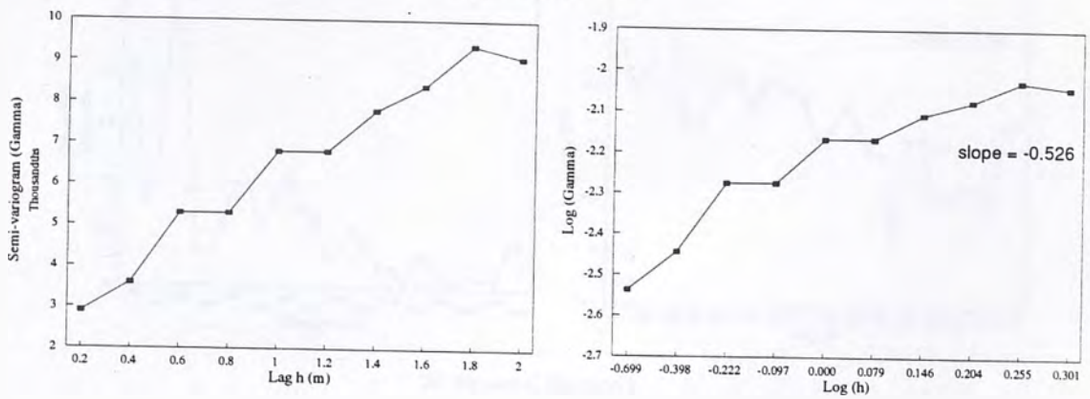

210 degrees, Secion II

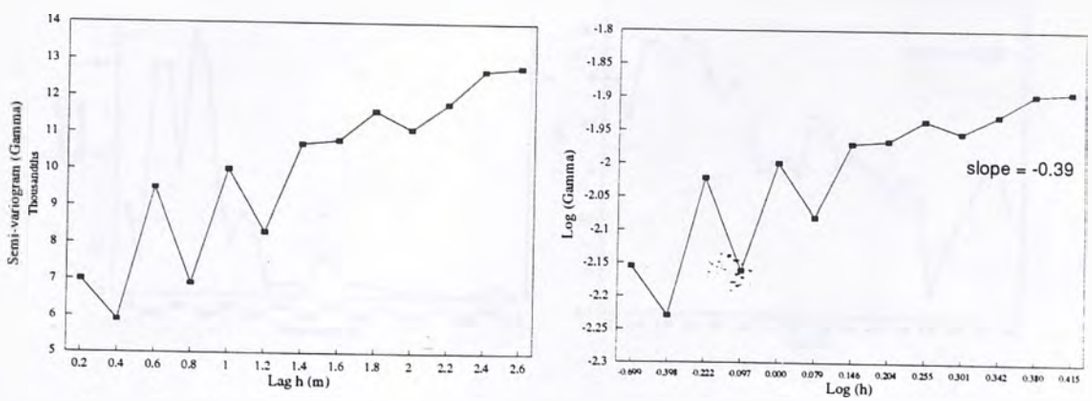

Plot of Power Spectrum

Plot of Log(Pf) vs Log(f)

-30 degrees, Section I

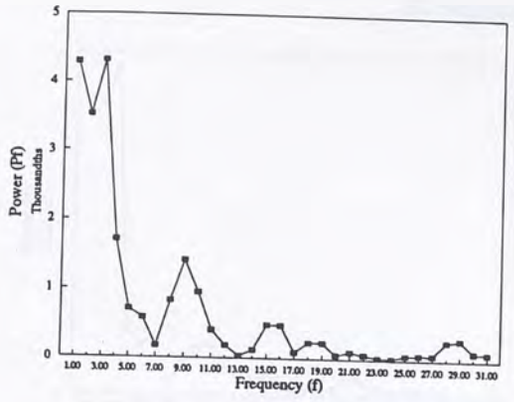

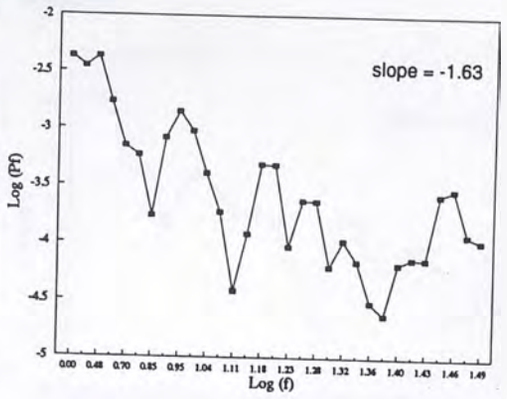

0 degree, Section I

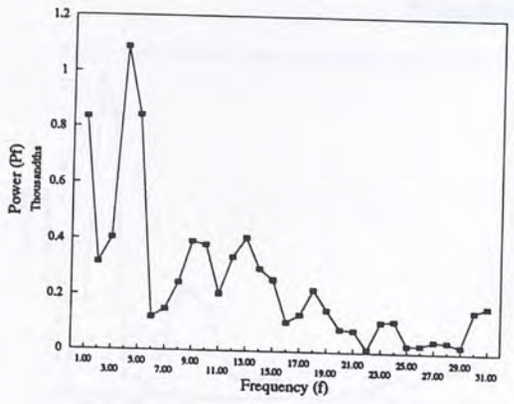

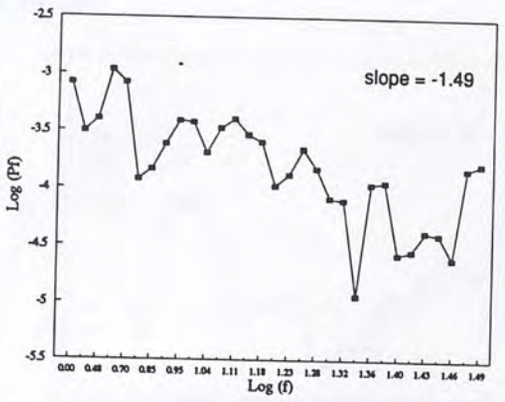

30 degrees, Section I

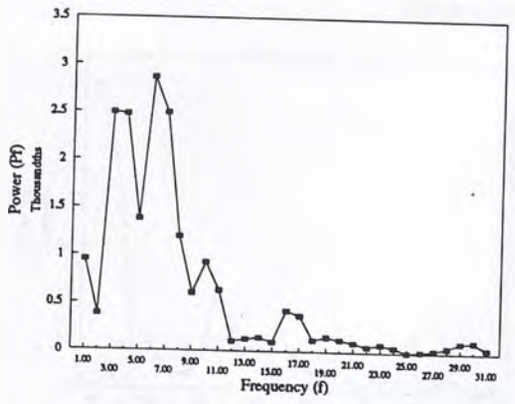

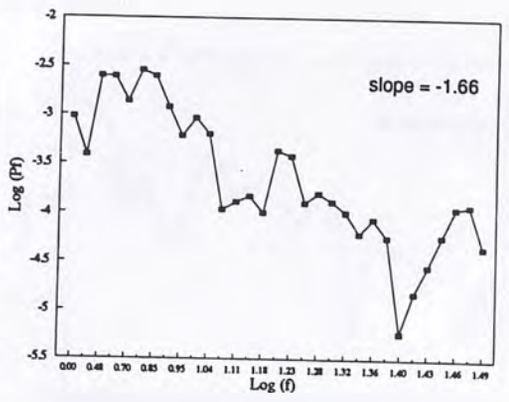

Plot of Power Spectrum

Plot of Log(Pf) vs Log(f)

60 degrees, Section I

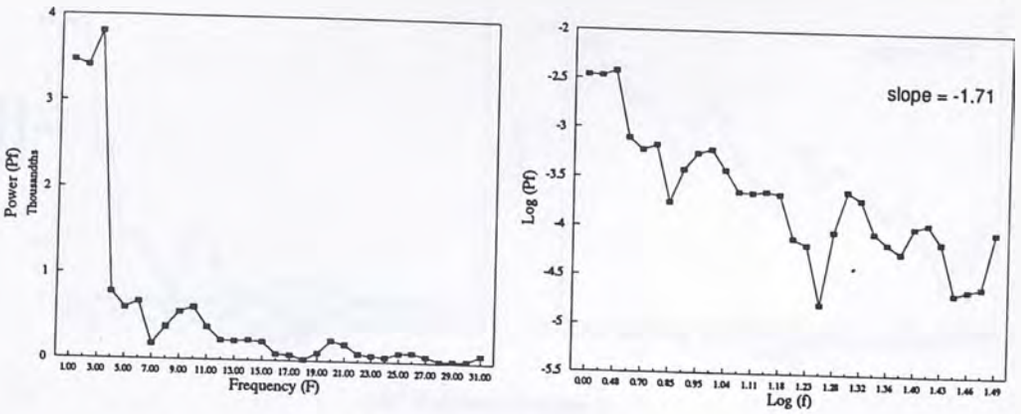

90 degrees, Section I

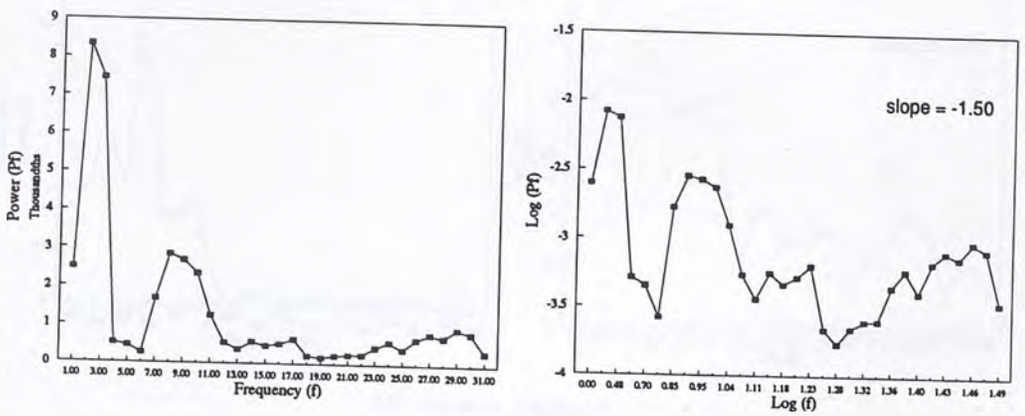

120 degrees, Section I

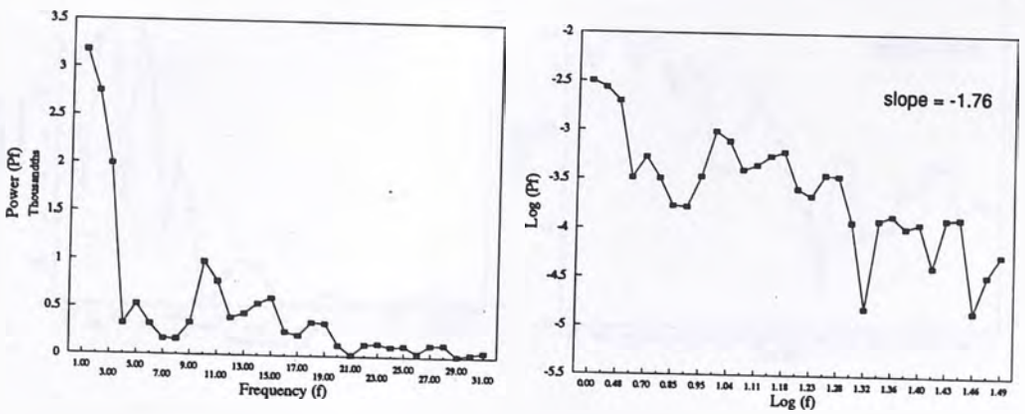

Plot of Power Spectrum

Plot of Log(Pf) vs Log(f)

150 degrees, Section I

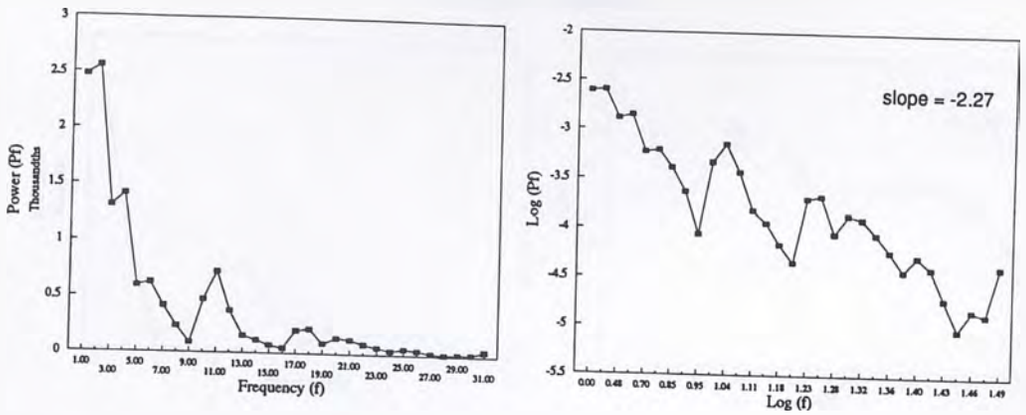

180 degrees, Section I

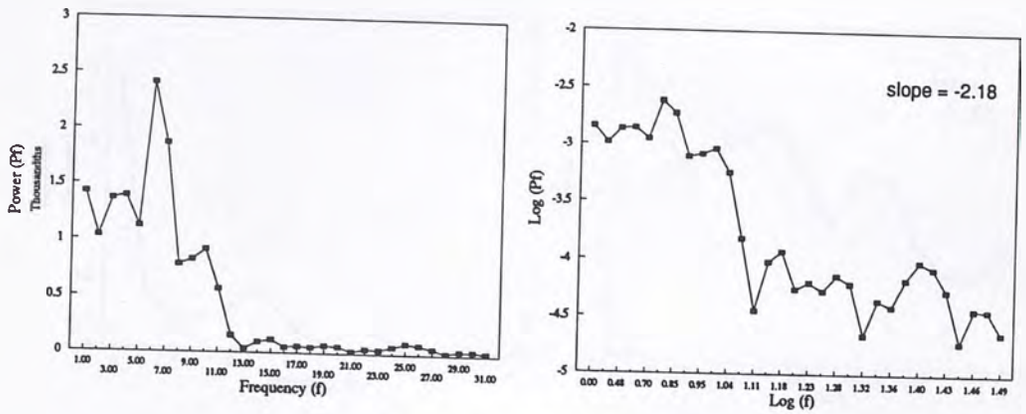

210 degrees, Section I

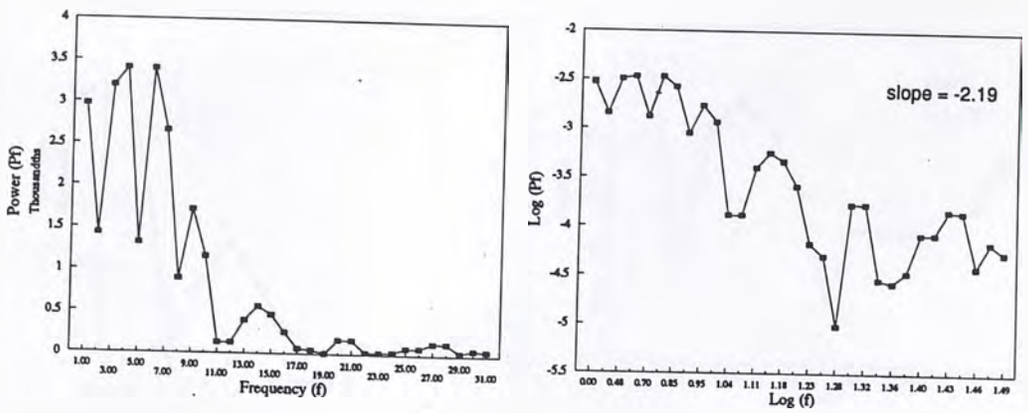

Plot Power Spectrum

Plot of Log(pf) vs. Log(f)

-30 degree, Section II

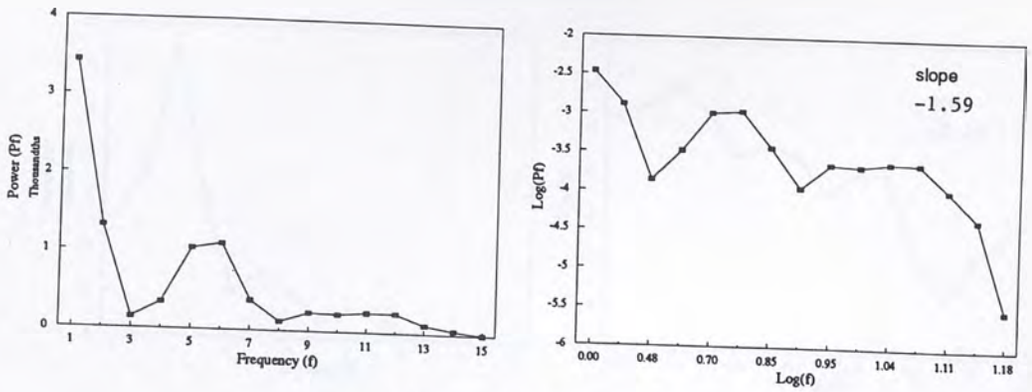

0 degree, Section II

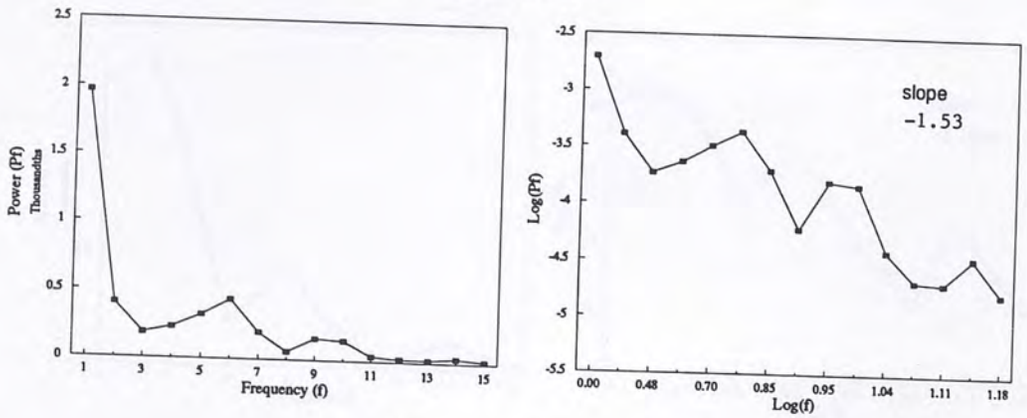

30 degree, Section II

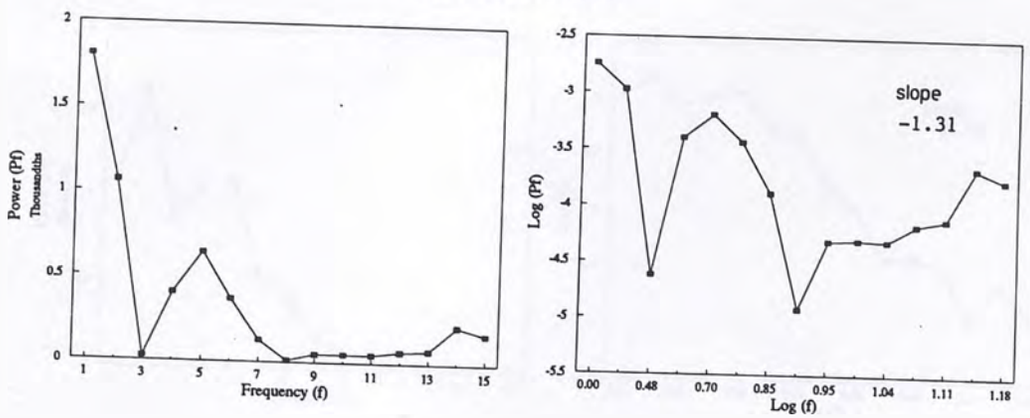

Plot of Power Spectrum

Plot of Log(Pf) vs. Log(f)

60 degree, Section II

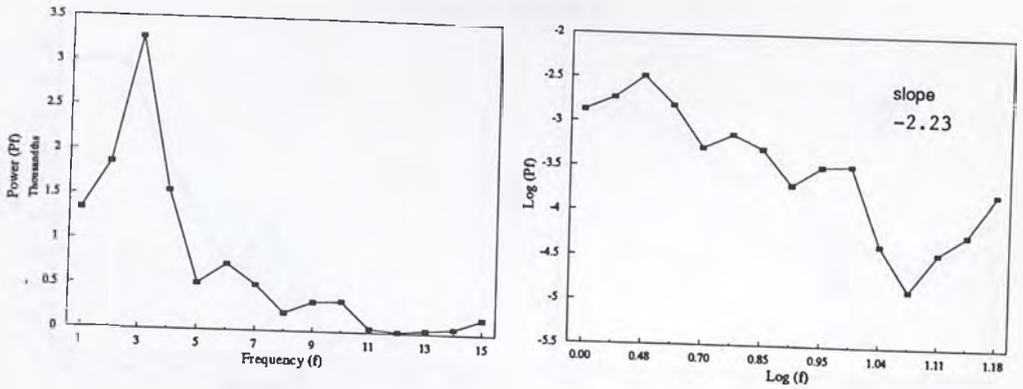

90 degree, Section II

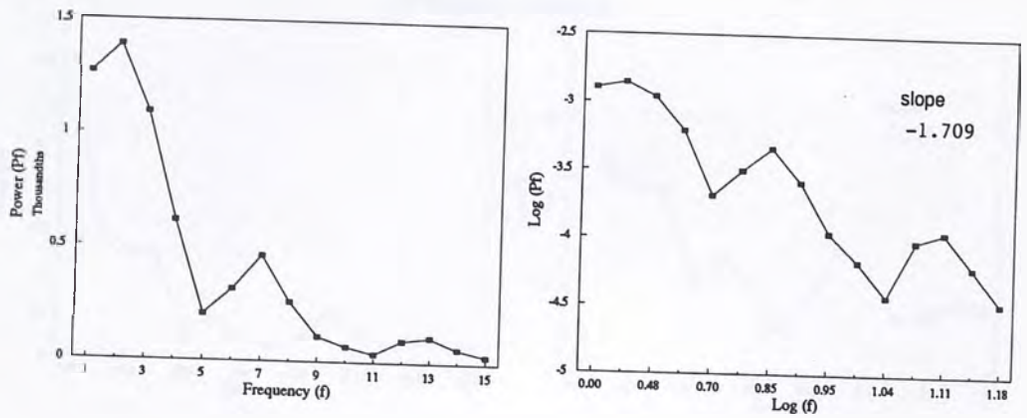

120 degree, Section II

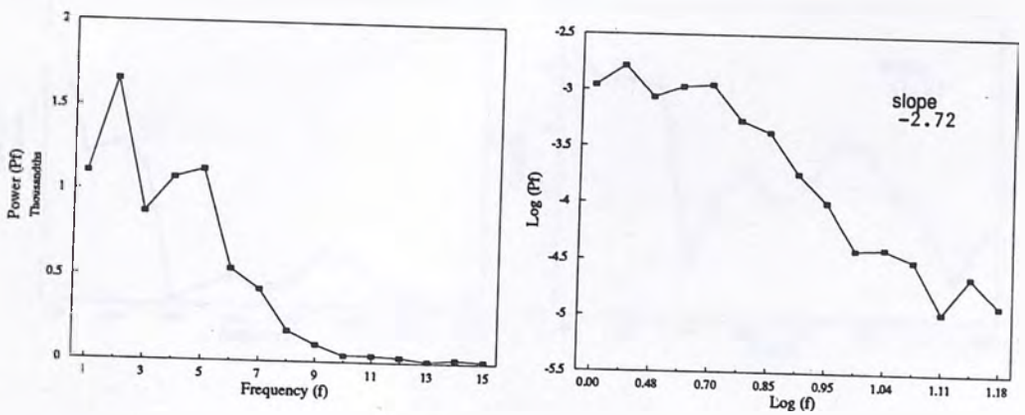

Plot of Power Spectrum

Plot of Log(Pf) vs. Log(f)

150 degree, Section II

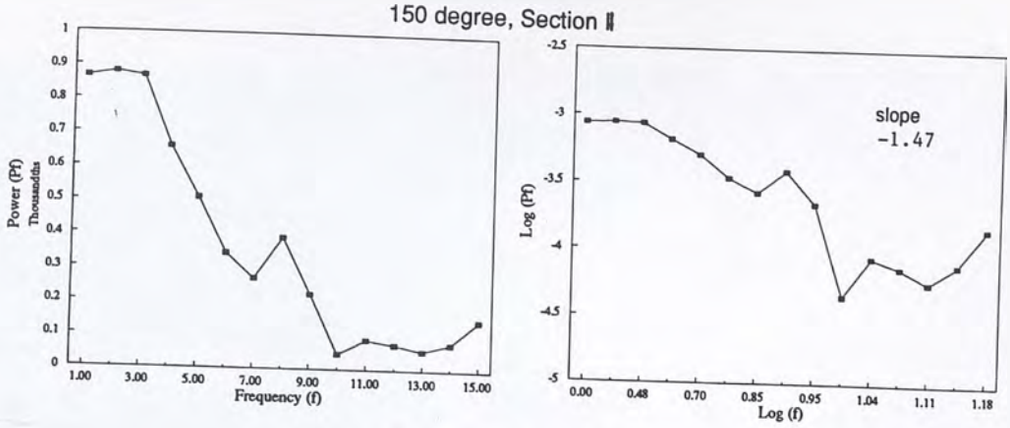

180 degree, Section II

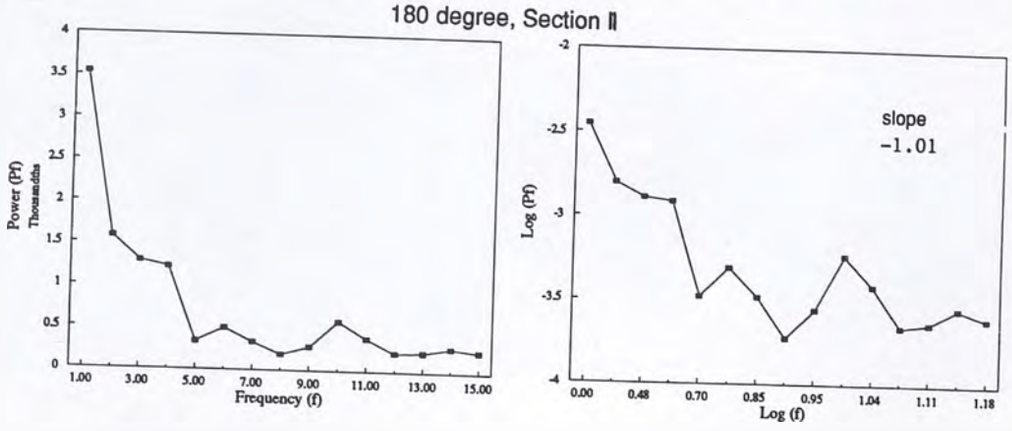

210 degree, Section II

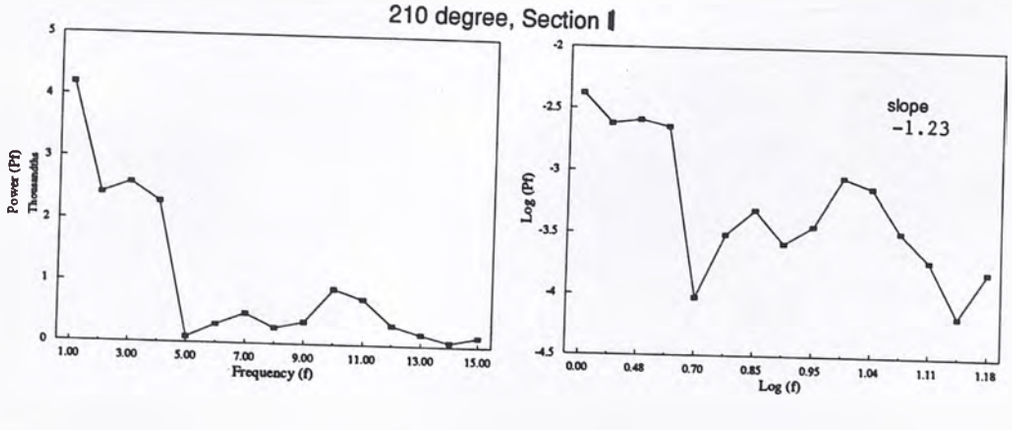

APPENDIX D

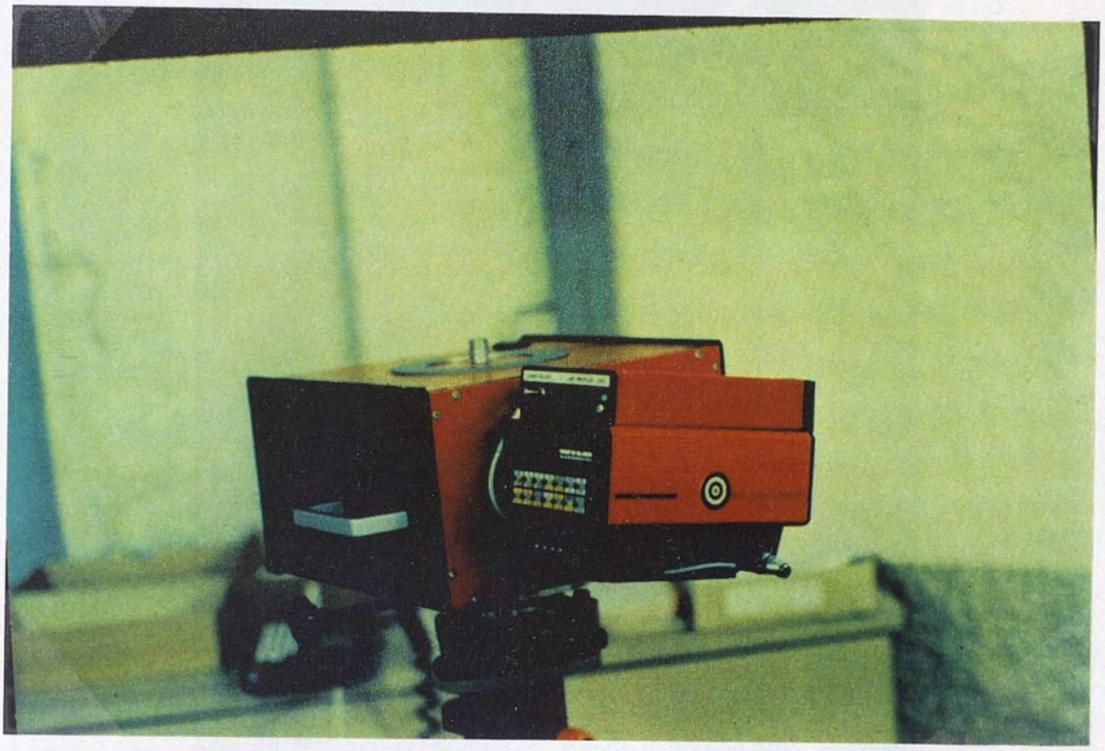

AMT 2000 Laser Profiler

Platform and Laser Profiler in the Sunshine Mine

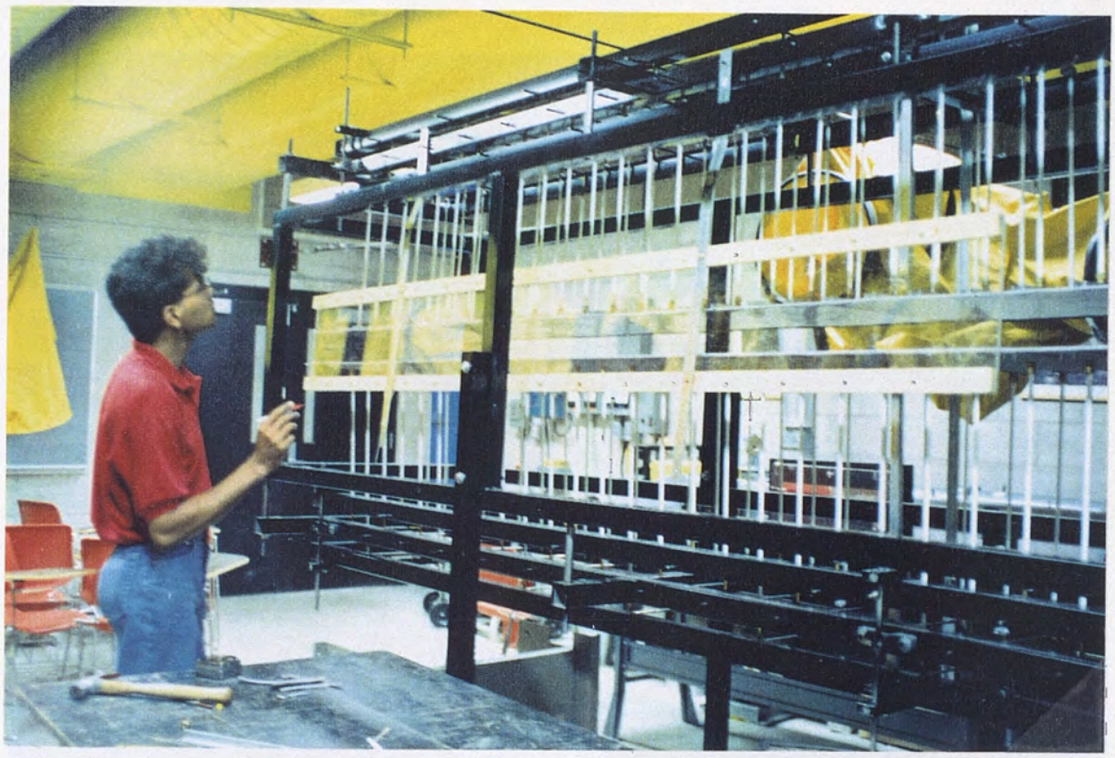

Assembling the Plexi-glass Side Walls

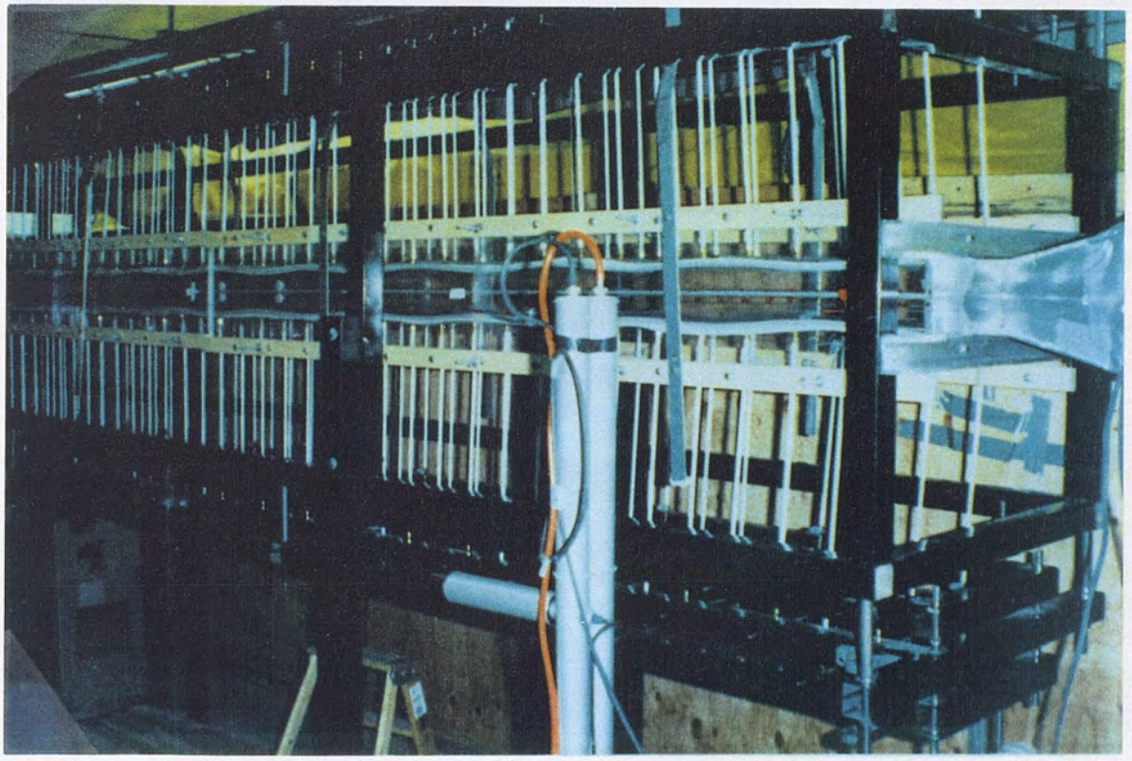

Model Drift and Betz Manometer

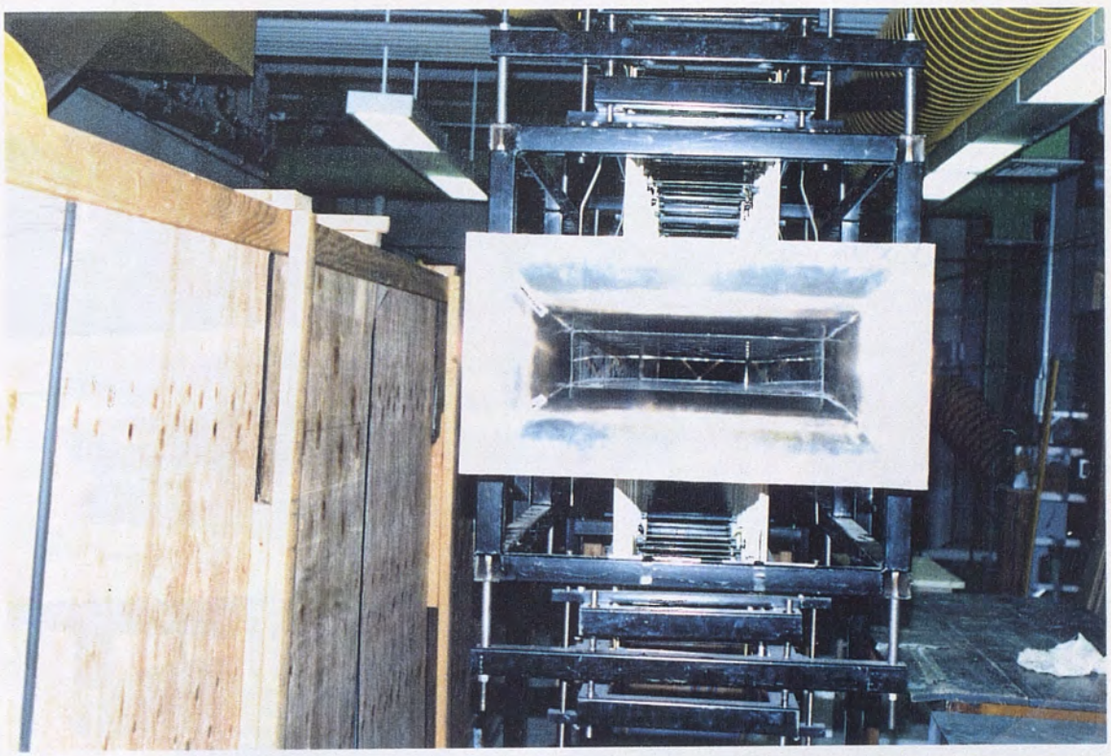

Front View of the Wind Tunnel and Parabola Shaped Inlet

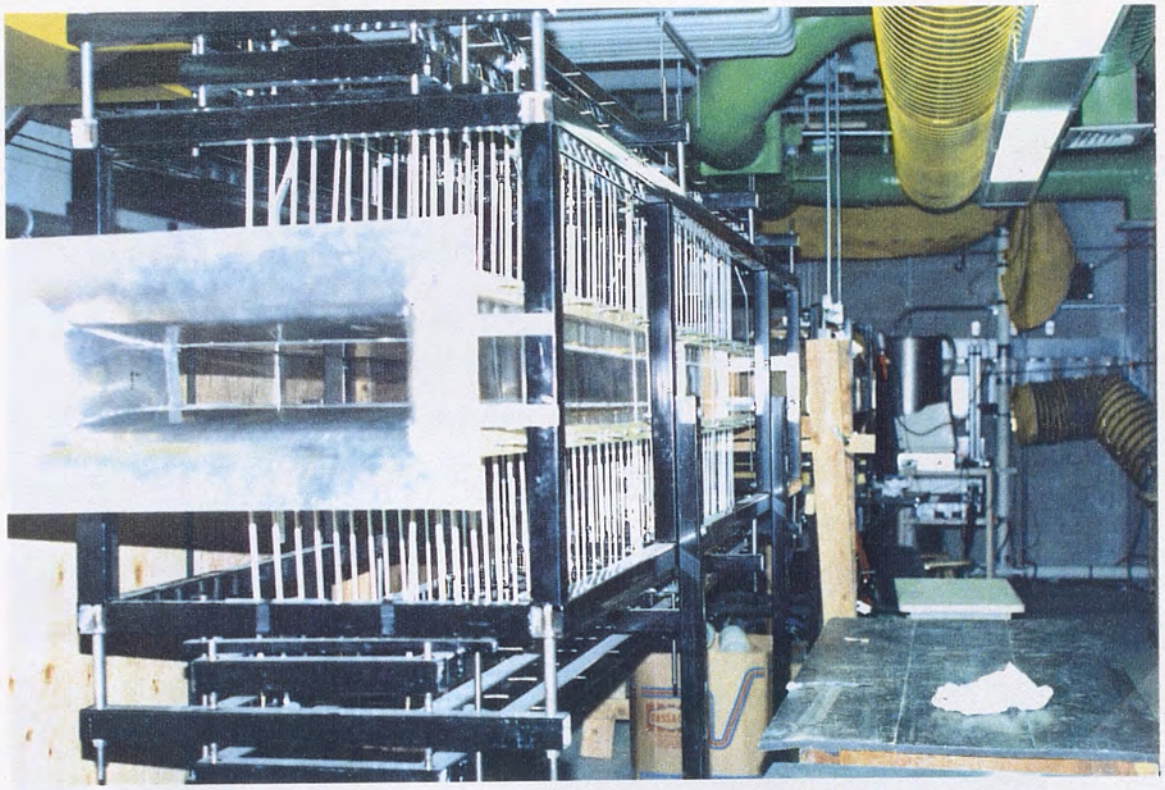

Another View of the Model

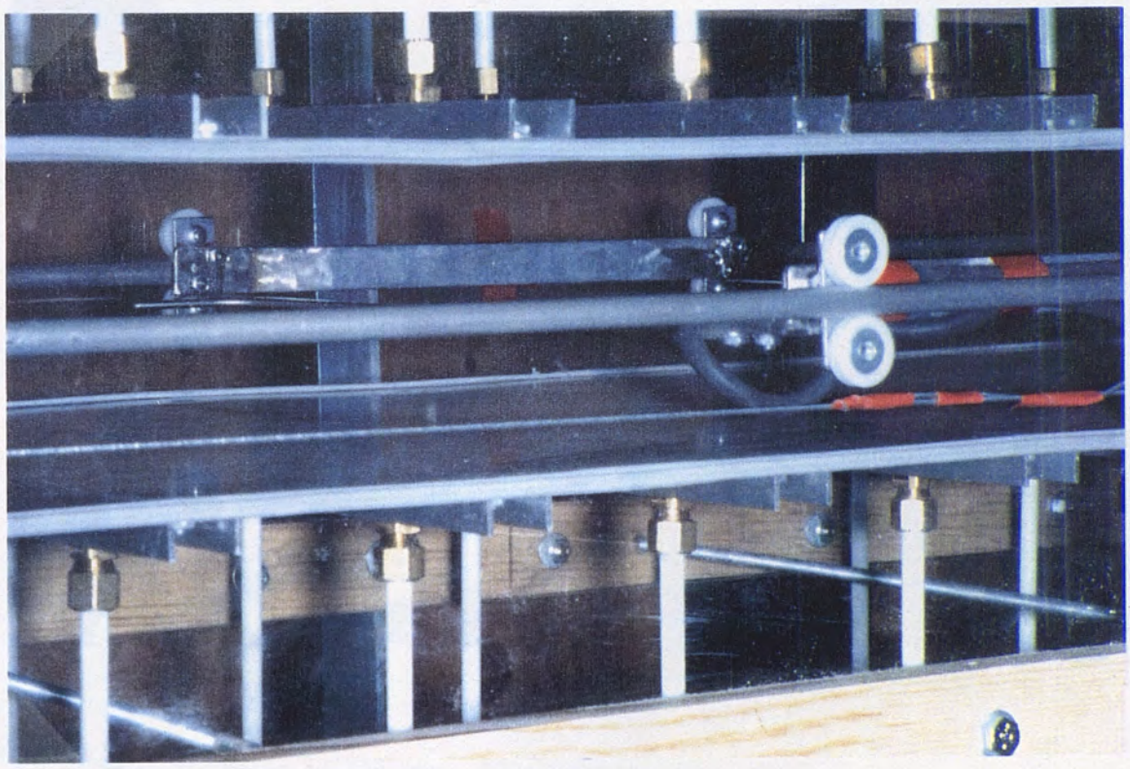

A Closer View Showing the Moving Platform, Pitot Tube and Other Arrangements

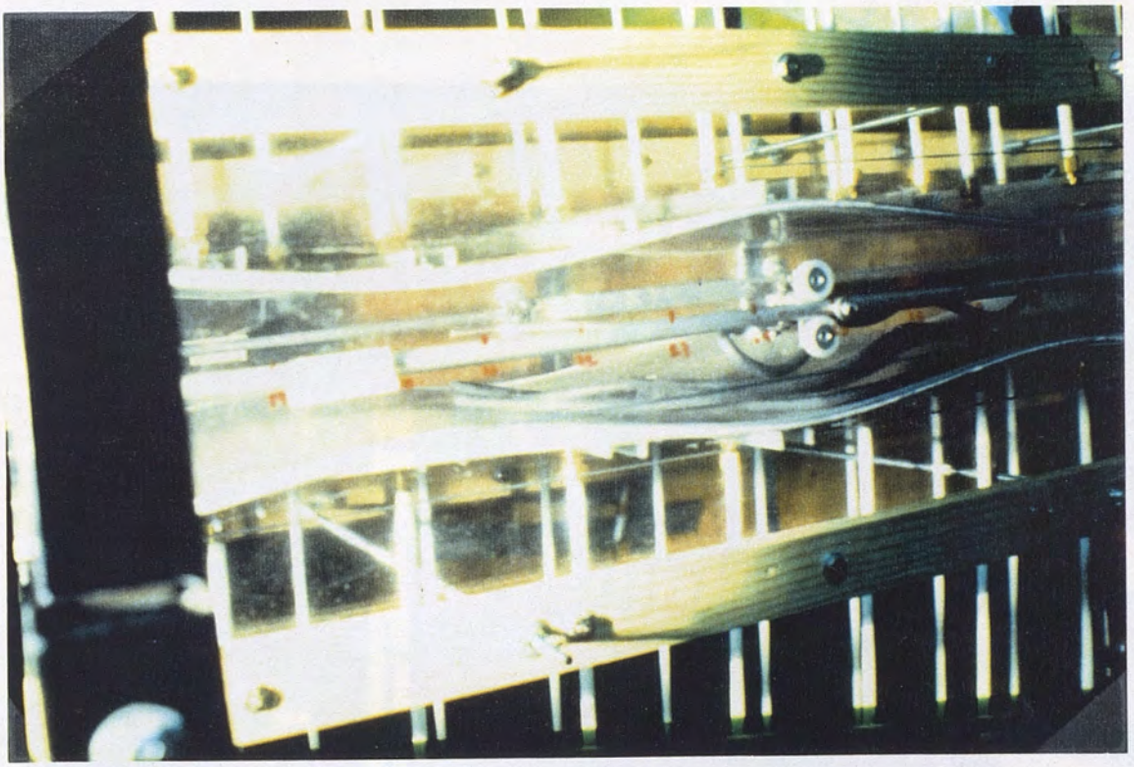

Moving Platform with Pitot Tube when the Roof and Floor are Wavy

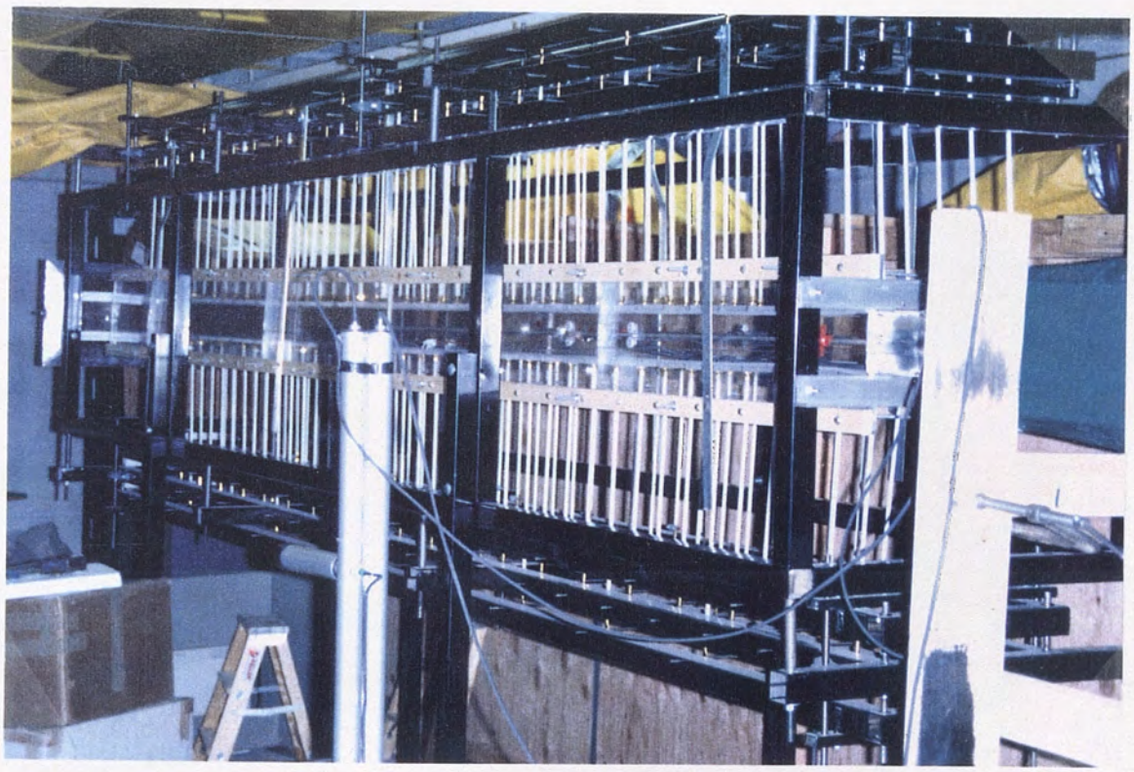

Experiment in Progress at a Set Waviness

APPENDIX E

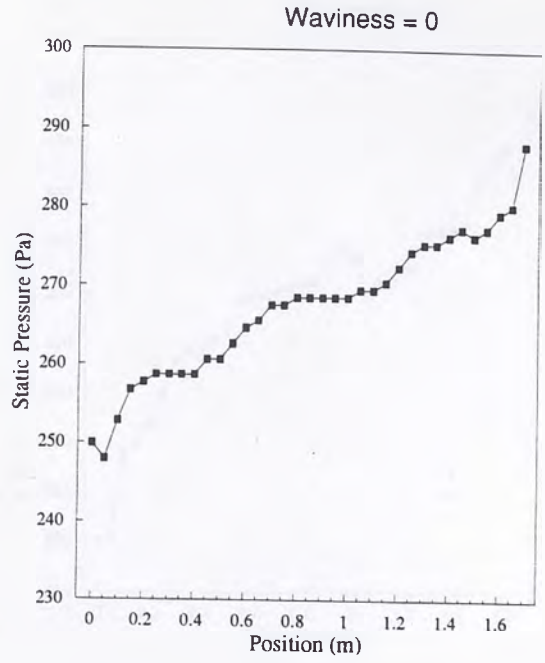
Waviness = 0
Static Pressure (Pa)
300
290
280
270
260
250
240
230
0
0.2
0.4
0.6
0.8
1
1.2
1.4
1.6
Position (m)

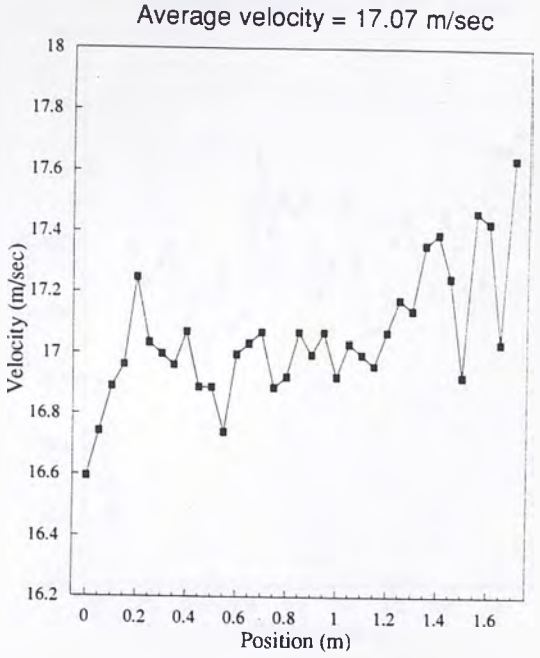
Average velocity = 17.07 m/sec
Velocity (m/sec)
18
17.8
17.6
17.4
17.2
17
16.8
16.6
16.4
16.2
0
0.2
0.4
0.6
0.8
1
1.2
1.4
1.6
Position (m)

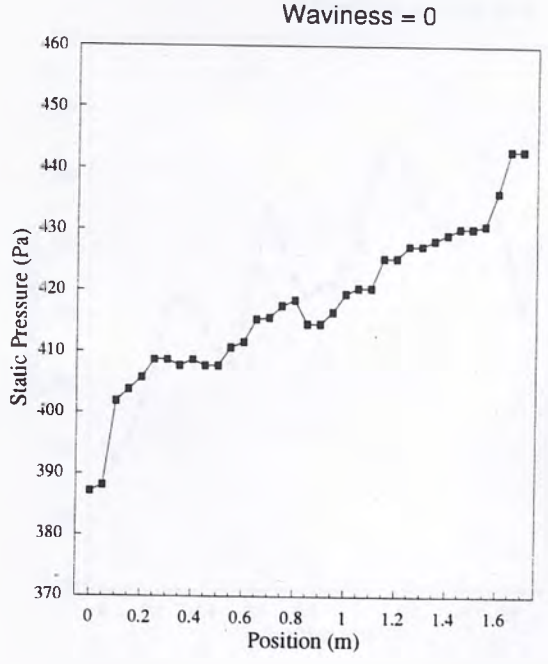
Waviness = 0
Static Pressure (Pa)
460
450
440
430
420
410
400
390
380
370
0
0.2
0.4
0.6
0.8
1
1.2
1.4
1.6
Position (m)

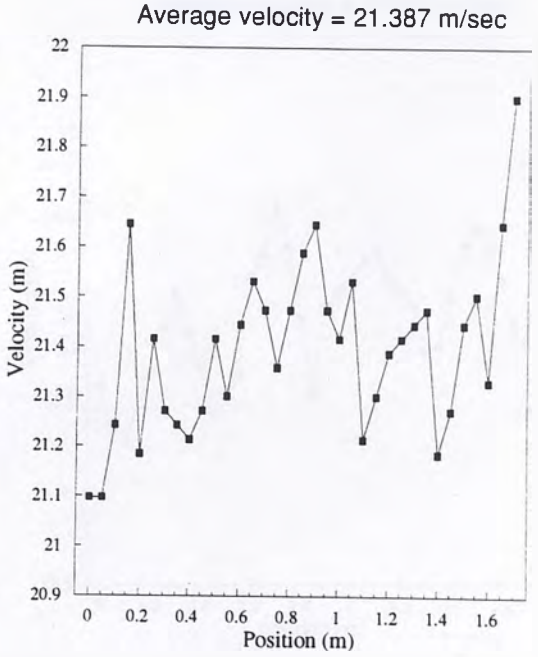
Average velocity = 21.387 m/sec
Velocity (m)
22
21.9
21.8
21.7
21.6
21.5
21.4
21.3
21.2
21.1
21
20.9
0
0.2
0.4
0.6
0.8
1
1.2
1.4
1.6
Position (m)

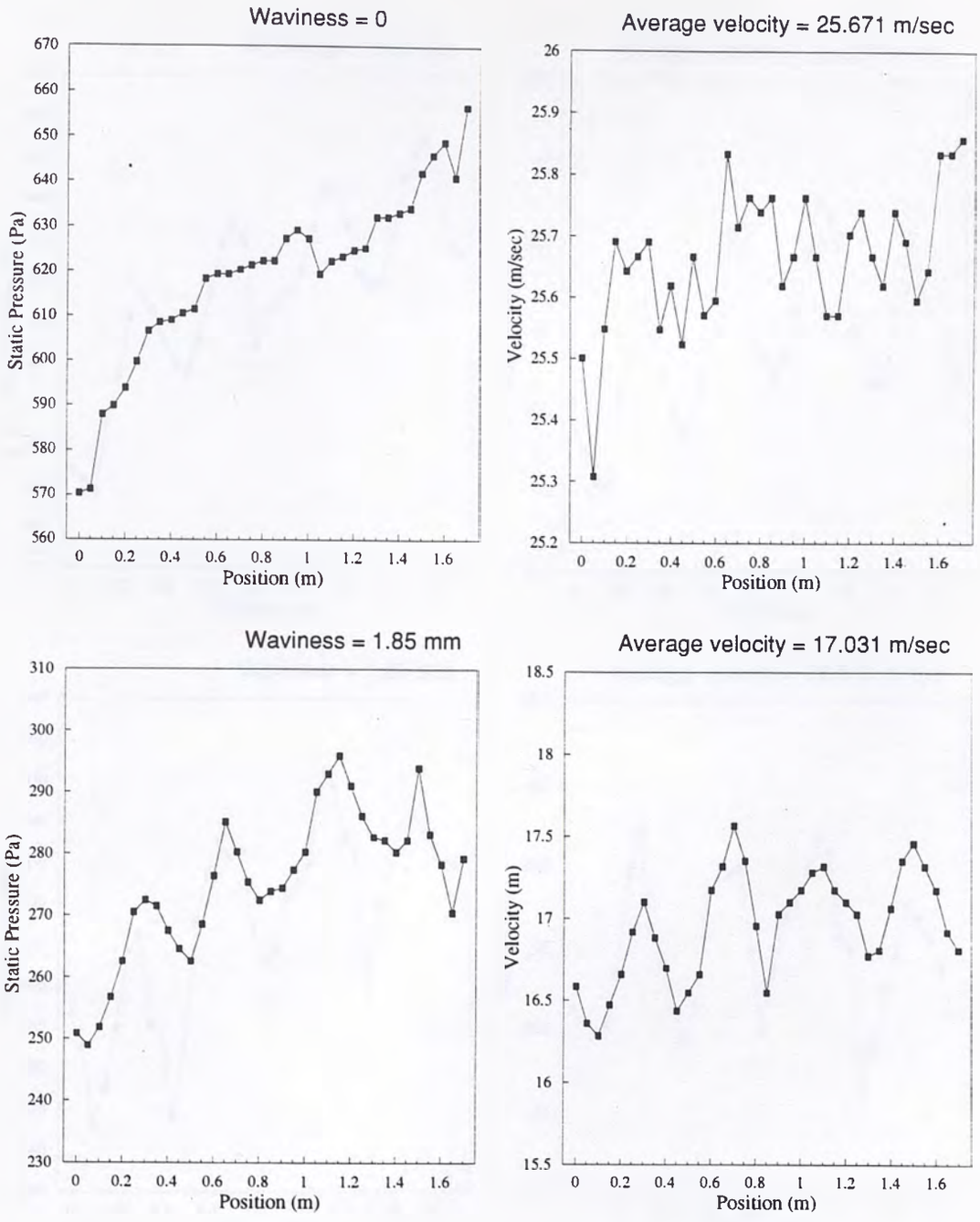
Waviness = 0
Static Pressure (Pa)
670
660
650
640
630
620
610
600
590
580
570
560
0 0.2 0.4 0.6 0.8 1 1.2 1.4 1.6
Position (m)
Average velocity = 25.671 m/sec
Velocity (m/sec)
26
25.9
25.8
25.7
25.6
25.5
25.4
25.3
25.2
0 0.2 0.4 0.6 0.8 1 1.2 1.4 1.6
Position (m)
Waviness = 1.85 mm
Static Pressure (Pa)
310
300
290
280
270
260
250
240
230
0 0.2 0.4 0.6 0.8 1 1.2 1.4 1.6
Position (m)
Average velocity = 17.031 m/sec
Velocity (m)
18.5
18
17.5
17
16.5
16
15.5
0 0.2 0.4 0.6 0.8 1 1.2 1.4 1.6
Position (m)

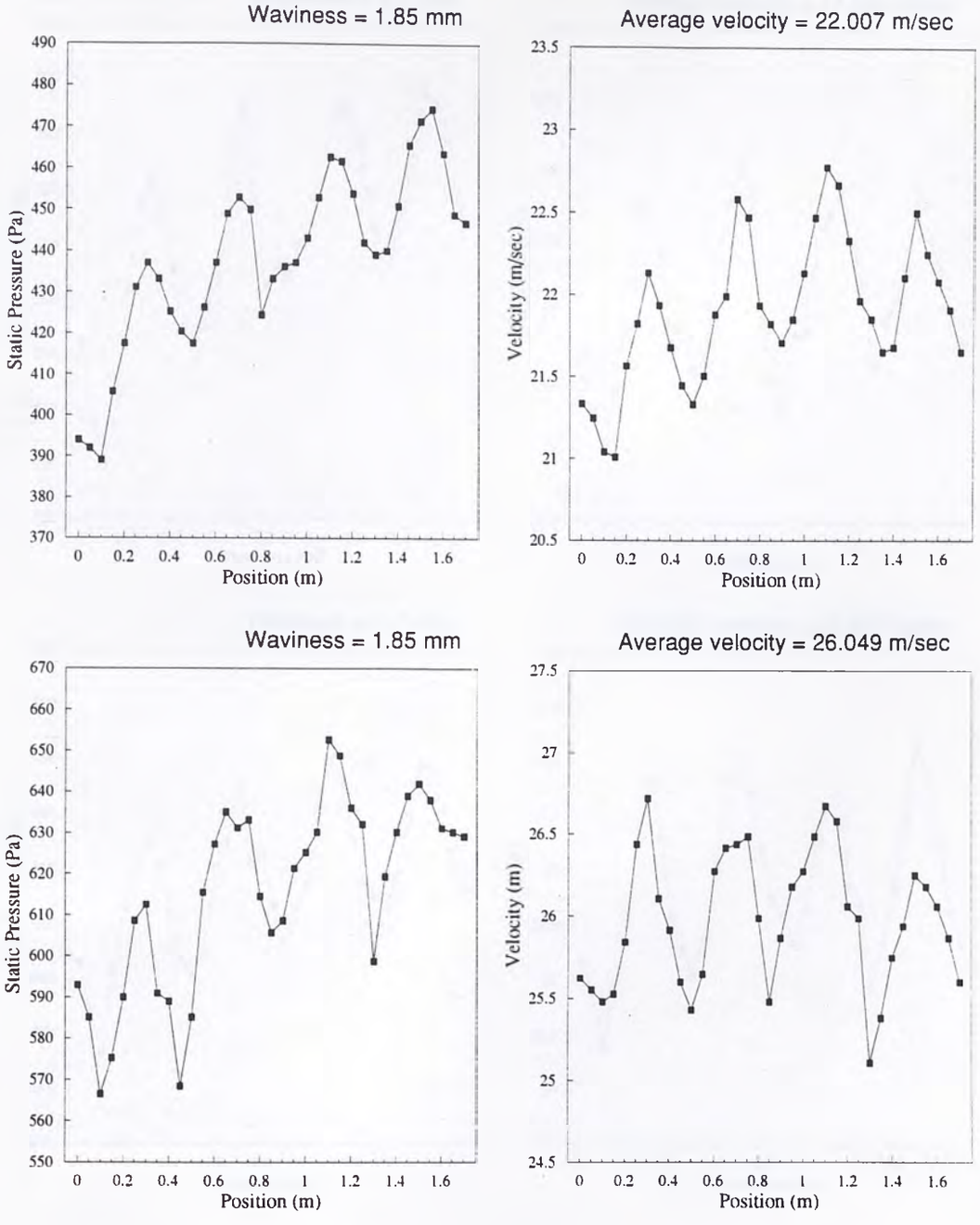
Waviness = 1.85 mm
Static Pressure (Pa)
Position (m)
Average velocity = 22.007 m/sec
Velocity (m/sec)
Position (m)
Waviness = 1.85 mm
Static Pressure (Pa)
Position (m)
Average velocity = 26.049 m/sec
Velocity (m)
Position (m)

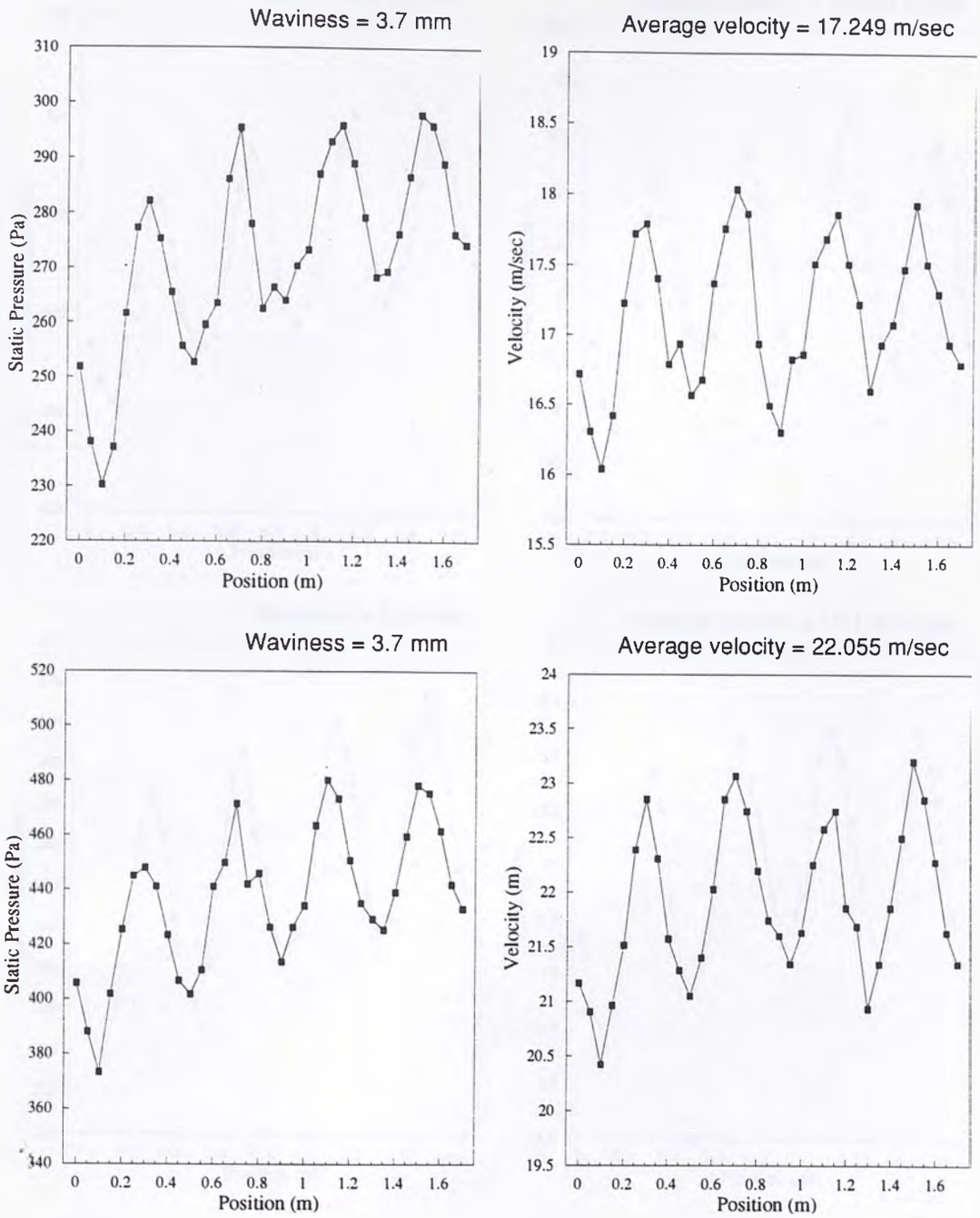
Waviness = 3.7 mm
Static Pressure (Pa)
Position (m)
Average velocity = 17.249 m/sec
Velocity (m/sec)
Position (m)
Waviness = 3.7 mm
Static Pressure (Pa)
Position (m)
Average velocity = 22.055 m/sec
Velocity (m)
Position (m)

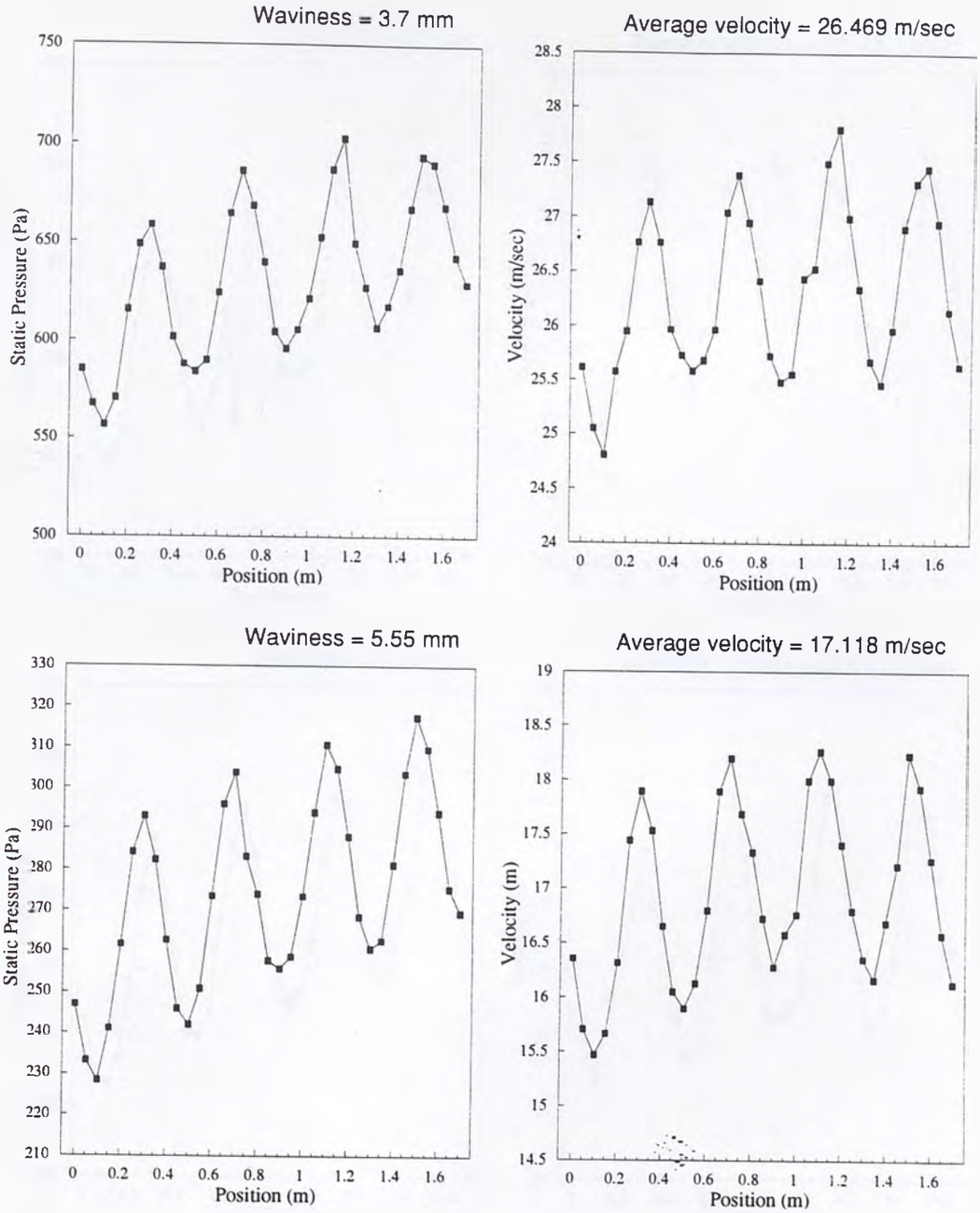
Waviness = 3.7 mm
Static Pressure (Pa)
750
700
650
600
550
500
0 0.2 0.4 0.6 0.8 1 1.2 1.4 1.6
Position (m)
Average velocity = 26.469 m/sec
Velocity (m/sec)
28.5
28
27.5
27
26.5
26
25.5
25
24.5
24
0 0.2 0.4 0.6 0.8 1 1.2 1.4 1.6
Position (m)
Waviness = 5.55 mm
Static Pressure (Pa)
330
320
310
300
290
280
270
260
250
240
230
220
210
0 0.2 0.4 0.6 0.8 1 1.2 1.4 1.6
Position (m)
Average velocity = 17.118 m/sec
Velocity (m)
19
18.5
18
17.5
17
16.5
16
15.5
15
14.5
0 0.2 0.4 0.6 0.8 1 1.2 1.4 1.6
Position (m)

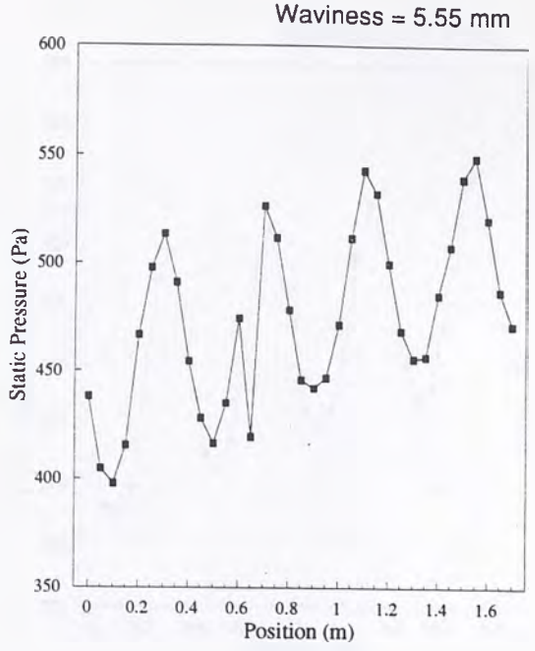
Waviness = 5.55 mm
Static Pressure (Pa)
600
550
500
450
400
350
0 0.2 0.4 0.6 0.8 1 1.2 1.4 1.6
Position (m)

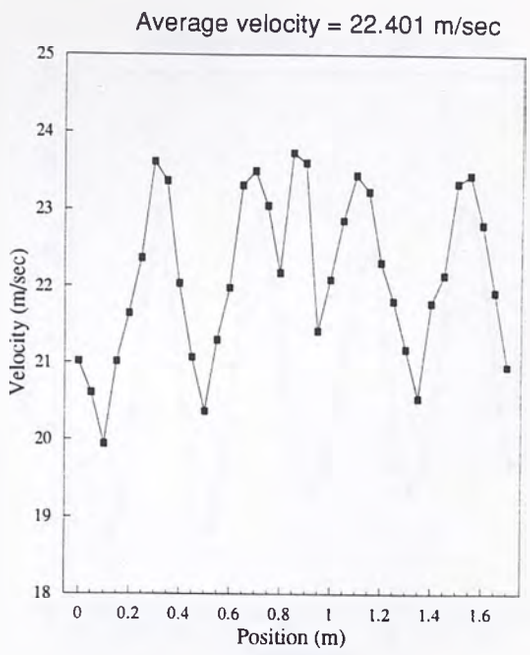
Average velocity = 22.401 m/sec
Velocity (m/sec)
25
24
23
22
21
20
19
18
0 0.2 0.4 0.6 0.8 1 1.2 1.4 1.6
Position (m)

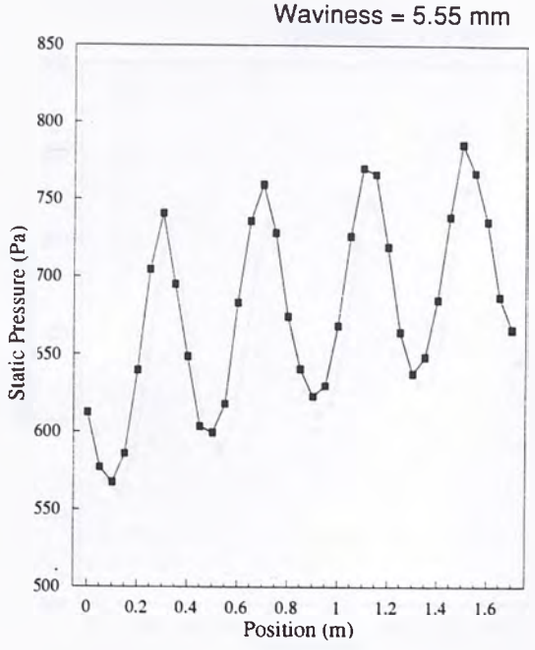
Waviness = 5.55 mm
Static Pressure (Pa)
850
800
750
700
650
600
550
500
0 0.2 0.4 0.6 0.8 1 1.2 1.4 1.6
Position (m)

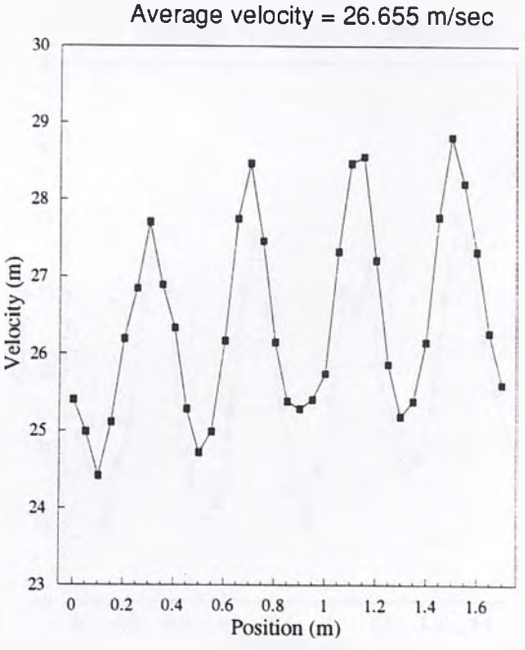
Average velocity = 26.655 m/sec
Velocity (m)
30
29
28
27
26
25
24
23
0 0.2 0.4 0.6 0.8 1 1.2 1.4 1.6
Position (m)

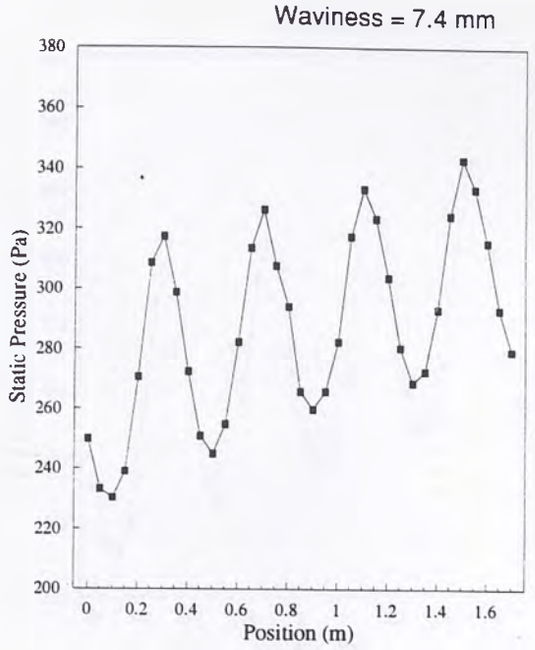
Waviness = 7.4 mm
Static Pressure (Pa)
380
360
340
320
300
280
260
240
220
200
0 0.2 0.4 0.6 0.8 1 1.2 1.4 1.6
Position (m)

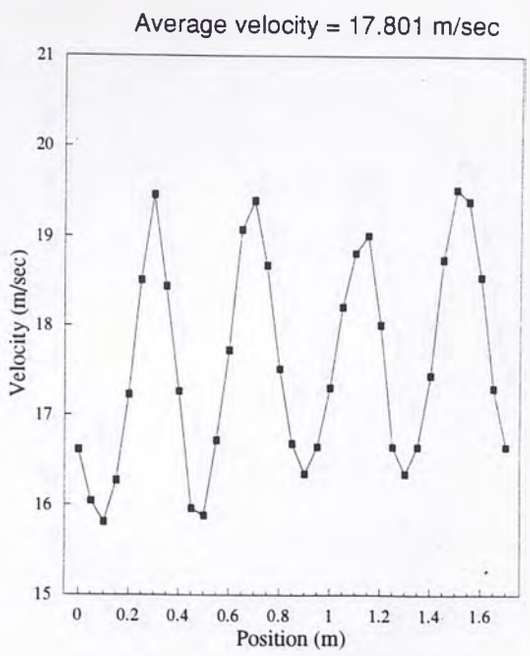
Average velocity = 17.801 m/sec
Velocity (m/sec)
21
20
19
18
17
16
15
0 0.2 0.4 0.6 0.8 1 1.2 1.4 1.6
Position (m)

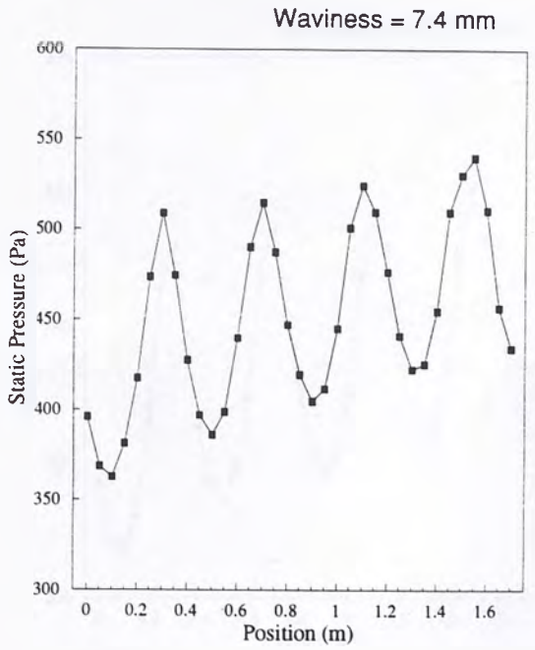
Waviness = 7.4 mm
Static Pressure (Pa)
600
550
500
450
400
350
300
0 0.2 0.4 0.6 0.8 1 1.2 1.4 1.6
Position (m)

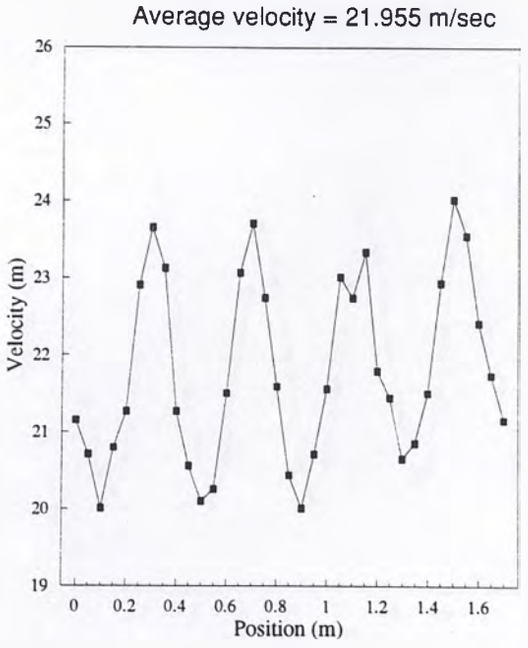
Average velocity = 21.955 m/sec
Velocity (m)
26
25
24
23
22
21
20
19
0 0.2 0.4 0.6 0.8 1 1.2 1.4 1.6
Position (m)

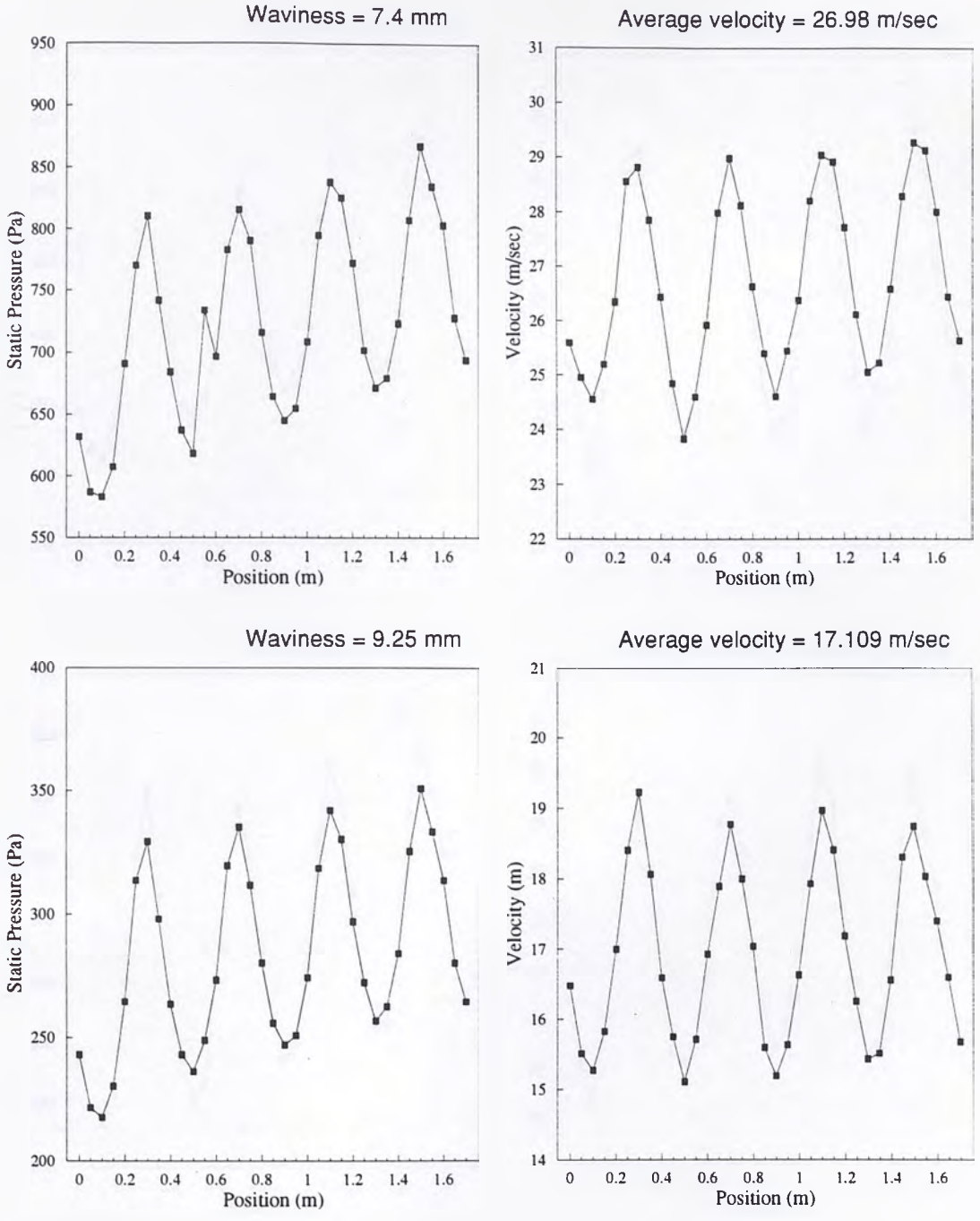
Waviness = 7.4 mm
Static Pressure (Pa)
950
900
850
800
750
700
650
600
550
0 0.2 0.4 0.6 0.8 1 1.2 1.4 1.6
Position (m)
Average velocity = 26.98 m/sec
Velocity (m/sec)
31
30
29
28
27
26
25
24
23
22
0 0.2 0.4 0.6 0.8 1 1.2 1.4 1.6
Position (m)
Waviness = 9.25 mm
Static Pressure (Pa)
400
350
300
250
200
0 0.2 0.4 0.6 0.8 1 1.2 1.4 1.6
Position (m)
Average velocity = 17.109 m/sec
Velocity (m)
21
20
19
18
17
16
15
14
0 0.2 0.4 0.6 0.8 1 1.2 1.4 1.6
Position (m)

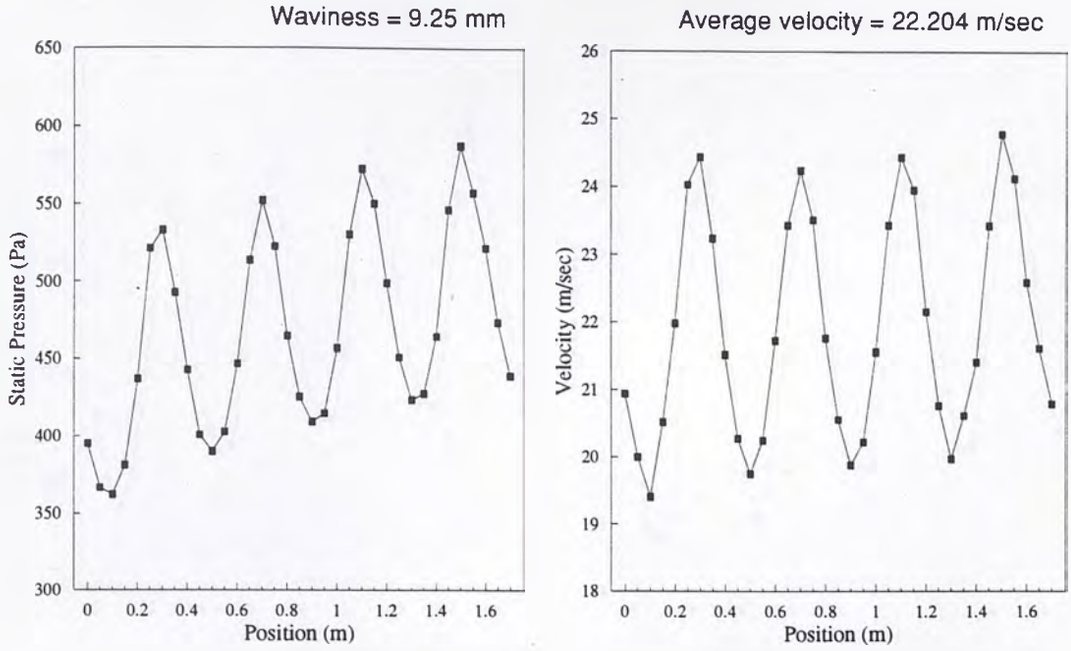
Waviness = 9.25 mm
Static Pressure (Pa)
650
600
550
500
450
400
350
300
0 0.2 0.4 0.6 0.8 1 1.2 1.4 1.6
Position (m)

Average velocity = 22.204 m/sec
Velocity (m/sec)
26
25
24
23
22
21
20
19
18
0 0.2 0.4 0.6 0.8 1 1.2 1.4 1.6
Position (m)

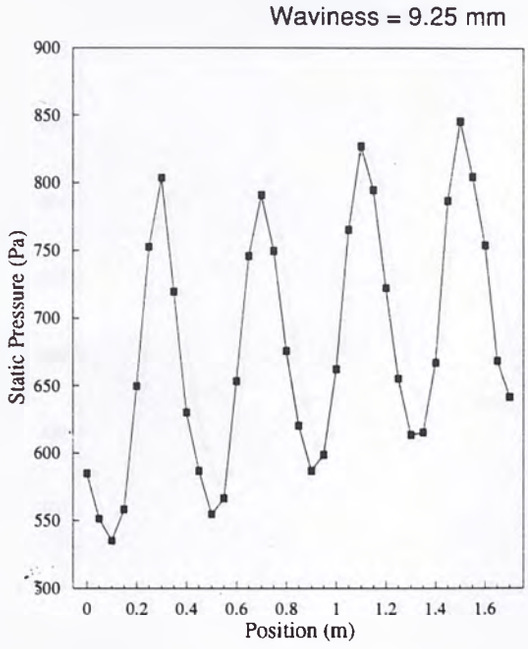
Waviness = 9.25 mm
Static Pressure (Pa)
900
850
800
750
700
650
600
550
300
0 0.2 0.4 0.6 0.8 1 1.2 1.4 1.6
Position (m)

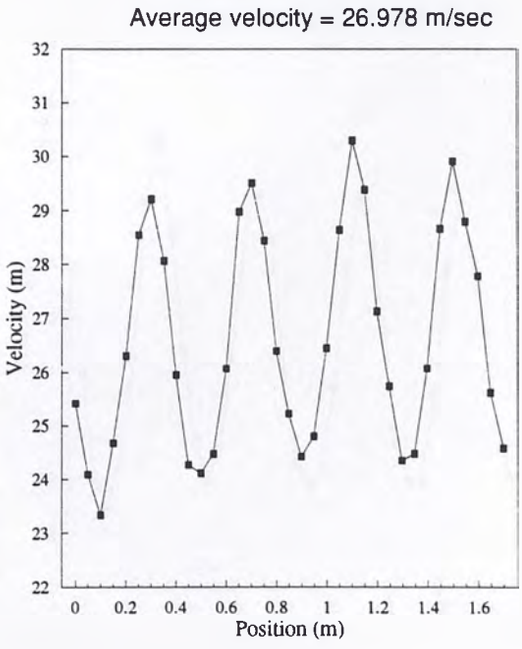
Average velocity = 26.978 m/sec
Velocity (m)
32
31
30
29
28
27
26
25
24
23
22
0 0.2 0.4 0.6 0.8 1 1.2 1.4 1.6
Position (m)

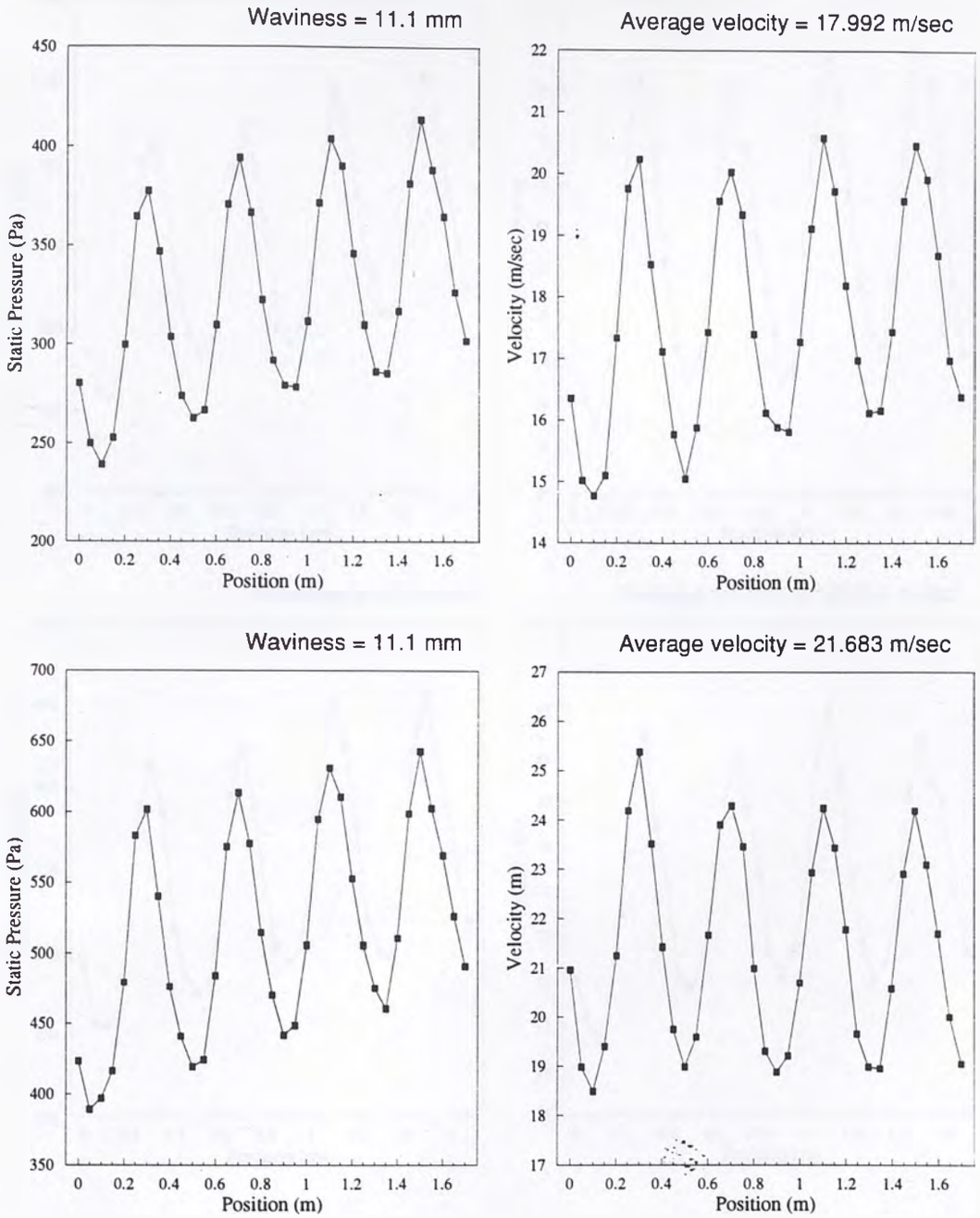
Waviness = 11.1 mm
Static Pressure (Pa)
Position (m)
Average velocity = 17.992 m/sec
Velocity (m/sec)
Position (m)
Waviness = 11.1 mm
Static Pressure (Pa)
Position (m)
Average velocity = 21.683 m/sec
Velocity (m)
Position (m)

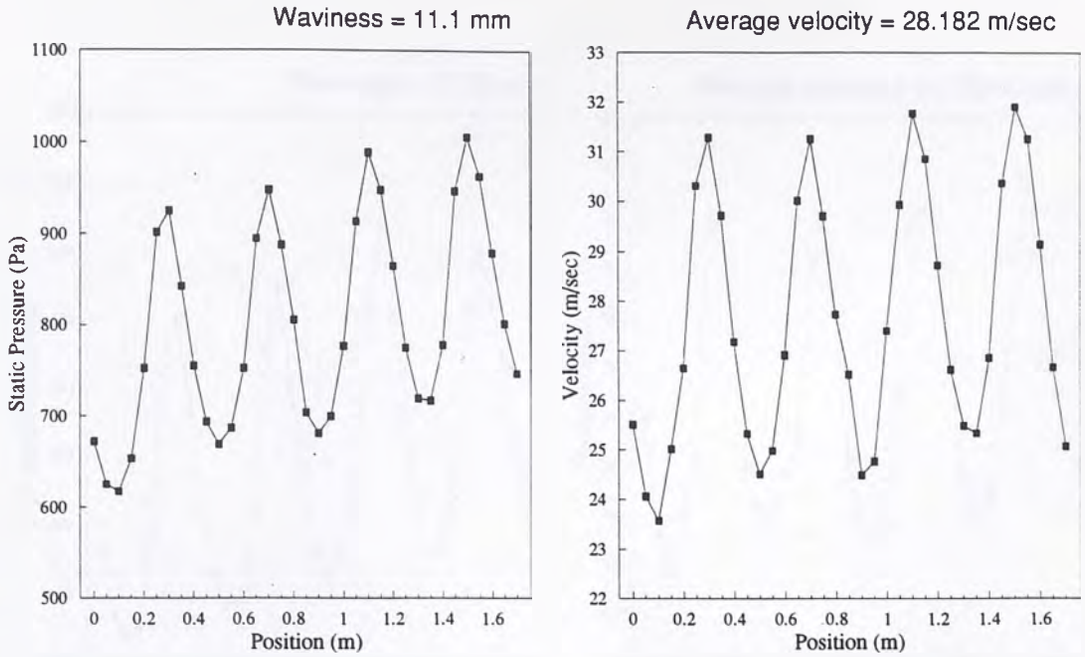
Waviness = 11.1 mm
Static Pressure (Pa)
1100
1000
900
800
700
600
500
0 0.2 0.4 0.6 0.8 1 1.2 1.4 1.6
Position (m)

Average velocity = 28.182 m/sec
Velocity (m/sec)
33
32
31
30
29
28
27
26
25
24
23
22
0 0.2 0.4 0.6 0.8 1 1.2 1.4 1.6
Position (m)

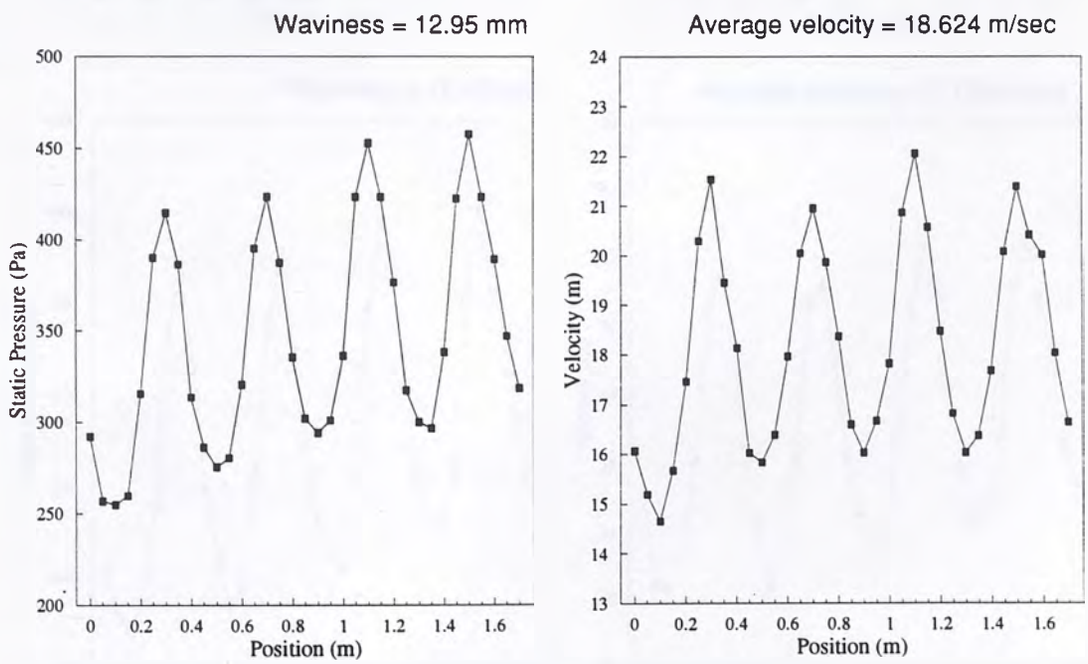
Waviness = 12.95 mm
Static Pressure (Pa)
500
450
400
350
300
250
200
0 0.2 0.4 0.6 0.8 1 1.2 1.4 1.6
Position (m)

Average velocity = 18.624 m/sec
Velocity (m)
24
23
22
21
20
19
18
17
16
15
14
13
0 0.2 0.4 0.6 0.8 1 1.2 1.4 1.6
Position (m)

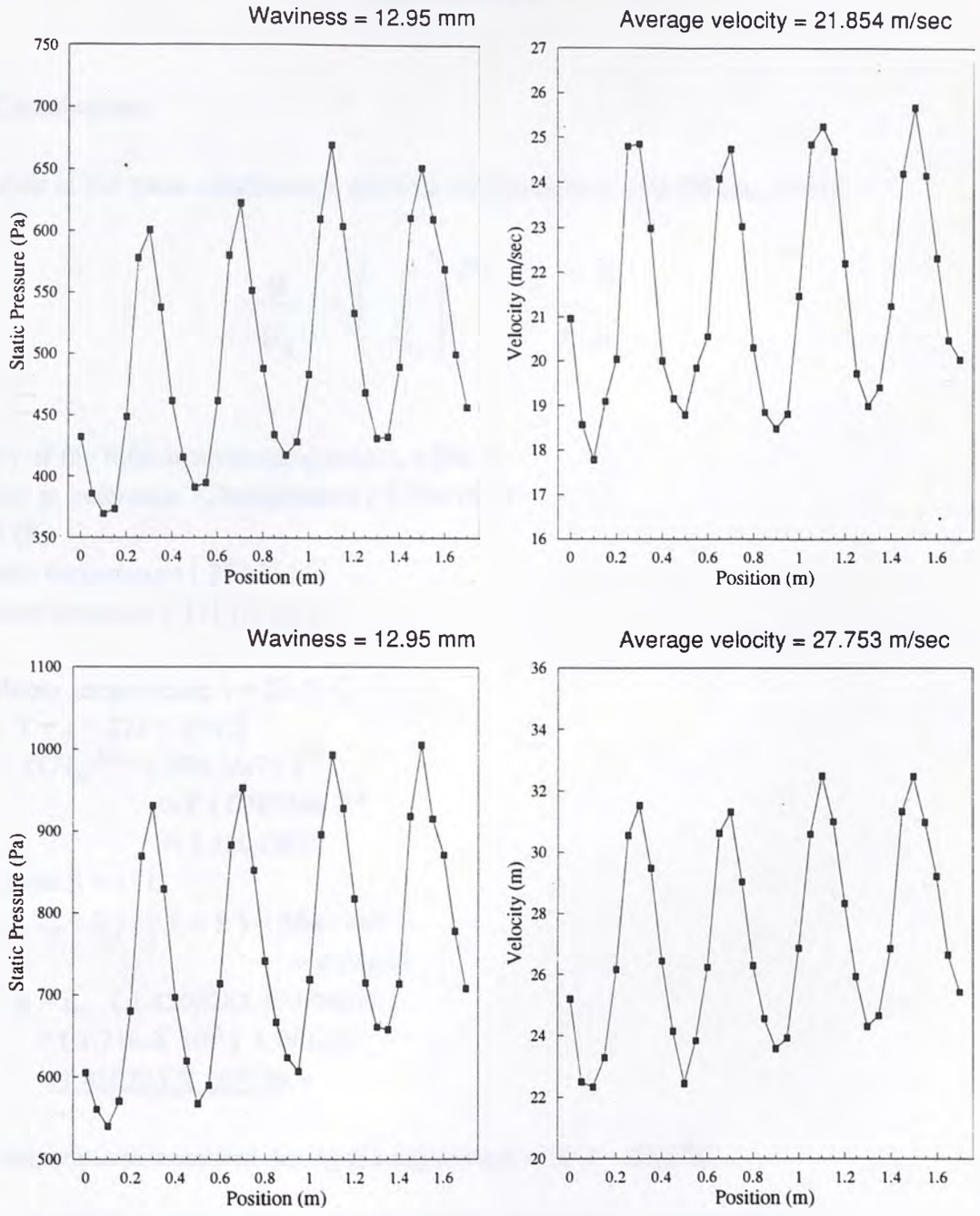
Waviness = 12.95 mm
Static Pressure (Pa)
Position (m)
Average velocity = 21.854 m/sec
Velocity (m/sec)
Position (m)
Waviness = 12.95 mm
Static Pressure (Pa)
Position (m)
Average velocity = 27.753 m/sec
Velocity (m)
Position (m)

APPENDIX F

Viscosity Calculations

Viscosity of air in the room conditions is given by the Sutherland Law (White, 1991):

$$\frac{\mu}{\mu_0} = \left(\frac{T}{T_0} \right)^{3/2} \frac{T_0 + S}{T + S}$$

where,
μ = viscosity of the fluid ar room temperature, t (Pa s)
μ_0 = viscosity at reference T_0 temperature (1.716 Pa s)
$T = t + 273$ (K)
T_0 = reference temperature (273 K)
S = Sutherland constant (111 for air)

Eg: Room temperature, $t = 21.5^0$ C

$\therefore T = t + 273 = 294.5$

$\therefore (T/T_0)^{3/2} = (294.5/273)^{3/2}$

$= (1.0787546)^{1.5}$

$= 1.1204281$

Given S = 111

$\therefore (T_0 + S) / (T + S) = 384 / 405.5$

$= 0.94698$

$\therefore \mu = \mu_0 . (1.1204281 \text{ X } 0.94698)$

$= (1.716 \text{ X } 10^{-5}) \ 1.061023$

$= \underline{1.820755 \text{ X } 10^{-5}}$ Pa s

Range of Temperatures measured during the experiment = 20.7 ~ 23.5 ^{0}C

For t = 20.7, Calculated Viscosity, μ is 1.81682 X 10^{-5} Pa s. For the highest room temperature, 23.5 ^{0}C, calculated Viscosity, μ is 1.83 X 10^{-5} Pa s. The average for all conditions is found to be 1.817 X 10^{-5} Pa s.

APPENDIX G

Waviness = 0 Temperature = 21.4^{0}C Density = 1.0195 Kg/m^3

Atm. pressure = 25.45 in. Hg Ave. velocity = 17.07 m/s Re = 152090

position m	vel. pr. mm. water	st. pr. mm water	vel. pr. Pa	st. pr. Pa	velocity m/s
0.00	22.4	25.5	219.132	249.90	16.5958
0.05	22.8	25.3	223.045	247.94	16.7433
0.10	23.2	25.8	226.958	252.84	16.8895
0.15	23.4	26.2	228.915	256.76	16.9622
0.20	24.2	26.3	236.741	257.74	17.2497
0.25	23.6	26.4	230.871	258.72	17.0345
0.30	23.5	26.4	229.893	258.72	16.9984
0.35	23.4	26.4	228.915	258.72	16.9622
0.40	23.7	26.4	231.849	258.72	17.0706
0.45	23.2	26.6	226.958	260.68	16.8895
0.50	23.2	26.6	226.958	260.68	16.8895
0.55	22.8	26.8	223.045	262.64	16.7433
0.60	23.5	27.0	229.893	264.60	16.9984
0.65	23.6	27.1	230.871	265.58	17.0345
0.70	23.7	27.3	231.849	267.54	17.0706
0.75	23.2	27.3	226.958	267.54	16.8895
0.80	23.3	27.4	227.936	268.52	16.9259
0.85	23.7	27.4	231.849	268.52	17.0706
0.90	23.5	27.4	229.893	268.52	16.9984
0.95	23.7	27.4	231.849	268.52	17.0706
1.00	23.3	27.4	227.936	268.52	16.9259
1.05	23.6	27.5	230.871	269.50	17.0345
1.10	23.5	27.5	229.893	269.50	16.9984
1.15	23.4	27.6	228.915	270.48	16.9622
1.20	23.7	27.8	231.849	272.44	17.0706
1.25	24.0	28.0	234.784	274.40	17.1782
1.30	23.9	28.1	233.806	275.38	17.1425
1.35	24.5	28.1	239.676	275.38	17.3563
1.40	24.6	28.2	240.654	276.36	17.3917
1.45	24.2	28.3	236.741	277.34	17.2497
1.50	23.3	28.2	227.936	276.36	16.9259
1.55	24.8	28.3	242.610	277.34	17.4622
1.60	24.7	28.5	241.632	279.30	17.4270
1.65	23.6	28.6	230.871	280.28	17.0345
1.70	25.3	29.4	247.502	288.12	17.6374

Waviness = 0 Temperature = 21.2^{0}C Density = 1.0182 Kg/m^3
Atm. pressure = 25.4 in. Hg Ave. velocity =21.387 m/s Re = 190408

position m	vel. pr. mm. water	st. pr. mm water	vel. pr. Pa	st. pr. Pa	velocity m/s
0.00	36.1	39.500	353.666	387.100	21.0970
0.05	36.1	39.600	353.666	388.080	21.0970
0.10	36.6	41.000	358.565	401.800	21.2426
0.15	38.0	41.200	372.280	403.760	21.6451
0.20	36.4	41.400	356.605	405.720	21.1845
0.25	37.2	41.700	364.443	408.660	21.4161
0.30	36.7	41.700	359.544	408.660	21.2716
0.35	36.6	41.600	358.565	407.680	21.2426
0.40	36.5	41.700	357.585	408.660	21.2136
0.45	36.7	41.600	359.544	407.680	21.2716
0.50	37.2	41.600	364.443	407.680	21.4161
0.55	36.8	41.900	360.524	410.620	21.3006
0.60	37.3	42.000	365.423	411.600	21.4448
0.65	37.6	42.375	368.362	415.275	21.5309
0.70	37.4	42.400	366.402	415.520	21.4735
0.75	37.0	42.600	362.483	417.480	21.3584
0.80	37.4	42.700	366.402	418.460	21.4735
0.85	37.8	42.300	370.321	414.540	21.5881
0.90	38.0	42.300	372.280	414.540	21.6451
0.95	37.4	42.500	366.402	416.500	21.4735
1.00	37.2	42.800	364.443	419.440	21.4161
1.05	37.6	42.900	368.362	420.420	21.5309
1.10	36.5	42.900	357.585	420.420	21.2136
1.15	36.8	43.400	360.524	425.320	21.3006
1.20	37.1	43.400	363.463	425.320	21.3873
1.25	37.2	43.600	364.443	427.280	21.4161
1.30	37.3	43.600	365.423	427.280	21.4448
1.35	37.4	43.700	366.402	428.260	21.4735
1.40	36.4	43.800	356.605	429.240	21.1845
1.45	36.7	43.900	359.544	430.220	21.2716
1.50	37.3	43.900	365.423	430.220	21.4448
1.55	37.5	43.950	367.382	430.710	21.5022
1.60	36.9	44.500	361.504	436.100	21.3295
1.65	38.0	45.200	372.280	442.960	21.6451
1.70	38.9	45.200	381.097	442.960	21.8999

Waviness = 0 Temperature = 21.2°C Density = 1.0262 Kg/m^3
Atm. pressure = 25.6 in. Hg Ave. velocity =25.671 m/s Re = 230348

position m	vel. pr. mm. water	st. pr. mm water	vel. pr. Pa	st. pr. Pa	velocity m/s
0.00	53.20	58.20	521.192	570.36	25.5006
0.05	52.40	58.30	513.355	571.34	25.3082
0.10	53.40	60.00	523.152	588.00	25.5485
0.15	54.00	60.20	529.030	589.96	25.6917
0.20	53.80	60.60	527.071	593.88	25.6440
0.25	53.90	61.20	528.050	599.76	25.6678
0.30	54.00	61.90	529.030	606.62	25.6917
0.35	53.40	62.10	523.152	608.58	25.5485
0.40	53.70	62.15	526.091	609.07	25.6202
0.45	53.30	62.30	522.172	610.54	25.5246
0.50	53.90	62.40	528.050	611.52	25.6678
0.55	53.50	63.10	524.131	618.38	25.5724
0.60	53.60	63.20	525.111	619.36	25.5963
0.65	54.60	63.20	534.908	619.36	25.8340
0.70	54.10	63.30	530.010	620.34	25.7154
0.75	54.30	63.40	531.969	621.32	25.7629
0.80	54.20	63.50	530.989	622.30	25.7392
0.85	54.30	63.50	531.969	622.30	25.7629
0.90	53.70	64.00	526.091	627.20	25.6202
0.95	53.90	64.20	528.050	629.16	25.6678
1.00	54.30	64.00	531.969	627.20	25.7629
1.05	53.90	63.20	528.050	619.36	25.6678
1.10	53.50	63.50	524.131	622.30	25.5724
1.15	53.50	63.60	524.131	623.28	25.5724
1.20	54.05	63.75	529.520	624.75	25.7035
1.25	54.20	63.80	530.989	625.24	25.7392
1.30	53.90	64.50	528.050	632.10	25.6678
1.35	53.70	64.50	526.091	632.10	25.6202
1.40	54.20	64.60	530.989	633.08	25.7392
1.45	54.00	64.70	529.030	634.06	25.6917
1.50	53.60	65.50	525.111	641.90	25.5963
1.55	53.80	65.90	527.071	645.82	25.6440
1.60	54.60	66.20	534.908	648.76	25.8340
1.65	54.60	65.40	534.908	640.92	25.8340
1.70	54.70	67.00	535.888	656.60	25.8576

Waviness = 1.85 mm Temperature = 21.5^{0}C Density = 1.0132 Kg/m^3
Atm. pressure = 25.3 in. Hg Ave. velocity = 17.031 m/s Re = 152757

position m	vel. pr. mm. water	st. pr. mm water	vel. pr. Pa	st. pr. Pa	velocity m/s
0.00	22.2	25.60	217.56	250.88	16.5833
0.05	21.6	25.40	211.68	248.92	16.3576
0.10	21.4	25.70	209.72	251.86	16.2818
0.15	21.9	26.20	214.62	256.76	16.4708
0.20	22.4	26.80	219.52	262.64	16.6578
0.25	23.1	27.60	226.38	270.48	16.9161
0.30	23.6	27.80	231.28	272.44	17.0982
0.35	23.0	27.70	225.40	271.46	16.8794
0.40	22.5	27.30	220.50	267.54	16.6950
0.45	21.8	27.00	213.64	264.60	16.4332
0.50	22.1	26.80	216.58	262.64	16.5458
0.55	22.4	27.40	219.52	268.52	16.6578
0.60	23.8	28.20	233.24	276.36	17.1705
0.65	24.2	29.10	237.16	285.18	17.3142
0.70	24.9	28.60	244.02	280.28	17.5628
0.75	24.3	28.10	238.14	275.38	17.3499
0.80	23.2	27.80	227.36	272.44	16.9526
0.85	22.1	27.95	216.58	273.91	16.5458
0.90	23.4	28.00	229.32	274.40	17.0255
0.95	23.6	28.30	231.28	277.34	17.0982
1.00	23.8	28.60	233.24	280.28	17.1705
1.05	24.1	29.60	236.18	290.08	17.2783
1.10	24.2	29.90	237.16	293.02	17.3142
1.15	23.8	30.20	233.24	295.96	17.1705
1.20	23.6	29.70	231.28	291.06	17.0982
1.25	23.4	29.20	229.32	286.16	17.0255
1.30	22.7	28.85	222.46	282.73	16.7690
1.35	22.8	28.80	223.44	282.24	16.8058
1.40	23.5	28.60	230.30	280.28	17.0619
1.45	24.3	28.80	238.14	282.24	17.3499
1.50	24.6	30.00	241.08	294.00	17.4566
1.55	24.2	28.90	237.16	283.22	17.3142
1.60	23.8	28.40	233.24	278.32	17.1705
1.65	23.1	27.60	226.38	270.48	16.9161
1.70	22.8	28.50	223.44	279.30	16.8058

Waviness = 1.85 mm Temperature = 213.5°C Density = 1.065 Kg/m^3
Atm. pressure = 25.3 in. Hg Ave. velocity = 22.007 m/s Re = 192507

position m	vel. pr. mm. water	st. pr. mm water	vel. pr. Pa	st. pr. Pa	velocity m/s
0.00	36.5	40.2	357.70	393.96	21.3341
0.05	36.2	40.0	354.76	392.00	21.2462
0.10	35.5	39.7	347.90	389.06	21.0398
0.15	35.4	41.4	346.92	405.72	21.0102
0.20	37.3	42.6	365.54	417.48	21.5666
0.25	38.2	44.0	374.36	431.20	21.8253
0.30	39.3	44.6	385.14	437.08	22.1373
0.35	38.6	44.2	378.28	433.16	21.9392
0.40	37.7	43.4	369.46	425.32	21.6819
0.45	36.9	42.9	361.62	420.42	21.4506
0.50	36.5	42.6	357.70	417.48	21.3341
0.55	37.1	43.5	363.58	426.30	21.5087
0.60	38.4	44.6	376.32	437.08	21.8823
0.65	38.8	45.8	380.24	448.84	21.9960
0.70	40.9	46.2	400.82	452.76	22.5834
0.75	40.5	45.9	396.90	449.82	22.4727
0.80	38.6	43.3	378.28	424.34	21.9392
0.85	38.2	44.2	374.36	433.16	21.8253
0.90	37.8	44.5	370.44	436.10	21.7107
0.95	38.3	44.6	375.34	437.08	21.8538
1.00	39.3	45.2	385.14	442.96	22.1373
1.05	40.5	46.2	396.90	452.76	22.4727
1.10	41.6	47.2	407.68	462.56	22.7758
1.15	41.2	47.1	403.76	461.58	22.6661
1.20	40.0	46.3	392.00	453.74	22.3335
1.25	38.7	45.1	379.26	441.98	21.9676
1.30	38.3	44.8	375.34	439.04	21.8538
1.35	37.6	44.9	368.48	440.02	21.6532
1.40	37.7	46.0	369.46	450.80	21.6819
1.45	39.2	47.5	384.16	465.50	22.1091
1.50	40.6	48.1	397.88	471.38	22.5004
1.55	39.7	48.4	389.06	474.32	22.2496
1.60	39.1	47.3	383.18	463.54	22.0809
1.65	38.5	45.8	377.30	448.84	21.9108
1.70	37.6	45.6	368.48	446.88	21.6532

Waviness = 1.85 mm Temperature = 21.4^{0}C Density = 1.0094 Kg/m^3
Atm. pressure = 25.2 in. Hg Ave. velocity = 26.049 m/s Re = 229782

position m	vel. pr. mm. water	st. pr. mm water	vel. pr. Pa	st. pr. Pa	velocity m/s
0.00	52.8	60.5	517.44	592.90	25.6218
0.05	52.5	59.7	514.50	585.06	25.5490
0.10	52.2	57.8	511.56	566.44	25.4759
0.15	52.4	58.7	513.52	575.26	25.5246
0.20	53.7	60.2	526.26	589.96	25.8394
0.25	56.2	62.1	550.76	608.58	26.4339
0.30	57.4	62.5	562.52	612.50	26.7146
0.35	54.8	60.3	537.04	590.94	26.1026
0.40	54.0	60.1	529.20	588.98	25.9114
0.45	52.7	58.0	516.46	568.40	25.5976
0.50	52.0	59.7	509.60	585.06	25.4270
0.55	52.9	62.8	518.42	615.44	25.6462
0.60	55.5	64.0	543.90	627.20	26.2688
0.65	56.1	64.8	549.78	635.04	26.4104
0.70	56.2	64.4	550.76	631.12	26.4339
0.75	56.4	64.6	552.72	633.08	26.4810
0.80	54.3	62.7	532.14	614.46	25.9833
0.85	52.2	61.8	511.56	605.64	25.4759
0.90	53.8	62.1	527.24	608.58	25.8634
0.95	55.1	63.4	539.98	621.32	26.1740
1.00	55.5	63.8	543.90	625.24	26.2688
1.05	56.4	64.3	552.72	630.14	26.4810
1.10	57.2	66.6	560.56	652.68	26.6681
1.15	56.8	66.2	556.64	648.76	26.5747
1.20	54.6	64.9	535.08	636.02	26.0550
1.25	54.3	64.5	532.14	632.10	25.9833
1.30	50.7	61.1	496.86	598.78	25.1072
1.35	51.8	63.2	507.64	619.36	25.3781
1.40	53.3	64.3	522.34	630.14	25.7429
1.45	54.1	65.2	530.18	638.96	25.9354
1.50	55.4	65.5	542.92	641.90	26.2451
1.55	55.1	65.1	539.98	637.98	26.1740
1.60	54.6	64.4	535.08	631.12	26.0550
1.65	53.8	64.3	527.24	630.14	25.8634
1.70	52.7	64.2	516.46	629.16	25.5976

Waviness = 3.7 mm Temperature = 21.0^{0}C Density = 1.0149 Kg/m^3
Atm. pressure = 25.3 in. Hg Ave. velocity = 17.249 m/s Re = 153147

position m	vel. pr. mm. water	st. pr. mm water	vel. pr. Pa	st. pr. Pa	velocity m/s
0.00	22.6	25.700	221.48	251.860	16.7175
0.05	21.5	24.300	210.70	238.140	16.3056
0.10	20.8	23.500	203.84	230.300	16.0380
0.15	21.8	24.200	213.64	237.160	16.4190
0.20	24.0	26.700	235.20	261.660	17.2275
0.25	25.4	28.300	248.92	277.340	17.7229
0.30	25.6	28.800	250.88	282.240	17.7925
0.35	24.5	28.100	240.10	275.380	17.4061
0.40	22.8	27.100	223.44	265.580	16.7913
0.45	23.2	26.100	227.36	255.780	16.9380
0.50	22.2	25.800	217.56	252.840	16.5689
0.55	22.5	26.500	220.50	259.700	16.6805
0.60	24.4	26.900	239.12	263.620	17.3705
0.65	25.5	29.200	249.90	286.160	17.7577
0.70	26.3	30.150	257.74	295.470	18.0342
0.75	25.8	28.375	252.84	278.075	17.8619
0.80	23.2	26.800	227.36	262.640	16.9380
0.85	22.0	27.200	215.60	266.560	16.4941
0.90	21.5	26.950	210.70	264.110	16.3056
0.95	22.9	27.600	224.42	270.480	16.8281
1.00	23.0	27.900	225.40	273.420	16.8648
1.05	24.8	29.300	243.04	287.140	17.5123
1.10	25.3	29.900	247.94	293.020	17.6880
1.15	25.8	30.200	252.84	295.960	17.8619
1.20	24.8	29.500	243.04	289.100	17.5123
1.25	24.0	28.500	235.20	279.300	17.2275
1.30	22.3	27.400	218.54	268.520	16.6062
1.35	23.2	27.500	227.36	269.500	16.9380
1.40	23.6	28.200	231.28	276.360	17.0834
1.45	24.7	29.250	242.06	286.650	17.4770
1.50	26.0	30.400	254.80	297.920	17.9310
1.55	24.8	30.200	243.04	295.960	17.5123
1.60	24.2	29.500	237.16	289.100	17.2992
1.65	23.2	28.200	227.36	276.360	16.9380
1.70	22.8	28.000	223.44	274.400	16.7913

Waviness= 3.7 mm Temperature = 20.6^{0}C Density = 0.9339 Kg/m^3
Atm. pressure = 25.25 in. Hg Ave. velocity = 22.055 m/s Re = 180386

position m	vel. pr. mm. water	st. pr. mm water	vel. pr. Pa	st. pr. Pa	velocity m/s
0.00	36.2	41.4	354.76	405.72	21.1644
0.05	35.3	39.6	345.94	388.08	20.8997
0.10	33.7	38.1	330.26	373.38	20.4205
0.15	35.5	41.0	347.90	401.80	20.9588
0.20	37.4	43.4	366.52	425.32	21.5124
0.25	40.5	45.4	396.90	444.92	22.3862
0.30	42.2	45.7	413.56	447.86	22.8512
0.35	40.2	45.0	393.96	441.00	22.3031
0.40	37.6	43.2	368.48	423.36	21.5698
0.45	36.6	41.5	358.68	406.70	21.2810
0.50	35.8	41.0	350.84	401.80	21.0472
0.55	37.0	41.9	362.60	410.62	21.3970
0.60	39.2	45.0	384.16	441.00	22.0240
0.65	42.2	45.9	413.56	449.82	22.8512
0.70	43.0	48.1	421.40	471.38	23.0668
0.75	41.8	45.1	409.64	441.98	22.7426
0.80	39.8	45.5	390.04	445.90	22.1919
0.85	38.2	43.5	374.36	426.30	21.7412
0.90	37.7	42.2	369.46	413.56	21.5985
0.95	36.8	43.5	360.64	426.30	21.3391
1.00	37.8	44.3	370.44	434.14	21.6271
1.05	40.0	47.3	392.00	463.54	22.2476
1.10	41.2	49.0	403.76	480.20	22.5788
1.15	41.8	48.3	409.64	473.34	22.7426
1.20	38.6	46.0	378.28	450.80	21.8548
1.25	38.0	44.4	372.40	435.12	21.6842
1.30	35.4	43.8	346.92	429.24	20.9293
1.35	36.8	43.4	360.64	425.32	21.3391
1.40	38.6	44.8	378.28	439.04	21.8548
1.45	40.9	46.9	400.82	459.62	22.4964
1.50	43.5	48.8	426.30	478.24	23.2005
1.55	42.2	48.5	413.56	475.30	22.8512
1.60	40.1	47.1	392.98	461.58	22.2753
1.65	37.8	45.1	370.44	441.98	21.6271
1.70	36.8	44.2	360.64	433.16	21.3391

Waviness = 3.7 mm Temperature = 20.75^{0}C Density = 1.0158 Kg/m^3
Atm. pressure = 25.3 in. Hg Ave. velocity = 26.469 m/s Re = 255363

position m	vel. pr. mm. water	st. pr. mm water	vel. pr. Pa	st. pr. Pa	velocity m/s
0.00	53.10	59.7	520.38	585.06	25.6142
0.05	50.80	57.9	497.84	567.42	25.0533
0.10	49.80	56.8	488.04	556.64	24.8055
0.15	52.95	58.2	518.91	570.36	25.5780
0.20	54.50	62.8	534.10	615.44	25.9496
0.25	58.00	66.2	568.40	648.76	26.7699
0.30	59.60	67.2	584.08	658.56	27.1367
0.35	58.00	65.0	568.40	637.00	26.7699
0.40	54.60	61.4	535.08	601.72	25.9734
0.45	53.60	60.0	525.28	588.00	25.7345
0.50	53.00	59.6	519.40	584.08	25.5900
0.55	53.40	60.2	523.32	589.96	25.6864
0.60	54.60	63.7	535.08	624.26	25.9734
0.65	59.20	67.8	580.16	664.44	27.0454
0.70	60.70	70.0	594.86	686.00	27.3859
0.75	58.80	68.2	576.24	668.36	26.9539
0.80	56.50	65.3	553.70	639.94	26.4215
0.85	53.60	61.7	525.28	604.66	25.7345
0.90	52.60	60.8	515.48	595.84	25.4933
0.95	52.90	61.8	518.42	605.64	25.5659
1.00	56.60	63.4	554.68	621.32	26.4449
1.05	57.00	66.6	558.60	652.68	26.5382
1.10	61.20	70.1	599.76	686.98	27.4985
1.15	62.60	71.7	613.48	702.66	27.8112
1.20	59.00	66.3	578.20	649.74	26.9997
1.25	56.20	64.0	550.76	627.20	26.3513
1.30	53.40	61.9	523.32	606.62	25.6864
1.35	52.50	63.0	514.50	617.40	25.4691
1.40	54.60	64.9	535.08	636.02	25.9734
1.45	58.60	68.1	574.28	667.38	26.9080
1.50	60.40	70.8	591.92	693.84	27.3182
1.55	61.00	70.4	597.80	689.92	27.4535
1.60	58.80	68.2	576.24	668.36	26.9539
1.65	55.30	65.6	541.94	642.88	26.1394
1.70	53.20	64.2	521.36	629.16	25.6383

Waviness = 5.5 mm Temperature = 20.6^{0}C Density = 1.0235 Kg/m^3
Atm. pressure = 25.48 in. Hg Ave. velocity = 17.118 m/s Re = 153435

position m	vel. pr. mm. water	st. pr. mm water	vel. pr. Pa	st. pr. Pa	velocity m/s
0.00	21.80	25.200	213.64	246.960	16.3514
0.05	20.10	23.800	196.98	233.240	15.7009
0.10	19.50	23.300	191.10	228.340	15.4647
0.15	20.00	24.600	196.00	241.080	15.6618
0.20	21.70	26.700	212.66	261.660	16.3138
0.25	24.80	29.000	243.04	284.200	17.4402
0.30	26.10	29.900	255.78	293.020	17.8915
0.35	25.05	28.800	245.49	282.240	17.5279
0.40	22.60	26.800	221.48	262.640	16.6487
0.45	21.00	25.100	205.80	245.980	16.0485
0.50	20.60	24.700	201.88	242.060	15.8949
0.55	21.20	25.600	207.76	250.880	16.1248
0.60	23.00	27.900	225.40	273.420	16.7954
0.65	26.10	30.200	255.78	295.960	17.8915
0.70	27.00	31.000	264.60	303.800	18.1973
0.75	25.50	28.900	249.90	283.220	17.6846
0.80	24.50	27.950	240.10	273.910	17.3344
0.85	22.80	26.300	223.44	257.740	16.7222
0.90	21.60	26.100	211.68	255.780	16.2762
0.95	22.40	26.400	219.52	258.720	16.5748
1.00	22.90	27.900	224.42	273.420	16.7588
1.05	26.40	30.000	258.72	294.000	17.9940
1.10	27.20	31.700	266.56	310.660	18.2646
1.15	26.40	31.100	258.72	304.780	17.9940
1.20	24.70	29.400	242.06	288.120	17.4050
1.25	23.00	27.400	225.40	268.520	16.7954
1.30	21.80	26.600	213.64	260.680	16.3514
1.35	21.30	26.800	208.74	262.640	16.1628
1.40	22.70	28.700	222.46	281.260	16.6855
1.45	24.15	30.975	236.67	303.555	17.2101
1.50	27.10	32.400	265.58	317.520	18.2310
1.55	26.20	31.600	256.76	309.680	17.9257
1.60	24.30	30.000	238.14	294.000	17.2635
1.65	22.40	28.100	219.52	275.380	16.5748
1.70	21.20	27.500	207.76	269.500	16.1248

Waviness = 5.55 mm Temperature = 21.0^{0}C Density = 1.0229 Kg/m^3
Atm. pressure = 25.5 in. Hg Ave. velocity = 22.401 m/s Re = 200462

position m	vel. pr. mm. water	st. pr. mm water	vel. pr. Pa	st. pr. Pa	velocity m/s
0.00	36.00	44.7	352.80	438.06	21.0164
0.05	34.60	41.3	339.08	404.74	20.6037
0.10	32.40	40.6	317.52	397.88	19.9380
0.15	36.00	42.4	352.80	415.52	21.0164
0.20	38.20	47.6	374.36	466.48	21.6491
0.25	40.80	50.8	399.84	497.84	22.3737
0.30	45.45	52.4	445.41	513.52	23.6143
0.35	44.50	50.1	436.10	490.98	23.3662
0.40	39.60	46.4	388.08	454.72	22.0422
0.45	36.20	43.7	354.76	428.26	21.0747
0.50	33.80	42.5	331.24	416.50	20.3642
0.55	37.00	44.4	362.60	435.12	21.3063
0.60	39.40	48.4	386.12	474.32	21.9865
0.65	44.30	42.8	434.14	419.44	23.3136
0.70	45.00	53.7	441.00	526.26	23.4971
0.75	43.30	52.2	424.34	511.56	23.0490
0.80	40.10	48.8	392.98	478.24	22.1810
0.85	45.90	45.5	449.82	445.90	23.7309
0.90	45.40	45.1	444.92	441.98	23.6013
0.95	37.40	45.6	366.52	446.88	21.4212
1.00	39.80	48.1	390.04	471.38	22.0978
1.05	42.60	52.2	417.48	511.56	22.8619
1.10	44.80	55.4	439.04	542.92	23.4448
1.15	44.00	54.3	431.20	532.14	23.2346
1.20	40.60	51.0	397.88	499.80	22.3188
1.25	38.80	47.8	380.24	468.44	21.8184
1.30	36.60	46.5	358.68	455.70	21.1909
1.35	34.40	46.6	337.12	456.68	20.5441
1.40	38.70	49.5	379.26	485.10	21.7903
1.45	40.00	51.8	392.00	507.64	22.1533
1.50	44.40	55.0	435.12	539.00	23.3399
1.55	44.80	56.0	439.04	548.80	23.4448
1.60	42.40	53.1	415.52	520.38	22.8082
1.65	39.20	49.7	384.16	487.06	21.9306
1.70	35.80	48.1	350.84	471.38	20.9580

Waviness = 5.55 mm Temperature = 21.0^{0}C Density = 1.0189 Kg/m^3
Atm. pressure = 25.4 in. Hg Ave. velocity = 26.655 m/s Re = 237595

position m	vel. pr. mm. water	st. pr. mm water	vel. pr. Pa	st. pr. Pa	velocity m/s
0.00	52.4	62.5	513.52	612.50	25.4054
0.05	50.7	58.9	496.86	577.22	24.9899
0.10	48.4	57.9	474.32	567.42	24.4165
0.15	51.2	59.8	501.76	586.04	25.1129
0.20	55.7	65.3	545.86	639.94	26.1932
0.25	58.5	71.9	573.30	704.62	26.8435
0.30	62.3	75.6	610.54	740.88	27.7016
0.35	58.7	70.9	575.26	694.82	26.8893
0.40	56.3	66.2	551.74	648.76	26.3339
0.45	51.9	61.6	508.62	603.68	25.2839
0.50	49.6	61.2	486.08	599.76	24.7174
0.55	50.7	63.1	496.86	618.38	24.9899
0.60	55.6	69.7	544.88	683.06	26.1697
0.65	62.5	75.1	612.50	735.98	27.7461
0.70	65.8	77.5	644.84	759.50	28.4691
0.75	61.2	74.3	599.76	728.14	27.4560
0.80	55.5	68.8	543.90	674.24	26.1461
0.85	52.3	65.4	512.54	640.92	25.3812
0.90	51.9	63.6	508.62	623.28	25.2839
0.95	52.4	64.3	513.52	630.14	25.4054
1.00	53.8	68.2	527.24	668.36	25.7426
1.05	60.6	74.1	593.88	726.18	27.3211
1.10	65.8	78.6	644.84	770.28	28.4691
1.15	66.2	78.2	648.76	766.36	28.5555
1.20	60.1	73.4	588.98	719.32	27.2081
1.25	54.3	67.8	532.14	664.44	25.8619
1.30	51.5	65.1	504.70	637.98	25.1863
1.35	52.3	66.2	512.54	648.76	25.3812
1.40	55.5	69.9	543.90	685.02	26.1461
1.45	62.6	75.4	613.48	738.92	27.7682
1.50	67.4	80.2	660.52	785.96	28.8132
1.55	64.6	78.3	633.08	767.34	28.2083
1.60	60.6	75.1	593.88	735.98	27.3211
1.65	56.0	70.1	548.80	686.98	26.2637
1.70	53.2	68.0	521.36	666.40	25.5986

Waviness = 7.4 mm Temperature = 21.2^{0}C Density = 1.0142 Kg/m^3
Atm. pressure = 25.3 in. Hg Ave. velocity = 17.801 m/s Re = 157858

position m	vel. pr. mm. water	st. pr. mm water	vel. pr. Pa	st. pr. Pa	velocity m/s
0.00	22.3	25.5	218.54	249.90	16.6118
0.05	20.8	23.8	203.84	233.24	16.0434
0.10	20.2	23.5	197.96	230.30	15.8103
0.15	21.4	24.4	209.72	239.12	16.2732
0.20	24.0	27.6	235.20	270.48	17.2334
0.25	27.7	31.5	271.46	308.70	18.5142
0.30	30.6	32.4	299.88	317.52	19.4593
0.35	27.5	30.5	269.50	298.90	18.4473
0.40	24.1	27.8	236.18	272.44	17.2693
0.45	20.6	25.6	201.88	250.88	15.9661
0.50	20.4	25.0	199.92	245.00	15.8884
0.55	22.6	26.0	221.48	254.80	16.7232
0.60	25.4	28.8	248.92	282.24	17.7289
0.65	29.4	32.0	288.12	313.60	19.0739
0.70	30.4	33.3	297.92	326.34	19.3956
0.75	28.2	31.4	276.36	307.72	18.6806
0.80	24.8	30.0	243.04	294.00	17.5183
0.85	22.5	27.1	220.50	265.58	16.6862
0.90	21.6	26.5	211.68	259.70	16.3490
0.95	22.4	27.1	219.52	265.58	16.6490
1.00	24.2	28.8	237.16	282.24	17.3051
1.05	26.8	32.4	262.64	317.52	18.2110
1.10	28.6	34.0	280.28	333.20	18.8126
1.15	29.2	33.0	286.16	323.40	19.0089
1.20	26.2	31.0	256.76	303.80	18.0060
1.25	22.4	28.6	219.52	280.28	16.6490
1.30	21.6	27.4	211.68	268.52	16.3490
1.35	22.4	27.8	219.52	272.44	16.6490
1.40	24.6	29.9	241.08	293.02	17.4475
1.45	28.4	33.1	278.32	324.38	18.7467
1.50	30.8	35.0	301.84	343.00	19.5227
1.55	30.4	34.0	297.92	333.20	19.3956
1.60	27.8	32.2	272.44	315.56	18.5476
1.65	24.2	29.9	237.16	293.02	17.3051
1.70	22.4	28.5	219.52	279.30	16.6490

Waviness = 7.4 mm Temperature = 21.5^{0}C Density = 1.0096 Kg/m^3
Atm. pressure = 25.21 in. Hg Ave. velocity = 21.955 m/s Re = 193653

position m	vel. pr. mm. water	st. pr. mm water	vel. pr. Pa	st. pr. Pa	velocity m/s
0.00	36.0	40.40	352.80	395.92	21.1549
0.05	34.5	37.60	338.10	368.48	20.7095
0.10	32.2	37.00	315.56	362.60	20.0073
0.15	34.8	38.90	341.04	381.22	20.7994
0.20	36.4	42.60	356.72	417.48	21.2721
0.25	42.2	48.30	413.56	473.34	22.9043
0.30	45.0	51.90	441.00	508.62	23.6519
0.35	43.0	48.40	421.40	474.32	23.1204
0.40	36.4	43.60	356.72	427.28	21.2721
0.45	34.0	40.50	333.20	396.90	20.5589
0.50	32.5	39.40	318.50	386.12	20.1003
0.55	33.0	40.70	323.40	398.86	20.2543
0.60	37.2	44.85	364.56	439.53	21.5046
0.65	42.8	50.00	419.44	490.00	23.0665
0.70	45.2	52.50	442.96	514.50	23.7044
0.75	41.6	49.70	407.68	487.06	22.7409
0.80	37.5	45.60	367.50	446.88	21.5912
0.85	33.6	42.80	329.28	419.44	20.4376
0.90	32.2	41.30	315.56	404.74	20.0073
0.95	34.5	42.00	338.10	411.60	20.7095
1.00	37.4	45.40	366.52	444.92	21.5624
1.05	42.6	51.10	417.48	500.78	23.0126
1.10	41.6	53.50	407.68	524.30	22.7409
1.15	43.8	52.00	429.24	509.60	23.3344
1.20	38.2	48.60	374.36	476.28	21.7918
1.25	37.0	45.00	362.60	441.00	21.4467
1.30	34.3	43.10	336.14	422.38	20.6494
1.35	35.0	43.40	343.00	425.32	20.8590
1.40	37.2	46.40	364.56	454.72	21.5046
1.45	42.3	52.00	414.54	509.60	22.9314
1.50	46.4	54.10	454.72	530.18	24.0170
1.55	44.6	55.10	437.08	539.98	23.5466
1.60	40.4	52.10	395.92	510.58	22.4105
1.65	38.0	46.60	372.40	456.68	21.7346
1.70	36.0	44.30	352.80	434.14	21.1549

Waviness = 7.4 mm Temperature = 21.0^{0}C Density = 1.0157 Kg/m^3
Atm. pressure = 25.32 in. Hg Ave. velocity = 26.98 m/s Re = 239735

position m	vel. pr. mm. water	st. pr. mm water	vel. pr. Pa	st. pr. Pa	velocity m/s
0.00	53.0	64.50	519.40	632.10	25.5908
0.05	50.4	59.90	493.92	587.02	24.9552
0.10	48.8	59.50	478.24	583.10	24.5559
0.15	51.4	62.00	503.72	607.60	25.2016
0.20	56.2	70.50	550.76	690.90	26.3521
0.25	66.0	78.60	646.80	770.28	28.5574
0.30	67.2	82.70	658.56	810.46	28.8158
0.35	62.8	75.70	615.44	741.86	27.8565
0.40	56.6	69.80	554.68	684.04	26.4457
0.45	50.0	65.00	490.00	637.00	24.8560
0.50	46.0	63.10	450.80	618.38	23.8410
0.55	49.0	74.90	480.20	734.02	24.6062
0.60	54.4	71.10	533.12	696.78	25.9266
0.65	63.4	79.90	621.32	783.02	27.9892
0.70	68.0	83.20	666.40	815.36	28.9868
0.75	64.0	80.65	627.20	790.37	28.1214
0.80	57.4	73.10	562.52	716.38	26.6319
0.85	52.2	67.80	511.56	664.44	25.3969
0.90	49.0	65.80	480.20	644.84	24.6062
0.95	52.4	66.80	513.52	654.64	25.4456
1.00	56.3	72.30	551.74	708.54	26.3755
1.05	64.4	81.10	631.12	794.78	28.2091
1.10	68.3	85.50	669.34	837.90	29.0507
1.15	67.7	84.20	663.46	825.16	28.9228
1.20	62.2	78.80	609.56	772.24	27.7231
1.25	55.2	71.60	540.96	701.68	26.1166
1.30	50.8	68.50	497.84	671.30	25.0541
1.35	51.5	69.30	504.70	679.14	25.2261
1.40	57.2	73.80	560.56	723.24	26.5855
1.45	64.8	82.40	635.04	807.52	28.2966
1.50	69.4	88.50	680.12	867.30	29.2837
1.55	68.7	85.20	673.26	834.96	29.1356
1.60	63.5	82.00	622.30	803.60	28.0113
1.65	56.6	74.30	554.68	728.14	26.4457
1.70	53.2	70.80	521.36	693.84	25.6391

Waviness = 9.25 mm Temperature = 21.0^{0}C Density = 1.0120 Kg/m^3
Atm. pressure = 25.23 in. Hg Ave. velocity = 17.109 m/s Re = 151474

position m	vel. pr. mm. water	st. pr. mm water	vel. pr. Pa	st. pr. Pa	velocity m/s
0.00	21.9	24.8	214.62	243.04	16.4799
0.05	19.4	22.6	190.12	221.48	15.5108
0.10	18.8	22.2	184.24	217.56	15.2690
0.15	20.2	23.5	197.96	230.30	15.8274
0.20	23.3	27.0	228.34	264.60	16.9986
0.25	27.3	32.0	267.54	313.60	18.3999
0.30	29.8	33.6	292.04	329.28	19.2239
0.35	26.3	30.4	257.74	297.92	18.0598
0.40	22.2	26.9	217.56	263.62	16.5924
0.45	20.0	24.8	196.00	243.04	15.7489
0.50	18.4	24.1	180.32	236.18	15.1058
0.55	19.9	25.4	195.02	248.92	15.7094
0.60	23.1	27.9	226.38	273.42	16.9254
0.65	25.8	32.6	252.84	319.48	17.8873
0.70	28.4	34.2	278.32	335.16	18.7669
0.75	26.1	31.8	255.78	311.64	17.9910
0.80	23.4	28.6	229.32	280.28	17.0350
0.85	19.6	26.1	192.08	255.78	15.5906
0.90	18.6	25.2	182.28	246.96	15.1876
0.95	19.7	25.6	193.06	250.88	15.6303
1.00	22.3	28.0	218.54	274.40	16.6298
1.05	25.9	32.5	253.82	318.50	17.9219
1.10	29.0	34.9	284.20	342.02	18.9642
1.15	27.3	33.7	267.54	330.26	18.3999
1.20	23.8	30.3	233.24	296.94	17.1800
1.25	21.3	27.8	208.74	272.44	16.2526
1.30	19.2	26.2	188.16	256.76	15.4306
1.35	19.4	26.8	190.12	262.64	15.5108
1.40	22.1	29.0	216.58	284.20	16.5550
1.45	27.0	33.2	264.60	325.36	18.2985
1.50	28.3	35.8	277.34	350.84	18.7338
1.55	26.2	34.0	256.76	333.20	18.0254
1.60	24.4	32.0	239.12	313.60	17.3952
1.65	22.2	28.6	217.56	280.28	16.5924
1.70	19.8	27.0	194.04	264.60	15.6699

Waviness = 9.25 mm Temperature = 20.7^{0}C Density = 1.0134 Kg/m^3
Atm. pressure = 25.24 in. Hg Ave. velocity = 22.204 m/s Re = 19700

position m	vel. pr. mm. water	st. pr. mm water	vel. pr. Pa	st. pr. Pa	velocity m/s
0.00	35.4	40.30	346.92	394.94	20.9385
0.05	32.3	37.40	316.54	366.52	20.0007
0.10	30.4	36.95	297.92	362.11	19.4035
0.15	34.0	38.90	333.20	381.22	20.5203
0.20	39.0	44.60	382.20	437.08	21.9774
0.25	46.6	53.20	456.68	521.36	24.0236
0.30	48.2	54.40	472.36	533.12	24.4325
0.35	43.6	50.30	427.28	492.94	23.2374
0.40	37.4	45.20	366.52	442.96	21.5219
0.45	33.2	40.90	325.36	400.82	20.2775
0.50	31.5	39.80	308.70	390.04	19.7515
0.55	33.1	41.10	324.38	402.78	20.2469
0.60	38.1	45.60	373.38	446.88	21.7224
0.65	44.3	52.40	434.14	513.52	23.4232
0.70	47.4	56.30	464.52	551.74	24.2289
0.75	44.6	53.30	437.08	522.34	23.5024
0.80	38.2	47.40	374.36	464.52	21.7508
0.85	34.1	43.40	334.18	425.32	20.5505
0.90	31.9	41.75	312.62	409.15	19.8765
0.95	33.0	42.30	323.40	414.54	20.2163
1.00	37.5	46.60	367.50	456.68	21.5506
1.05	44.3	54.10	434.14	530.18	23.4232
1.10	48.2	58.40	472.36	572.32	24.4325
1.15	46.3	56.10	453.74	549.78	23.9461
1.20	39.6	50.90	388.08	498.82	22.1458
1.25	34.8	46.00	341.04	450.80	20.7603
1.30	32.2	43.20	315.56	423.36	19.9697
1.35	34.3	43.60	336.14	427.28	20.6106
1.40	37.0	47.35	362.60	464.03	21.4065
1.45	44.3	55.70	434.14	545.86	23.4232
1.50	49.6	59.90	486.08	587.02	24.7848
1.55	47.0	56.80	460.60	556.64	24.1264
1.60	41.2	53.20	403.76	521.36	22.5888
1.65	37.7	48.30	369.46	473.34	21.6080
1.70	34.9	44.80	342.02	439.04	20.7901

Waviness = 9.25 mm Temperature = 21.0°C Density = 1.0120 Kg/m³
Atm. pressure = 25.23 in. Hg Ave. velocity = 26.978 m/s Re = 238849

position m	vel. pr. mm. water	st. pr. mm water	vel. pr. Pa	st. pr. Pa	velocity m/s
0.00	52.1	59.70	510.58	585.06	25.4186
0.05	46.8	56.25	458.64	551.25	24.0911
0.10	43.9	54.60	430.22	535.08	23.3327
0.15	49.1	56.95	481.18	558.11	24.6760
0.20	55.8	66.30	546.84	649.74	26.3058
0.25	65.7	76.80	643.86	752.64	28.5441
0.30	68.8	82.00	674.24	803.60	29.2098
0.35	63.5	73.40	622.30	719.32	28.0622
0.40	54.3	64.30	532.14	630.14	25.9498
0.45	47.5	59.90	465.50	587.02	24.2706
0.50	46.9	56.60	459.62	554.68	24.1168
0.55	48.3	57.80	473.34	566.44	24.4742
0.60	54.8	66.70	537.04	653.66	26.0690
0.65	67.7	76.10	663.46	745.78	28.9753
0.70	70.2	80.70	687.96	790.86	29.5054
0.75	65.2	76.50	638.96	749.70	28.4353
0.80	56.2	69.00	550.76	676.20	26.3998
0.85	51.3	63.30	502.74	620.34	25.2227
0.90	48.1	59.90	471.38	587.02	24.4234
0.95	49.6	61.10	486.08	598.78	24.8013
1.00	56.4	67.60	552.72	662.48	26.4468
1.05	66.1	78.10	647.78	765.38	28.6309
1.10	74.0	84.40	725.20	827.12	30.2935
1.15	69.6	81.10	682.08	794.78	29.3791
1.20	59.3	73.70	581.14	722.26	27.1182
1.25	53.4	66.90	523.32	655.62	25.7338
1.30	47.8	62.60	468.44	613.48	24.3471
1.35	48.3	62.80	473.34	615.44	24.4742
1.40	54.8	68.10	537.04	667.38	26.0690
1.45	66.2	80.30	648.76	786.94	28.6525
1.50	72.1	86.30	706.58	845.74	29.9021
1.55	66.8	82.10	654.64	804.58	28.7821
1.60	62.2	76.95	609.56	754.11	27.7734
1.65	52.9	68.25	518.42	668.85	25.6130
1.70	48.7	65.50	477.26	641.90	24.5753

Waviness = 11.1 mm Temperature = 20.4^{0}C Density = 1.0184 Kg/m^3
Atm. pressure = 25.33 in. Hg Ave. velocity = 17.992 m/s Re = 160543

position m	vel. pr. mm. water	st. pr. mm water	vel. pr. Pa	st. pr. Pa	velocity m/s
0.00	21.70	28.60	212.66	280.28	16.3534
0.05	18.30	25.50	179.34	249.90	15.0177
0.10	17.70	24.40	173.46	239.12	14.7694
0.15	18.50	25.80	181.30	252.84	15.0995
0.20	24.40	30.60	239.12	299.88	17.3410
0.25	31.70	37.20	310.66	364.56	19.7654
0.30	33.25	38.50	325.85	377.30	20.2429
0.35	27.90	35.40	273.42	346.92	18.5430
0.40	23.80	31.00	233.24	303.80	17.1264
0.45	20.20	27.95	197.96	273.91	15.7780
0.50	18.40	26.80	180.32	262.64	15.0586
0.55	20.50	27.20	200.90	266.56	15.8948
0.60	24.70	31.60	242.06	309.68	17.4472
0.65	31.10	37.80	304.78	370.44	19.5775
0.70	32.60	40.20	319.48	393.96	20.0441
0.75	30.40	37.40	297.92	366.52	19.3559
0.80	24.60	32.90	241.08	322.42	17.4118
0.85	21.10	29.80	206.78	292.04	16.1257
0.90	20.50	28.50	200.90	279.30	15.8948
0.95	20.30	28.40	198.94	278.32	15.8170
1.00	24.25	31.80	237.65	311.64	17.2875
1.05	29.70	37.90	291.06	371.42	19.1318
1.10	34.40	41.20	337.12	403.76	20.5900
1.15	31.60	39.80	309.68	390.04	19.7342
1.20	26.90	35.30	263.62	345.94	18.2076
1.25	23.40	31.60	229.32	309.68	16.9818
1.30	21.10	29.20	206.78	286.16	16.1257
1.35	21.20	29.10	207.76	285.18	16.1638
1.40	24.70	32.30	242.06	316.54	17.4472
1.45	31.10	38.90	304.78	381.22	19.5775
1.50	34.00	42.20	333.20	413.56	20.4699
1.55	32.20	39.60	315.56	388.08	19.9207
1.60	28.35	37.20	277.83	364.56	18.6919
1.65	23.40	33.30	229.32	326.34	16.9818
1.70	21.80	30.80	213.64	301.84	16.3910

Waviness = 11.1 mm Temperature = 20.8^{0}C Density = 1.0171 Kg/m^3
Atm. pressure = 25.34 in. Hg Ave. velocity = 21.683 m/s Re = 193042

position m	vel. pr. mm. water	st. pr. mm water	vel. pr. Pa	st. pr. Pa	velocity m/s
0.00	35.6	43.20	348.88	423.36	20.9587
0.05	29.2	39.70	286.16	389.06	18.9815
0.10	27.7	40.50	271.46	396.90	18.4875
0.15	30.5	42.50	298.90	416.50	19.3994
0.20	36.6	48.90	358.68	479.22	21.2510
0.25	47.4	59.50	464.52	583.10	24.1840
0.30	52.2	61.40	511.56	601.72	25.3790
0.35	44.8	55.10	439.04	539.98	23.5114
0.40	37.2	48.60	364.56	476.28	21.4245
0.45	31.6	45.00	309.68	441.00	19.7462
0.50	29.2	42.80	286.16	419.44	18.9815
0.55	31.1	43.30	304.78	424.34	19.5893
0.60	38.0	49.40	372.40	484.12	21.6536
0.65	46.3	58.70	453.74	575.26	23.9018
0.70	47.8	62.60	468.44	613.48	24.2858
0.75	44.6	58.95	437.08	577.71	23.4588
0.80	35.7	52.50	349.86	514.50	20.9881
0.85	30.2	48.00	295.96	470.40	19.3038
0.90	28.9	45.10	283.22	441.98	18.8837
0.95	29.9	45.80	293.02	448.84	19.2077
1.00	34.7	51.60	340.06	505.68	20.6921
1.05	42.6	60.70	417.48	594.86	22.9268
1.10	47.6	64.40	466.48	631.12	24.2350
1.15	44.5	62.30	436.10	610.54	23.4325
1.20	38.4	56.40	376.32	552.72	21.7673
1.25	31.3	51.60	306.74	505.68	19.6522
1.30	29.2	48.50	286.16	475.30	18.9815
1.35	29.1	47.00	285.18	460.60	18.9490
1.40	34.3	52.10	336.14	510.58	20.5725
1.45	42.5	61.10	416.50	598.78	22.8999
1.50	47.4	65.60	464.52	642.88	24.1840
1.55	43.2	61.50	423.36	602.70	23.0877
1.60	38.1	58.10	373.38	569.38	21.6821
1.65	32.4	53.70	317.52	526.26	19.9946
1.70	29.4	50.10	288.12	490.98	19.0464

Waviness = 11.1 mm Temperature = 22.0^{0}C Density = 1.0121 Kg/m^3
Atm. pressure = 25.31 in. Hg Ave. velocity = 28.182 m/s Re = 248864

position m	vel. pr. mm. water	st. pr. mm water	vel. pr. Pa	st. pr. Pa	velocity m/s
0.00	52.5	68.60	514.50	672.28	25.5156
0.05	46.7	63.80	457.66	625.24	24.0649
0.10	44.8	63.00	439.04	617.40	23.5703
0.15	50.5	66.70	494.90	653.66	25.0249
0.20	57.3	76.80	561.54	752.64	26.6565
0.25	74.1	92.00	726.18	901.60	30.3135
0.30	78.9	94.40	773.22	925.12	31.2799
0.35	71.2	86.05	697.76	843.29	29.7144
0.40	59.6	77.10	584.08	755.58	27.1863
0.45	51.8	70.80	507.64	693.84	25.3449
0.50	48.5	68.30	475.30	669.34	24.5243
0.55	50.4	70.10	493.92	686.98	25.0001
0.60	58.5	76.80	573.30	752.64	26.9342
0.65	72.7	91.30	712.46	894.74	30.0257
0.70	78.8	96.70	772.24	947.66	31.2600
0.75	71.2	90.60	697.76	887.88	29.7144
0.80	62.1	82.20	608.58	805.56	27.7506
0.85	56.8	71.80	556.64	703.64	26.5400
0.90	48.4	69.50	474.32	681.10	24.4990
0.95	49.5	71.40	485.10	699.72	24.7759
1.00	60.6	79.30	593.88	777.14	27.4134
1.05	72.3	93.20	708.54	913.36	29.9430
1.10	81.4	100.90	797.72	988.82	31.7716
1.15	76.8	96.70	752.64	947.66	30.8608
1.20	66.6	88.30	652.68	865.34	28.7385
1.25	57.2	79.10	560.56	775.18	26.6333
1.30	52.4	73.40	513.52	719.32	25.4913
1.35	51.8	73.20	507.64	717.36	25.3449
1.40	58.2	79.40	570.36	778.12	26.8651
1.45	74.4	96.60	729.12	946.68	30.3748
1.50	82.1	102.60	804.58	1005.48	31.9079
1.55	78.8	98.20	772.24	962.36	31.2600
1.60	68.5	89.70	671.30	879.06	29.1455
1.65	57.4	81.80	562.52	801.64	26.6798
1.70	50.7	76.20	496.86	746.76	25.0744

Waviness = 12.95 mm Temperature = 22.0^{0}C Density = 1.0121 Kg/m^3
Atm. pressure = 25.31 in. Hg Ave. velocity = 18.624 m/s Re = 164461

position m	vel. pr. mm. water	st. pr. mm water	vel. pr. Pa	st. pr. Pa	velocity m/s
0.00	20.80	29.80	203.84	292.04	16.0605
0.05	18.60	26.20	182.28	256.76	15.1874
0.10	17.30	26.00	169.54	254.80	14.6470
0.15	19.80	26.50	194.04	259.70	15.6696
0.20	24.60	32.20	241.08	315.56	17.4660
0.25	33.20	39.80	325.36	390.04	20.2906
0.30	37.40	42.30	366.52	414.54	21.5359
0.35	30.50	39.40	298.90	386.12	19.4481
0.40	26.50	32.00	259.70	313.60	18.1280
0.45	20.70	29.20	202.86	286.16	16.0218
0.50	20.20	28.10	197.96	275.38	15.8271
0.55	21.65	28.60	212.17	280.28	16.3853
0.60	26.00	32.70	254.80	320.46	17.9561
0.65	32.40	40.30	317.52	394.94	20.0447
0.70	35.40	43.20	346.92	423.36	20.9521
0.75	31.80	39.50	311.64	387.10	19.8582
0.80	27.20	34.20	266.56	335.16	18.3658
0.85	22.20	30.80	217.56	301.84	16.5922
0.90	20.70	30.00	202.86	294.00	16.0218
0.95	22.40	30.70	219.52	300.86	16.6667
1.00	25.60	34.30	250.88	336.14	17.8175
1.05	35.10	43.20	343.98	423.36	20.8632
1.10	39.20	46.20	384.16	452.76	22.0480
1.15	34.10	43.20	334.18	423.36	20.5638
1.20	27.50	38.40	269.50	376.32	18.4668
1.25	22.80	32.40	223.44	317.52	16.8149
1.30	20.70	30.60	202.86	299.88	16.0218
1.35	21.60	30.25	211.68	296.45	16.3664
1.40	25.20	34.50	246.96	338.10	17.6777
1.45	32.50	43.10	318.50	422.38	20.0756
1.50	36.90	46.70	361.62	457.66	21.3914
1.55	33.60	43.20	329.28	423.36	20.4125
1.60	32.30	39.70	316.54	389.06	20.0137
1.65	26.20	35.40	256.76	346.92	18.0251
1.70	22.30	32.50	218.54	318.50	16.6295

Waviness = 12.95 mm Temperature = 22.0^{0}C Density = 1.0119 Kg/m^3
Atm. pressure = 25.31 in. Hg Ave. velocity = 21.854 m/s Re = 192954

position m	vel. pr. mm. water	st. pr. mm water	vel. pr. Pa	st. pr. Pa	velocity m/s
0.00	35.4	44.1	346.92	432.18	20.9521
0.05	27.8	39.4	272.44	386.12	18.5673
0.10	25.5	37.7	249.90	369.46	17.7827
0.15	29.4	38.1	288.12	373.38	19.0941
0.20	32.4	45.8	317.52	448.84	20.0447
0.25	49.6	59.0	486.08	578.20	24.8009
0.30	49.8	61.3	488.04	600.74	24.8508
0.35	42.6	54.9	417.48	538.02	22.9843
0.40	32.3	47.1	316.54	461.58	20.0137
0.45	29.6	42.4	290.08	415.52	19.1590
0.50	28.5	39.9	279.30	391.02	18.7996
0.55	31.8	40.3	311.64	394.94	19.8582
0.60	34.1	47.1	334.18	461.58	20.5638
0.65	46.8	59.2	458.64	580.16	24.0907
0.70	49.4	63.5	484.12	622.30	24.7508
0.75	42.8	56.3	419.44	551.74	23.0382
0.80	33.3	49.8	326.34	488.04	20.3212
0.85	28.7	44.3	281.26	434.14	18.8655
0.90	27.6	42.6	270.48	417.48	18.5004
0.95	28.6	43.7	280.28	428.26	18.8326
1.00	37.2	49.3	364.56	483.14	21.4782
1.05	49.8	62.2	488.04	609.56	24.8508
1.10	51.4	68.3	503.72	669.34	25.2469
1.15	49.2	61.6	482.16	603.68	24.7007
1.20	39.8	54.4	390.04	533.12	22.2161
1.25	31.4	47.8	307.72	468.44	19.7329
1.30	29.1	44.0	285.18	431.20	18.9965
1.35	30.4	44.1	297.92	432.18	19.4162
1.40	36.4	49.9	356.72	489.02	21.2460
1.45	47.3	62.3	463.54	610.54	24.2190
1.50	53.2	66.4	521.36	650.72	25.6852
1.55	47.1	62.2	461.58	609.56	24.1678
1.60	40.2	58.1	393.96	569.38	22.3275
1.65	33.8	51.0	331.24	499.80	20.4732
1.70	32.4	46.6	317.52	456.68	20.0447

Waviness = 12.95 mm Temperature = 21.0°C Density = 1.0145 Kg/m³
Atm. pressure = 25.29 in. Hg Ave. velocity = 27.753 m/s Re = 246324

position m	vel. pr. mm. water	st. pr. mm water	vel. pr. Pa	st. pr. Pa	velocity m/s
0.00	51.3	61.70	502.74	604.66	25.1913
0.05	40.9	57.20	400.82	560.56	22.4933
0.10	40.3	55.10	394.94	539.98	22.3277
0.15	43.8	58.20	429.24	570.36	23.2771
0.20	55.3	69.40	541.94	680.12	26.1550
0.25	75.4	88.70	738.92	869.26	30.5406
0.30	80.3	95.00	786.94	931.00	31.5174
0.35	70.2	84.60	687.96	829.08	29.4687
0.40	56.5	71.10	553.70	696.78	26.4373
0.45	47.1	63.20	461.58	619.36	24.1381
0.50	40.7	57.90	398.86	567.42	22.4383
0.55	45.9	60.20	449.82	589.96	23.8286
0.60	55.6	72.80	544.88	713.44	26.2259
0.65	75.8	90.10	742.84	882.98	30.6215
0.70	79.2	97.20	776.16	952.56	31.3008
0.75	68.1	86.95	667.38	852.11	29.0246
0.80	55.8	75.60	546.84	740.88	26.2730
0.85	48.7	68.00	477.26	666.40	24.5446
0.90	44.9	63.60	440.02	623.28	23.5676
0.95	46.2	61.90	452.76	606.62	23.9063
1.00	58.3	73.30	571.34	718.34	26.8551
1.05	75.6	91.40	740.88	895.72	30.5811
1.10	85.3	101.30	835.94	992.74	32.4838
1.15	77.6	94.70	760.48	928.06	30.9830
1.20	64.8	83.40	635.04	817.32	28.3126
1.25	54.3	72.90	532.14	714.42	25.9174
1.30	47.7	67.40	467.46	660.52	24.2913
1.35	49.1	67.10	481.18	657.58	24.6452
1.40	58.2	72.80	570.36	713.44	26.8320
1.45	79.3	93.70	777.14	918.26	31.3205
1.50	85.2	102.60	834.96	1005.48	32.4647
1.55	77.5	93.40	759.50	915.32	30.9630
1.60	68.9	88.90	675.22	871.22	29.1946
1.65	57.3	79.35	561.54	777.63	26.6238
1.70	52.2	72.20	511.56	707.56	25.4113